Master thesis

GPS/INS Integrity in Airborne Mapping

Presented by

Yannick STEBLER

Supervised by

Dr. Jan SKALOUD

Philipp SCHAER

Swiss Federal Institute of Technology, Lausanne

Geodetic Engineering Laboratory

July 2008

Abstract

The quality of the laser point cloud georeferencing in airborne laser scanning missions is largely related to the quality of the GPS solution. The latter is obtained by post-processing the differential carrier-phase measurements in order to reach the required accuracy. This implies that errors or unacceptable quality in the gathered data that cause problems for the ambiguity resolution in the post-processing step are detected much later. The objective of this thesis is to investigate new concepts of GPS data quality monitoring and to improve the GPS solution by using RAIM and WAAS/EGNOS integrity enhancement techniques. To do that, quality check algorithms based on indicators such as the signal-to-noise ratio, the cycle slip detection results or the phase tracking loop output are proposed and successfully tested. Furthermore, a new global quality check algorithm based on RAIM and cycle slip detection has been designed and tested with a focus on the chances to resolve correctly the ambiguities during the carrier-phase post-processing. The algorithms are implemented in a real-time quality check tool developed in a C/C++ environment whose performance shows that the provided quality indications enhance the GPS integrity by providing crucial information on the signal quality during the flight. This information enables problematic epoch identification and warns immediately the mission operator about problematic flightlines that should be flown again. This avoids final product quality degradation or expensive mission repetition. The thesis also presents the design of an RTK-GPS on-board solution via radio communication channel. The design has been tested during a flight and the results show that a sub-decimetric accuracy can be reached by this mean. The potential of using such a solution is high since this provides ultimate integrity test for phase data. Also, as the final laser point cloud has been georeferenced quite accurately using the real-time sensor observations and Kalman filtering, the economical gain of avoiding post-processing is substantial.

Acknowledgments

I would like to take this opportunity to thank a few people who have support me in my time at EPFL.

First, I want to thank my thesis supervisor, Dr. Jan Skaloud, who gave me the chance to work in a fascinating domain. His leadership, support and uncompromising quest for excellence has been able to fascinate me for the navigation and laser-scanning domains. It's for me a huge satisfaction to continue to work with him in this lab.

To Philipp Schaer of the Geodetic Engineering Laboratory, thank you for the support and advice during the thesis, as well as the good times spent together on the bike.

To the other members of the Geodetic Engineering Laboratory, Prof. Bertrand Merminod, Pierre-Yves Gilliéron, Christian Baumann and Adrian Waegli, thank you for the good atmosphere and the good times we spent together. The friendly and supportive atmosphere inherent in the whole lab contributed essentially to the final outcome of my thesis.

To the directors of GEOSAT S.A., Christian Hagin and Patrick Lathion, thank you for the time you have spent with me and for the equipment without which the RTK-GPS flight would not have been possible.

Finally, I want to particularly thank my parents, Ruth and Franz Stebler, who gave me the opportunity to study and focus on exactly what I wanted to do. Thank you for your continual support of me in all my endeavors. Thank you to Valérie for her enduring patience, understanding, and love.

Contents

List of Figures

List of Tables

Key acronyms

ABAS	Aircraft Based Augmentation System
AL	Alarm Limit
ALS	Airborne Laser Scanning
CDF	Cumulative Density Function
CEP	Circular Error Probable
DD	Double-Difference
DGPS	Differential GPS
DOP	Dilution Of Precision
EGNOS	European Geostationary Navigation Overlay Service
FDI	Fault Detection and Isolation
GBAS	Ground Based Augmentation System
GNSS	Global Navigation System
GPS	Global Positioning System
GRIL	GPS Receiver Interface Language
ICAO	International Civil Aviation Organisation
INS	Inertial Navigation System
JNS	Javad Navigation Systems
MSAS	Multi-transport Satellite Based Augmentation System
MT	Message Type
PDF	Probability Density Function
PL	Protection Level
PM	Post-Mission
PP	Post-Processing
PRN	Pseudo-Random Noise
QI	Quality Indicator
RAIM	Receiver Autonomous Integrity Monitoring
RF	Radio-Frequency
RMS	Root Mean Square
RNP	Required Navigation Performance
RT	Real Time
RTCM	Radio Technical Commission of Maritime services
RTK	Real Time Kinematic
SARP	Standards And Recommended Practices
SBAS	Space Based Augmentation System
SEP	Spherical Error Probable

SIS	Signal In Space
SNR	Signal-to-Noise Ratio
SQM	Signal Quality Monitoring
SV	Space Vehicle
TD	Triple-Difference
TOA	Time Of Alert
UERE	User Equivalent Range Error
UHF	Ultra High Frequency
VHF	Very High Frequency
WAAS	Wide Area Augmentation System

Chapter 1

Introduction

This chapter introduces the research domain and the main objectives of this master thesis. The adopted strategy for achieving the goals and the structure of the present report are presented.

1.1 Context

The lack of information on the reliability of the acquired data shortly or during the survey flight is one of the main problem of today's mapping system providers. Therefore, errors or unacceptable quality in the gathered data are often detected much later, when no more actions can be taken to improve the data quality. In airborne-mapping mission, the position of the carrier determined by one dual frequency GPS receiver is usually improved off-line by carrier-phase differential data using forward/backward processing of ambiguity determination/validation for one or more base stations. This implies that possible occurrences of local signal distortions affecting both the GNSS code and phase measurements become apparent only during the Post-Processing (PP) step. The remaining solutions for data quality assessment can therefore be resumed by flight repetition or acceptance of a serious final product quality degradation implying severe economical consequences.

1.2 Objectives of the thesis

New concepts for GPS data quality monitoring and assessment and their implementation into a flexible online monitoring tool need to be developed. Information on the reliability of GPS data in Real-Time (RT) allow to take actions during the flight like repetition of flight lines or direct identification of major problems. Several strategies will be pursued in order to improve the quality of GPS data and to provide a reliability information in RT or near RT. These strategies are:

- the monitoring of the carrier-phase quality by detecting cycle slips on raw measurements,

- RT GPS data quality assessment using WAAS/EGNOS/SBAS and RAIM equipped GPS receiver,
- evaluation of benefits using RTK-GPS on-board solution via radio communication channel and,
- evaluation of the GPS provided position and velocity accuracy measures, and identification of possible estimation improvements.

1.3 Methodology

1.3.1 Adopted approach

The first step of the thesis deals with the identification of relevant Quality Indicators (QI) and the design of an Airborne Laser Scanning (ALS) global quality check environment. The adopted methodology for achieving the latter separates the work in two approaches. The first approach is to develop algorithms based on the identified QI and the usually used integrity enhancement techniques like Receiver Autonomous Integrity Monitoring (RAIM) or Spatial Based Augmentation Systems (SBAS) like Wide Area Augmentation System (WAAS) or European Geostationary Navigation Overlay Service (EGNOS). These algorithms are then implemented in a Post-Mission (PM) quality check tool. The second approach consists in implementing the developed PM algorithms in a RT quality check tool, according to the results obtained by the PM tool within number of missions.

The second step is to test the performance of the tool by simulating past flights and comparing the detected problems with those obtained during the PP step. A particular attention will be given to flights that caused major problems on the GPS quality level.

The third step consists in analyzing the relevance of the GPS receiver provided position and velocity accuracy measures and in investigating if these measures could be improved. This will be used in order to improve the quality of the GPS stochastic model in the RT Kalman filtering step. Furthermore, the use of EGNOS corrected differential observations for improving GPS observation quality is also evaluated during this step.

Finally, a Real-Time-Kinematic (RTK)-GPS solution via radio communication channel will be designed and tested in order to evaluate its potential for obtaining direct georeferencing of the laser point cloud and its ability to supply integrity information.

1.3.2 Report structure

The present report is organized as follows. The next chapter deals with the integrity concept taken in the particular context of the airborne-mapping missions. The usually used QI in the literature are identified and the main integrity enhancement techniques (RAIM and WAAS/EGNOS) reported in this chapter. Chapter 3 presents the chosen QI and the performance of the tested cycle slip detection algorithms. A new global integrity check algorithm is also proposed and tested. The relevance of the GPS stochastic modeling by using receiver estimates as well as the result of the data quality assessment by means of EGNOS differential corrections are discussed in chapter 4. Chapter 5 deals with the potential of using an RTK-GPS solution and presents the first results obtained after a test flight above Sion. Finally, chapter 6 presents the final implementation of the developed PM and RT quality check tools as well as their performances on simulated survey flights.

Chapter 2

Integrity concept in airborne mapping

The basic concepts on which this thesis is based are defined in this chapter. The sense given to the integrity term placed in the particular context of airborne-mapping is exposed. Furthermore, currently used QI as well as integrity enhancement technologies are outlined and related to the objectives of the thesis. Finally, the concepts of accuracy and precision are defined and their importance for mapping missions outlined.

2.1 Current definition of integrity

For the aviation, safety is a critical issue. The International Civil Aviation Organisation (ICAO) has defined four parameters that encompasses the Required Navigation Performance (RNP[1]): accuracy, integrity, continuity and availability. These four parameters will be defined in order to understand the features of the navigation performance.

The *accuracy* is defined as (according to [22])

> *the position error that will be experienced by a user with a certain probability at any instant in time and at any location in the coverage area. In general, the probability is required to be 95%.*

The parameter directly linked to safety is *integrity* and is defined according to the ICAO GNSS Standards And Recommended Practices (SARPs) as

> *a measure of the trust which can be placed in the correctness of the information supplied by the total system. Integrity includes the ability of a system to provide timely and valid warnings to users (alerts).*

The *availability* is (according to [22])

---

[1] The RNP concept is statement of the navigation performance necessary for operation in all phases of flight developed by the ICAO.

> *the probability that a user is able to determine his position with the required accuracy and is able to monitor the integrity of his determined position at any instant in time and at any location in the coverage area.*

Finally, the *continuity* can be defined as (according to [22])

> *the probability that a user is able to determine his position with the required accuracy and is able to monitor the integrity of his determined position at any location in the coverage area over a minimum time interval applicable to the corresponding phase flight.*

Integrity requirements are generally specified in terms of three parameters with values fixed by governing institutions: the *alarm limit* (AL), the *time-to-alert* (TOA) and a probability of non-integrity (or missed) detection [3]. Moreover, the integrity is often specified by its inverse, *integrity risk*, that is related to the third parameter and defined according to the ICAO by *the probability of providing a signal that is out of tolerance without warning the user in a given period of time.* The AL parameter is *the error tolerance that should not be exceeded without issuing an alert to the user*, and represents therefore the largest error that results in a safe operation. The TOA parameter is *the maximum permitted time interval between the onset of a failure and an alert being issued by the user's receiver.* So, the error tolerance given in the definition of the integrity risk is the AL while the period of time is traduced by the TOA parameter. Institutions like the ICAO or the International Maritime Organisation fix values depending on specific applications and intended operations for the three parameters.

Note The concept of integrity is strongly related to the idea of *reliability* in the geodesy domain. The reliability of point coordinates in a geodesic network is related to the idea that a fault on a point's coordinates could be detected by mean of other (redundant) observations in the network. The difference between the two concepts lies in the fact that integrity implies an instantaneous dimension through the TOA parameter, and is therefore used in the navigation domain.

2.2 Meaning of integrity in the airborne mapping context

As seen in the previous section, the classical integrity concept is related to the ability of a system to provide timely warnings to users in periods where the system should not be used. The integrity problem is crucial for aviation since the user is traveling at high speeds and can quickly deviate from the flight path [11]. Integrity is not motivated by this safety dimension in the airborne-mapping context, but rather by the ability to provide informations on the reliability of the acquired GPS data. The knowledge of these informations is necessary to predict possible difficulties in the carrier-phase PP step induced by bad GPS signal quality as introduced in chapter 1. Identification of bad GPS observation quality and the supply of warnings at these epochs during the flight allow to make provision against difficulties in the ambiguity resolution during PP of the final solution, or even to avoid situations where no solution at all can be computed (for example due to poor satellite number). The GPS integrity is therefore derived from the quality of the signal which should be quantified. The next section deals with commonly used GPS QI as well as existing integrity enhancement techniques.

2.3 Identification of relevant quality indicators

2.3.1 Current quality indicators

There are two important aspects to the optimal processing of GPS observations. The first is the definition of the functional model through the design matrix, describing the mathematical relationship between the GPS observations and the unknown parameters, and the second is the stochastic model describing the statistics of the observations. The construction of the functional model by data differencing techniques enables the elimination of many GPS biases such as the atmospheric bias or the receiver and satellite clock biases. However, the data differencing doesn't eliminate some residual biases like cycle slips, receiver clock jumps, multipath, diffraction, or ionospheric scintillation. Such effects should therefore be correctly detected or otherwise handled at the data quality control stage either for RT or PP needs in order to attain a reliable positioning.

The effects of cycle slips and receiver clock jumps seriously affect the GPS observation quality and their detection and correction is crucial for reliability. If cycle slips and receiver clock can be easily captured either in the measurement or parameter domain due to their systematic characteristics, multipath and ionospheric scintillation are more difficult to eliminate since they are of quasi-random nature. The idea developed in [12] for handling such errors is to separate the systematic errors from the quasi-random ones and then to estimate the quasi-random errors after removing the systematic part in order the get more reliable results the least-squares sense. Moreover, many researchers like [13] or [6] have emphasised the relevance of using Signal-to-Noise Ratio (SNR) and satellite elevation as QI for GPS observations. The relationship between SNR or Carrier-to-Noise density ratio (C/N0), and multipath, which is a major concern in GPS positioning, has been investigated by several authors like [19] for example. [13] claims that C/N0 directly affects the precision of GPS observations and that it can be seen like a key parameter in analyzing receiver performance. Furthermore, [7] states that SNR data directly expresses the quality of the individual GPS phase values. Concerning the elevation indicator, [10] has demonstrated that satellite elevation angle and accuracy of GPS code observations are strongly correlated. GPS accuracy decreases with decreasing satellite elevation angle following an exponential function expressed as

$$y = a_0 + a_1 \cdot e^{-\epsilon/x_0} \tag{2.3.1}$$

where

y = RMS error
a_0, a_1, x_0 = coefficients dependent on the receiver brand and the observation type
ϵ = satellite elevation angle

It is also generally accepted that SNR is almost directly proportional to satellite elevation. Nevertheless, [12] shows that this relationship may not be true for high satellite elevations. He makes a comparative analysis between the use of satellite elevation and SNR and concludes that both can be used as QI but that they do not always reflect the reality. Furthermore, [16] states that RF interferences can surreptitiously degrade accuracy and thereby compromise system integrity. Since interferences can be related to SNR, the latter can be used to detect them and to minimize the integrity risk.

2.3.2 Integrity technologies

The aviation domain has devoted much effort to developing techniques to provide integrity for airborne use of GPS. The augmentation systems enable the improvement of the previously mentioned RNP attributes (accuracy, integrity, continuity and reliability) through integration of additional information. Several systems exist and are usually classified based on how the GNSS sensor receives this additional information. Three types of GNSS augmentation systems can be formed:

- Ground Based Augmentation System (GBAS),
- Aircraft Based Augmentation System (ABAS),
- Satellite Based Augmentation System (SBAS).

The GBAS are local Differential GPS systems (DGPS) that transmit differential corrections to the users. The corrections are computed by mean of some accurately surveyed ground stations, which take measurements concerning the GNSS. After the processing step, the corrections are directly sent to the users by mean of radio transmitters operating in the Very High Frequency (VHF) or Ultra High Frequency (UHF) bands. Other GBAS approaches are based on the use of pseudolites, which are ground-based pseudo-satellites that send GPS signals. By combining them with a classical DGPS reference station, the number of signals can be increased, inducing an assessment of the precision and integrity.

The ABAS compute the integrity information by mean of a RAIM function and/or additional navigation sensors operating via different principles than the GNSS. The latter are therefore not subject to the same sources of errors or interference. Such additional sensors may include automated celestial navigation systems, Inertial Navigation Systems (INS), or simple dead reckoning systems composed for example of gyro compasses and a distance measurement.

The SBAS is a system that supports wide-area or regional augmentation through the use of additional satellite-broadcast messages. Due to the size of the covered area, SBAS systems must send differential corrections based on spatial and temporal modelisation. Similarly to the GBAS, the corrections and the integrity information are computed by mean of ground based stations and then sent via geostationary satellites to the users. The user specific corrections are computed by interpolation functions. Three various SBAS are implemented:

- WAAS is the american SBAS,
- Multi-transport Satellite Based Augmentation System (MSAS) is the japanese SBAS,
- EGNOS is the european SBAS.

The main informations present in the EGNOS signal are related to the integrity and the precision of the user's position. EGNOS provides additional GPS signals and contributes to the improvement of the constellation. Furthermore, the corrections messages sent to the user enable to reduce residual biases and errors. Finally, the integrity information is given by a standard-deviation that enables the calculation of the user Protection Level (PL). Details on the WAAS/EGNOS/SBAS, i.e. the meaning of PL and the processing of the integrity information can be found in [3].

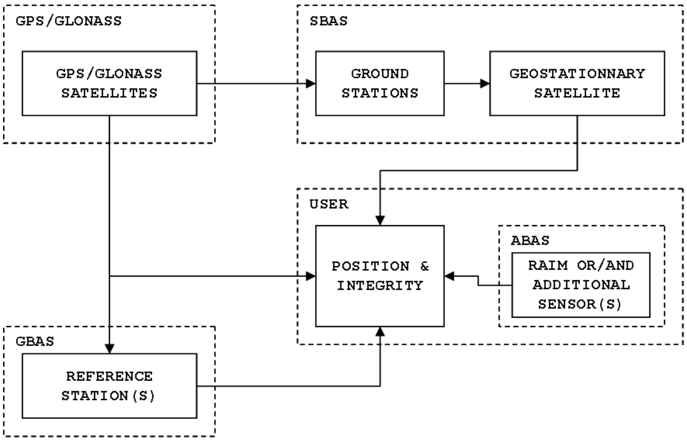

Figure 2.1: Principle of the different types of augmentation systems.

2.3.3 Relevant quality indicators in airborne mapping

The main interest of implementing an online quality-monitoring tool in the airborne-mapping context is the detection of the periods where the ambiguities cannot be resolved by using forward/backward carrier-phase PP. Furthermore, conditions where the number of satellites is very low should be known by the user, especially in the case where the mapping flight is performed in mountainous areas causing variable signal obstructions.

Usually used QI related to the code measurements have been described in the previous section. The most important are those giving an indication on the carrier-phase quality. Thus the detection of cycle slips[2] occurring on the signals is of great importance. Furthermore, the carrier tracking loop is always the weak link in a standalone GPS receiver and its threshold characterizes the receiver performance [11]. So, the nature of the carrier tracking loop output can form a good phase signal quality factor.

One of the main objective of this thesis is to check the advantages of using RAIM function not only to assess GPS data quality, but also to provide a relevant integrity information for the airborne-mapping missions. The advantage of using RAIM is that it doesn't depend on external informations like it is the case for WAAS/EGNOS. The provided integrity warnings can be used as indicator for bad signal and satellite constellation quality. In addition, epochs affected by low satellite number are immediately indicated by RAIM.

The use of the informations provided by WAAS/EGNOS could also be advantageous. While the application of the differential corrections in the computed positions is possible with receivers having WAAS/EGNOS capabilities, the RT derivation of the PL is specific to aircraft GPS receivers. Thus the use of this technology in the airborne-mapping could be advantageous for improving the GPS data quality and the RT estimation of the position and velocity accuracy.

Finally, the use of RTK-GPS positioning could give direct informations on the ability to resolve the ambiguities, and perhaps even provide a definitive navigation solution for georeferencing the laser point cloud. The basic RTK-GPS principles will be explained in chapter 5.

---

[2] The notion of cycle slip will be explained in chapter 3.

2.4 Real-time position and velocity error estimation

The estimation of the position and velocity accuracy is also of great importance for the navigation performance. Accuracy and precision are often used to describe how good is the position acquired by the receiver. It is important to understand the difference between the two concepts. The term *accuracy* is used to express the degree of closeness of the obtained solution, to the true but unknown value. The term *precision*, however, is used to describe the degree of closeness of repeated measurements of the same quantity to each other. That means that in absence of systematic errors, precision and accuracy would be equivalent. The relevance of the accuracy measures provided by the receiver is especially important in the airborne-mapping context since the GPS observations are integrated with the inertial data through Kalman filtering. The latter requires a relevant GPS stochastic model that is actually based on the receiver position and velocity accuracy estimations.

2.5 Development strategy

The adopted strategy for the development of new concepts for GPS data quality assessment is summarized in figure 2.2. The idea of this thesis is to use the identified QI in order to provide a quality information for each position and at any time during the airborne-mapping mission. The used QI could also be supported by the RAIM function and WAAS/EGNOS differential corrections for improving the quality of the positioning. Finally, one of the purpose of this thesis is to check if these tools could be used to improve the receiver position and velocity accuracy measures. This could be of great importance for the definition of a relevant stochastic model that is used in the RT Kalman filter implemented in the actual processing environment[3].

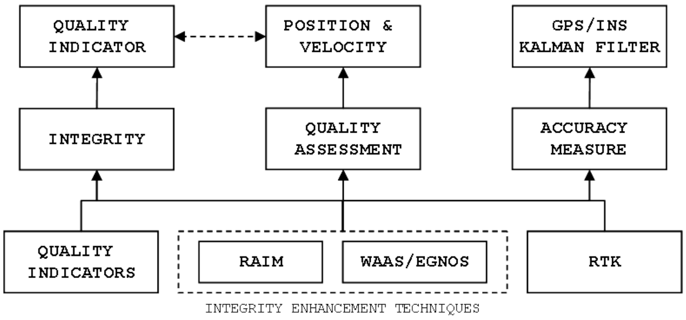

Figure 2.2: Global development strategy adopted in the present thesis.

---

[3] Details on this environment under development at EPFL are given in chapter ??

Chapter 3

GPS integrity indicators

The main purpose of the thesis is to develop and implement algorithms capable performing both PM and RT quality check. This chapter describes and tests the proposed algorithms and provides an analysis of the obtained results. Their performance will be central for the final PM and RT quality check tool architectures. In order to understand the concepts on which the algorithms are based, some basics about positioning by GPS will be presented.

3.1 GPS observables

The basic observations of GPS are code pseudoranges, carrier phases and Doppler measurements. The related concepts will be briefly described in this section. The equations of this section are derived from [25] where further informations can be found.

3.1.1 Code pseudorange

The code pseudorange is a measure of the distance between the receiver's antenna and the satellite. It is computed by measuring the signal transmitting time from the satellite to the receiver by analyzing maximum correlation between the receiver code and the GPS signal. The measured pseudorange will be different from the geometric distance between the receiver and the satellite due to the errors of the receiver and satellite clocks and the influence of the signal transmitting mediums. The simplified pseudorange model can be expressed by

$$R_j = \rho_j - (\delta t_r - \delta t_s)c + \delta_{ion} + \delta_{tro} + \delta_{tide} + \delta_{rel} + \varepsilon_c \tag{3.1.1}$$

where

R_j = pseudorange measure of satellite j
ρ_j = geometric distance between the receiver and the satellite j
t_r = GPS signal reception time of the receiver
t_s = GPS emission time of the satellite
δt_r, δt_s = clock error of the receiver and the satellite
δ_{ion} = ionospheric effects

δ_{tro} = tropospheric effects
δ_{tide} = earth tide and ocean loading tide effects
δ_{rel} = relativistic effects
ε_c = remaining errors
c = speed of light

3.1.2 Carrier phase measurements

The carrier-phase is a measure of the received satellite signal's phase relative to the carrier-phase generated by the receiver at the reception time. The measure is made by shifting the phase generated by the receiver to track the received phase. This implies that the full number of carrier waves comprised between the receiver and the satellite is not known at the initial signal acquisition. So, measuring carrier-phase means measuring the fractional phase and keeping track of changes in cycles. The ambiguous integer number of cycles in the carrier-phase measurement is known under the term of *ambiguity*. The initial observation has correct fractional phase and an arbitrary integer counter set at the start epoch and that will be corrected by an ambiguity resolution procedure [25]. The simplified carrier-phase model where all terms have units of length instead of cycles is given by

$$\lambda_i \Phi_j = \rho_j - (\delta t_r - \delta t_s)c + \lambda_i N_j - \delta_{ion} + \delta_{tro} + \delta_{tide} + \delta_{rel} + \varepsilon_p \tag{3.1.2}$$

where

λ_i = wavelength of frequency i
Φ_j = measured phase of satellite j
N_j = ambiguity related to satellite j
ε_p = remaining errors

3.1.3 Doppler measurements

The Doppler effect is a frequency shift of the signal caused by a relative motion of the emitter (satellite) and the receiver. By considering that the emitted signal has a nominal frequency f_i, the expression of the radial velocity of the emitter related to the receiver, noted $\mathbf{V}_{\rho_j}$, is formed by

$$\mathbf{V}_{\rho_j} = \mathbf{V} \cdot \mathbf{U}_{\rho_j} = |\mathbf{V}|\, cos(\alpha) \tag{3.1.3}$$

where

$\mathbf{V}$ = velocity vector of the emitter related to the receiver
$\mathbf{U}_{\rho_j}$ = identity vector in the direction from the receiver to the emitter
α = projection angle of the vector $\mathbf{V}$ to $\mathbf{U}_{\rho_j}$

The received signal will have a frequency f_r of

$$f_r = f_i \left(1 + \frac{|\mathbf{V}_{\rho_j}|}{c}\right)^{-1} \approx f_i \left(1 - \frac{|\mathbf{V}_{\rho_j}|}{c}\right) \tag{3.1.4}$$

It can be demonstrated [25] that the frequency shift f_d is given by

$$f_d = f_i - f_r \approx f_i \frac{|\mathbf{V}_{\rho_j}|}{c} = \frac{|\mathbf{V}_{\rho_j}|}{\lambda_i} = \frac{d\rho_j}{\lambda_i dt} \tag{3.1.5}$$

The Doppler count, noted D, represents the integration of the frequency shift over a time interval. If this interval is small enough, D will be the same as the instantaneous frequency shift and can so be written by

$$D = \frac{d\rho_j}{\lambda_i dt} \tag{3.1.6}$$

In facts, the receiver will predict D in order to predict the phase change, and then the phase change is compared with the measured value to obtain the precise value of f_d. In other words, the Doppler shift is derived from the carrier phase measurements but is considered like an independent observable and a measure of the instantaneous range rate. The model is given by

$$D = \frac{d\rho_j}{\lambda_i dt} - f_i \frac{d(\delta t_r - \delta t_s)}{dt} + \varepsilon_d \tag{3.1.7}$$

where

ε_d = remaining errors

This result is obtained by considering that $d\rho_j/(\lambda_i dt)$ is the same as $d\Phi_j/dt$.

3.2 Cycle slip detection algorithms

The use of carrier-phase measurements for positioning is submitted to an ambiguity problem which has to be solved. If a loss of lock of the signal occurs, the ambiguity resolution, which is a time and computation expensive task, has to be restarted again. Such a phenomenon is called *cycle slip* and can occur in cases where tracking is interrupted by shadowing, weak satellite signal (low SNR or C/N0) or receiver software failure implying incorrect signal processing. Cycle slips, i.e. integer ambiguity losses, imply that the adjacent carrier-phase observation jumps by an integer number of cycles and that the integer ambiguity parameter should be calculated again. Numerous researchers are interested in cycle slip detection and correction methods in order to avoid new ambiguity resolution. Several methods for detecting and correcting cycle slips can be found in the literature. [12] presents methods based on dual-frequency carrier-phase observations and by forming double/triple differenced (DD/TD) phase observations. Nevertheless, the use of DD and TD observations are less interesting for RT detection applications because of the unavailability of the base observations. Other approaches described in [9] use linear combinations of dual-frequency phase observations and code pseudoranges. For example, [5] uses the Melbourne-Wübbena combination which combines L1/L2 carrier-phases and code pseudoranges for both frequencies in order to eliminate the effect of the ionosphere, the clocks, the geometry and the troposphere. [15] uses changes of the residuals between the Doppler measurement and a calculated Doppler based on least-squares solution to detect any cycle slip and repair the jumps by mean of inertial measurements. Nevertheless, [25] summaries several methods for detecting cycle slips that are applicable for RT purposes

- time-differential phases,

- phase-phase ionospheric residual,
- Doppler integration,
- time derivative of the ionospheric delay and
- phase-code comparison.

These methods will be implemented and tested by comparing their results with the one obtained by *GrafNav* PP software. All the implemented algorithms have been evaluated by applying them on GPS data samples acquired during survey flights. In the following sections, only one data sample is taken as an illustration. The reference detection result provided by *GrafNav* is shown in appendix F.

Note A particular attention is given on the detection of cycle slips on L2 phase signal because the numerous airborne-mapping missions show that in periods where the L2 signal is badly conditioned, problems in the carrier-phase post-processing step can appear. Furthermore, high density of cycle slips on the L1 phase often involves bad L2 phase quality, too. The graphic in figure 3.2 presents the number of epochs where either only one carrier or both were affected. It can be seen that cycle slip presence on L1 is often characterized by cycle slip presence on L2. Furthermore, the higher cycle slip occurrence on the L2 phase comes from the higher sensitivity of the L2 carrier-phase due to lower transmitting power and absence of C/A code on this frequency. The cycle slips were detected by using time derivative of ionospheric delay (see section 3.2.4) and L2 phase lock time analysis for L1 and L2 carrier phase, respectively. The following sections will present the different implemented algorithms and their performances.

3.2.1 Phase lock time analysis

The probably easiest method for detecting bad phase quality is to analyze the availability of the phase signal acquired by the phase tracking loop of the receiver. By decoding the receiver phase signal, the obtained output is corrupted in cases where the tracking loop hasn't locked the phase. The assumption of cycle slip presence can be made in such conditions. The test on

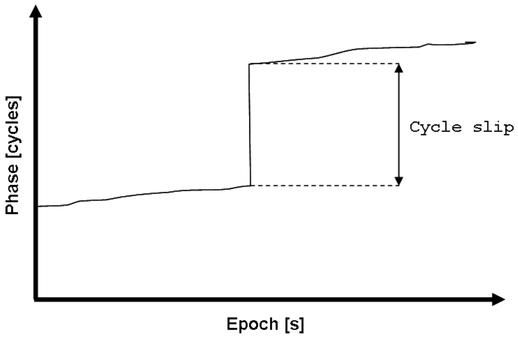

Figure 3.1: Cycle slip occurrence induces a jump in the carrier phase measurement. After such an epoch, the ambiguity has a different value than before.

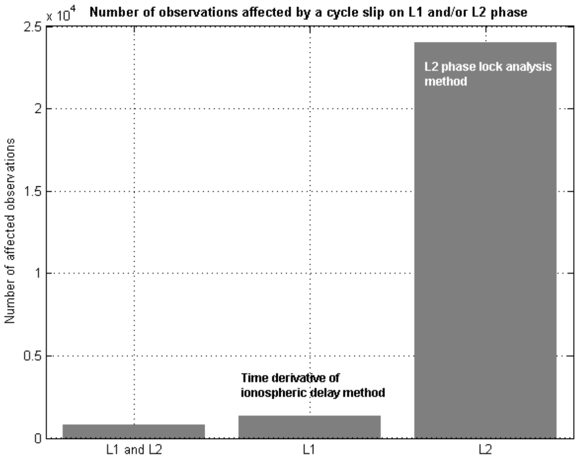

Figure 3.2: Number of epochs that were affected by cycle slips. The first bar corresponds to the number of epochs were both L1 and L2 are affected while the two others represent epochs where only L1 (second bar) or only L2 (third bar) carrier-phase is affected.

the nature of the receiver phase measurement has been implemented in the decoding step and the obtained results have been compared with the solution obtained by the *GrafNav* software[1]. An example of obtained results for a given survey flight is shown in figure 3.3. The comparison

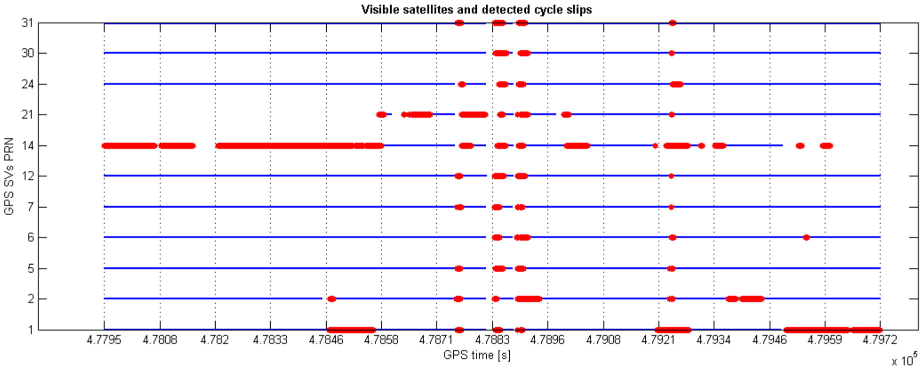

Figure 3.3: Result of cycle slip detection on L2 carrier-phase by analyzing if the phase was locked or not by the receiver's phase tracking loop. The detected cycle slips are shown in red.

with the *GrafNav* output shows that the results obtained by this mean are identical. This fact was observed on all the analyzed samples. However, applying the test on L1 signal gives less good results because L1 carrier-phase is much less sensitive to perturbations than L2 carrier. The cycle slip detection on L1 will therefore be more difficult to perform and requires other methods described in the following sections.

---

[1] *GrafNav* uses lock time informations and Doppler measurements for detecting cycle slips.

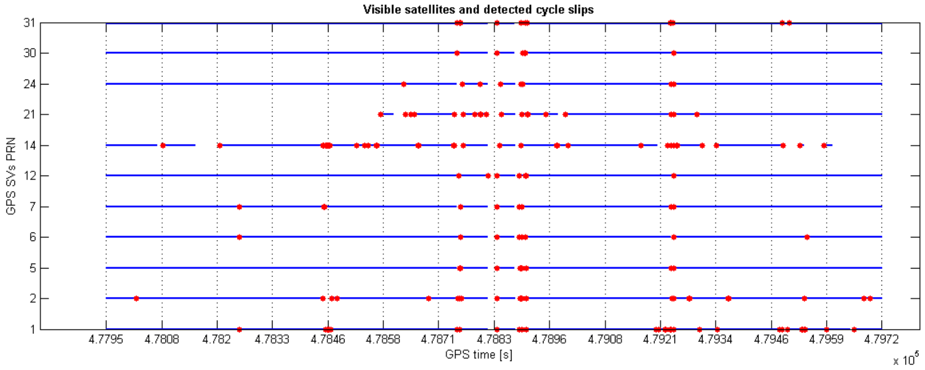

Figure 3.4: Result of cycle slip detection on L1 using Doppler integration. The detected cycle slips are shown in red.

3.2.2 Doppler integration

The integration of the instantaneous Doppler given in equation 3.1.7 can be formed as

$$\lambda_j \int_{t_{j-1}}^{t_j} D_j dt = \Delta_t \rho - \Delta_t(\delta t_r - \delta t_s)c + \varepsilon_d \tag{3.2.1}$$

where

Δ_t = numerical time difference operator

By applying the operator Δ_t on equations 3.1.1 and 3.1.2, the latter can be written as

$$\Delta_t R_j = \Delta_t \rho - \Delta_t(\delta t_r - \delta t_s)c + \varepsilon_c \tag{3.2.2}$$

$$\lambda_j \Delta_t \Phi_j = \Delta_t \rho - \Delta_t(\delta t_r - \delta t_s)c + \lambda_j \Delta_t N_j + \varepsilon_p \tag{3.2.3}$$

Differencing equation 3.2.3 with equation 3.2.1 leads to

$$\Delta_t N_j = \Delta_t \Phi_j - \int_{t_{j-1}}^{t_j} D_j dt + \varepsilon \tag{3.2.4}$$

where

$\Delta_t N_j$ = time difference of ambiguity

The integrated Doppler is theoretically speaking a good method for cycle slip detection [25]. The Doppler integration was processed for L1 carrier-phase frequency by means of numerical integration using the trapezoidal rule. The algorithm gives good results in cases where several adjacent cycle slips were detected by *GrafNav*. An example of result obtained with this method is presented in figure 3.4. Groups of adjacent cycle slips as well as a lot of isolated cycle slips are detected according to the *GrafNav* processing. The graphic on figure 3.5 shows the time difference of ambiguities calculated by means of Doppler integration. The time differences are less affected by noise because no code ranges are used. This allows the use of a single

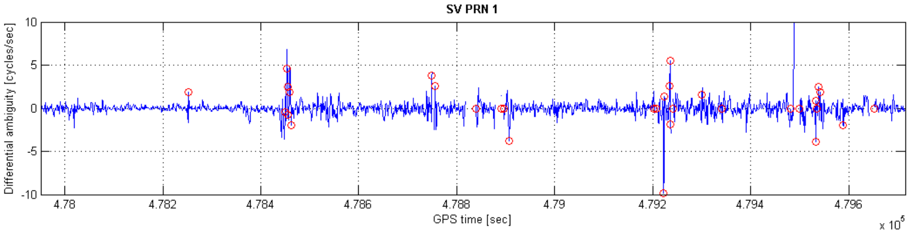

Figure 3.5: Time difference of ambiguity computed by Doppler integration for one PRN and detected cycle slips (red circles).

decision threshold. The raise of the noise after time 478'440 [GPS s] is due the engine start, i.e. rotor rotation beginning. This demonstrates that GPS data that were acquired in a noisy environment are much more difficult to process. The figure 3.6 shows the autocorrelation functions of the time differences ambiguities of tree SVs. The mean of the $\Delta_t N_j$ signal is approximately zero and the ε_d term can be modeled like a white noise process, in accord with equation 3.2.4. The numerical integration step could be improved by first fitting the Doppler data with a polynomial of suitable order, and then integrating within the desired time interval [25]. However, the trapezoidal rule is sufficient for quality check purposes and less expensive in terms of time computation for RT applications.

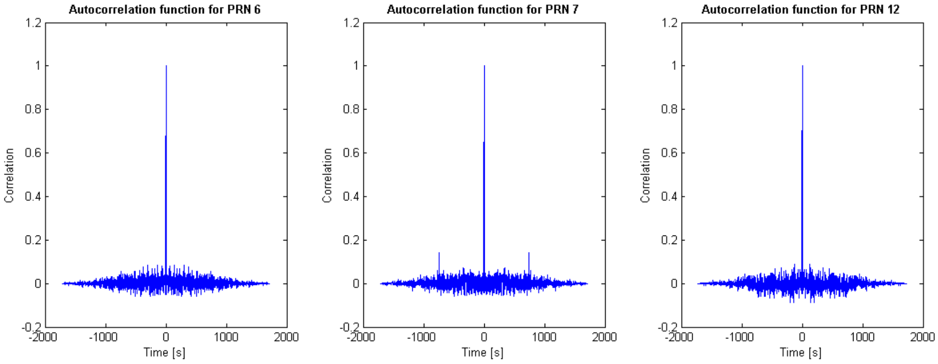

Figure 3.6: Autocorrelation functions of time difference of ambiguity computed by Doppler integration for three visible SVs.

3.2.3 Phase-code comparison

By comparing the equation 3.2.2 with equation 3.2.3, the following equation can be formed

$$\Delta_t R_j = \lambda_j \Delta_t \Phi_j - \lambda_j \Delta_t N_j + \varepsilon \tag{3.2.5}$$

Equation 3.2.5 is originally used for smoothing the code survey by phase in cases where no cycle slips happen. The time difference of the ambiguity $\Delta_t N_j$, should then be zero. Because the code range is affected by a much higher noise level than that of the phase, the $\Delta_t N_j$

value will not be exactly zero, allowing only the detection of big cycle slips. A fixed decision threshold was set by comparing the detected cycle slips with the *GrafNav* solution. The threshold was then validated by testing the algorithm on several other GPS data samples. An example of result is presented in figure 3.7 where cycle slips are marked with red dots for each visible SV. With respect to the PP solution, the detected cycle slip number is too low and this was observed for all the flight data samples that were analyzed. This is essentially due to the intrinsic nature of equation 3.2.5 and to the fact that helicopter GPS data are especially noisy. The graphic on figure 3.8 shows the time differenced ambiguities for one visible satellite. The high noise level of the code range, represented by the ε value in equation 3.2.5, affects the values which should be near to zero. The red circles indicate the presence of cycle slips as well as signal receiver tracking losses where cycle slips are presumed.

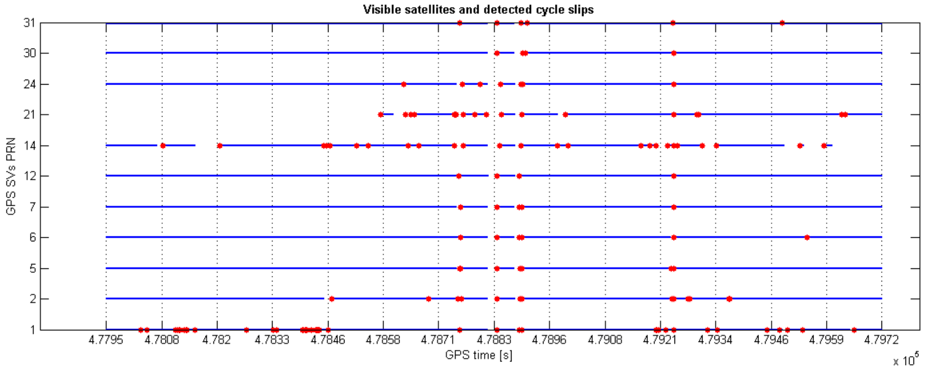

Figure 3.7: Result of cycle slip detection on L1 using the phase-code comparison formula. The detected cycle slips are shown in red.

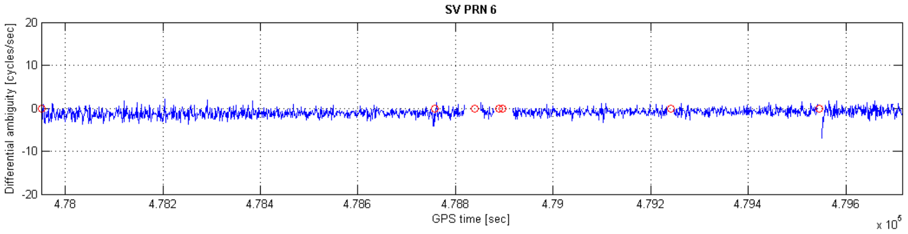

Figure 3.8: Time difference of the ambiguity computed by phase-code comparison for one PRN and detected cycle slips (red circles).

3.2.4 Ionospheric delay time derivative

The time derivative of the ionospheric delay can be used to detect jumps in the phase measurements. This is the algorithm used in the *TEQC* quality check tool and detailed informations on the following theory can be found in [4]. Comparing equation 3.1.1 with equation 3.1.2 reveals that the sign of the $\delta_{ion}(i)$ changes. This is due to the ionosphere being dispersive at GPS frequencies meaning that the carrier-phase measurements travel at the phase velocity (a phase advance) and that the pseudorange measurements travel at the group velocity (a group delay). They can be modeled by considering the index of refraction for the phase and group propagation in the ionosphere noted $n_{ph,i}$ and $n_{gr,i}$, respectively. These terms are approximated by the first-order polynoms

$$n_{ph,i} \cong 1 + \frac{c_2}{f_i^2} \tag{3.2.6}$$

$$n_{gr,i} \cong 1 - \frac{c_2}{f_i^2} \tag{3.2.7}$$

where

$n_{ph,i}$ = index of refraction for the phase of frequency i
$n_{gr,i}$ = index of refraction for the group velocity of frequency i
c_2 = coefficient proportional to the electron density

and

$$\alpha \equiv \frac{f_1^2}{f_2^2} \tag{3.2.8}$$

$$f_2^2 \delta_{ion}(1) = f_1^2 \delta_{ion}(2) \tag{3.2.9}$$

By starting with $\Phi_1 - \Phi_2$ and assuming that the paths for the two frequencies i are the same through the atmosphere, the relation

$$\delta_{ion}(1) + \frac{1}{\alpha - 1}\left(\lambda_1 N_1 - \lambda_2 N_2 + \delta_{mul}(1) - \delta_{mul}(2)\right) = \frac{1}{\alpha - 1}(\Phi_1 - \Phi_2) \tag{3.2.10}$$

where

$\delta_{mul}(i)$ = phase multipath for frequency i

can be written. The time derivative of the ionospheric delay can then be formed as

$$I_{(2)}OD = \frac{\alpha}{\alpha - 1} \frac{\Delta_t(\Phi_1 - \Phi_2)}{\Delta t} \tag{3.2.11}$$

This value can be computed at each epoch and then be compared with a defined threshold. The results of cycle slip detection using ionospheric variations are presented in figure 3.9. Satellite motion, ionospheric time variation and motion of the receiver antenna induce a minimum amount of variability that is fixed, according to [4], at 400 [cm/min] (see figure 3.10). That means that if the time difference goes beyond this value, cycle slip presence can be supposed. The value of this threshold can vary with ionospheric variations. Figure 3.10 shows $I_{(2)}OD$ values for one PRN. The red circles represent the detected cycle slips and the L2 phase tracking losses.

3.2.5 Results and discussion

By applying the presented algorithms on six data samples, it appears that the solution provided by the ionospheric delay time derivative and the Doppler integration give the best results for

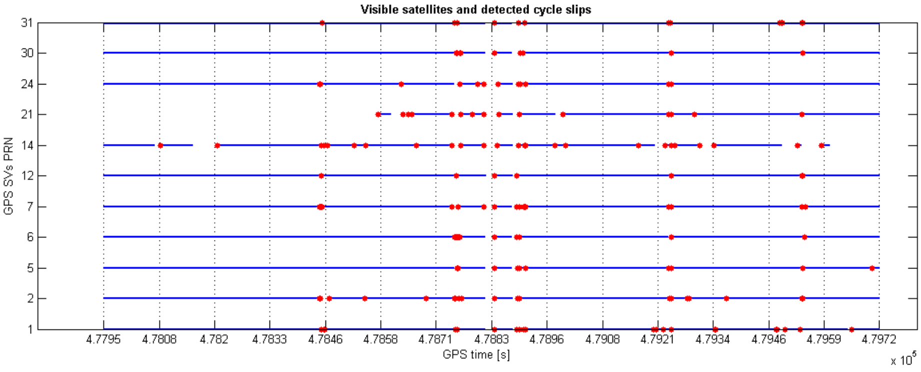

Figure 3.9: Result of cycle slip detection using time derivative of ionospheric delay. The detected cycle slips are indicated in red.

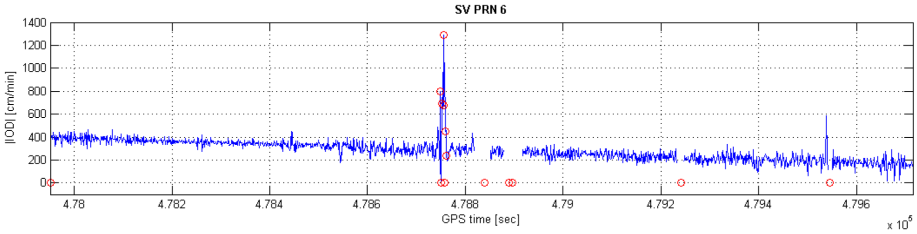

Figure 3.10: Time differenced ionospheric delay for one PRN and detected cycle slips (red circles).

L1 cycle slip detection. However, it was observed that the sensitivity of the decision threshold in the Doppler integration algorithm is a bit higher. Anyway, the difference in the results of detection is not significant enough to qualify an algorithm as better than the other. By analyzing PP solutions of different samples, it can be seen that a large cycle slip density on L2 carrier-phase induces a high probability of cycle slip presence on L1 carrier-phase in the same period. In a context of RT quality check, only the worst scenario is of importance and the limitation on L2 signal analysis is therefore relevant. In addition, L2 cycle slips can simply be detected by evaluating if L2 carrier was locked by the phase tracking loop, making it the ideal method for RT applications.

3.3 Interference detection algorithm

3.3.1 Interference sources

GPS receivers are vulnerable to Radio-Frequency (RF) interference. The latter can result in degraded navigation accuracy or complete loss of signal tracking [11]. RF interference detection is of particular interest in the airborne-mapping context since avionic equipments, rotor rotation and cellular phones constitute potential interference sources that degrade satellite signals. There are several types of RF interference that can be summarized in table 3.1. [16]

presents a receiver autonomous interference detection algorithm based on low-level or raw receiver measurements. Thresholds are computed by means of receiver measurements like correlator output power, variance of correlator output power, carrier-phase vacillation and analog-to-digital converter. But many researchers claim that the precision of the receiver's pseudorange and carrier-phase observation is largely influenced by the C/N0. The latter describes the ratio of the power level of the signal carrier to the noise level. Typical values for nominal receivers are comprised in the 30 to 60 [dB*Hz] range. RF interferences will have effects on code correlation and loop filtering functions by reducing the C/N0 of all the GPS signals. In other words, they have the same effect as signal blockage, foliage attenuation, ionospheric scintillation and multipath, which are all factors that reduce the effective C/N0 of the GPS signals. Furthermore, many authors like [13] claim that there is a strong relationship between multipath and C/N0 or SNR, implying that C/N0 values directly affect the precision of GPS observations [18]. For all these reasons, it is relevant to use C/N0 values to detect possible interferences since signal power is the basic measure of its quality.

3.3.2 Proposed interference detection algorithm

An RF interference detection algorithm based on receiver C/N0 signal has been tested and implemented. The algorithm performs two tests. The first test computes continuously the standard deviation of the C/N0 time series as well as the averaged C/N0 value in a buffer of fixed size. By default, the window size has been set to 15 observations. The difference

Type	**Typical sources**
Wideband-Gaussian	Intentional noise jammers
Wideband phase/frequency modulation	Television transmitter's harmonic or near-band microwave link transmitters overcoming front-end filter of GPS receiver
Wideband-spread spectrum	Intentional spread spectrum jammers or near-field of pseudolites
Wideband-pulse	Radar transmitters
Narrowband phase/frequency modulation	AM stations transmitter's harmonic or CB transmitter's harmonic
Narrowband-swept continuous wave	Intention CW jammers or FM stations transmitter's harmonics
Narrowband-continuous wave	Intentional CW jammers or near-band unmodulated transmitter's carriers

Table 3.1: Types of RF interference and typical sources (from [11])

between the local mean and the detected minimum C/N0 in the window range is compared with the standard deviation multiplied by a coefficient K. The test is expressed as

$$\overline{cn_0}^{(buf)} - \min\left[cn_0^{(buf)}\right] > K \cdot \sigma \tag{3.3.1}$$

where

$\overline{cn_0}^{(buf)}$ = mean of C/N0 in the buffer window
K = coefficient
σ = global C/N0 time series standard-deviation

The coefficient K is selected as 3. This value is based on empirical adjustments. If the left term of equation 3.3.1 is above the right term, the presence of an interference can be presumed.

The second performed test is to check how many signals have their C/N0 value below a single absolute threshold. This test is of particular interest in RT quality check since RF interferences caused by avionic equipments, antenna connection default or due to the particular environment of helicopter flights will significantly decrease the C/N0 value of all satellite signals. Typical C/N0 thresholds are ranged between 20 and 30 [dB*Hz] according to the model given in [16].

3.3.3 Results and discussion

The algorithm was first tested by applying interferences caused by *Bluetooth* signals near a static receiver antenna. The algorithm was able to detect precisely the epochs were the perturbations have been applied (figure 3.11). Nevertheless, GPS observations coming from airborne-mapping missions are much more affected by noise and possible interferences are more difficult to detect. A particular characteristic of helicopter GPS data is the effect of the rotor on C/N0 values. The rotor rotation induces a decrease of the C/N0 values of about 10 - 15 [dB*Hz] depending mainly on the satellite elevation angle. The efficiency of the algorithm for such signals is shown in figure 3.12. The algorithm validates the detection only

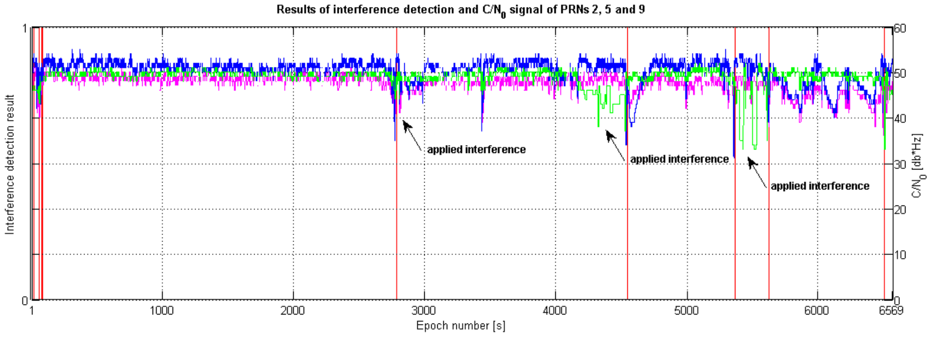

Figure 3.11: Results provided by the interference detection algorithm (red bars). The three applied interferences have been detected at the epochs where several C/N0 signals decrease. The three lines (blue, green and magenta) represent C/N0 values for three satellites.

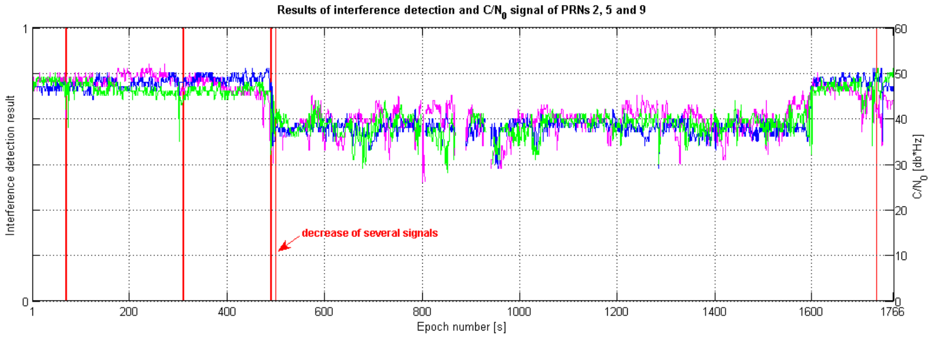

Figure 3.12: Results provided by the interference detection algorithm for a survey flight (red bars). The C/N0 decrease caused by the rotor rotation is clearly visible.

in cases where less than five satellites have their C/N0 signal above the threshold. That is, if only a few satellites are affected by a C/N0 decrease, the algorithm won't detect it like an interference since only the worst scenario is of interest in a quality check. The C/N0 decrease due to rotor start was optimally detected and the other detected interferences were also confirmed by global C/N0 decreasing. That is, the main goal of such an algorithm is fulfilled since only significant C/N0 decreases affecting a large number of satellites must be announced. Nevertheless, the high sensitivity of the results on parameter K and on the buffer size represent the main weakness of the method and could involve high false alarm rates. For these reasons, the given results are particularly interesting for PM quality check where more interpretation time is possible but could seriously affect the reliability of the RT quality check. Furthermore, important interferences that could occur during the flight can be detected by performing the single threshold test (second test). The use of a fixed threshold despite the fact that the C/N0 signal depends mainly on satellite elevation angle is also motivated by the interpretation of figure 3.13. Eight GPS data samples provided by survey flights have been used in order to isolate all obtained C/N0 values for a given satellite elevation angle. For each sample specific to an angle, the median value was calculated (indicated in red in figure 3.13). The tendency of having higher C/N0 values when the elevation angle increases is visible. Nevertheless, the median value for each elevation angle tends to be nearly constant. So, in the case of an interference all C/N0 values will decrease and only those which are below a certain threshold will be problematic. These considerations motivate for the choice of a single threshold test for RT interference detection.

3.4 Proposed integrity check algorithm based on RAIM and cycle slip detection

One of the main purpose of this thesis is to check if the use of RAIM could be relevant in the context of airborne-mapping integrity.

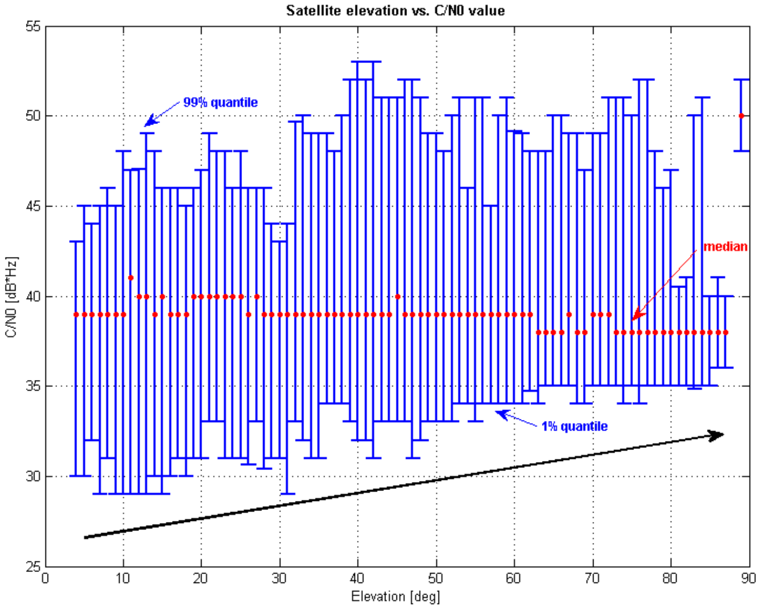

Figure 3.13: Relation between satellite elevation and C/N0 values. The red dots represent the median of all the obtained C/N0 values for the given elevation. The upper and lower bound represent the 99% and 1% empirical quantile respectively.

3.4.1 Use of RAIM function

The related detailed theory on which RAIM is based is treated in [11]. Only the basic principles will be described in this section.

RAIM is a receiver based, i.e. independent from external integrity information, augmentation system using redundant observations to perform a consistency check. It allows to detect an anomaly and to remove the faulty satellite from the navigation solution by identifying which satellite is problematic. This procedure is known as *Fault Detection and Isolation* (FDI). Before carrying out this test, a first test is needed in order to determine if the conditions exist to execute a RAIM calculation (RAIM *availability test*). Only a positive outcome of this test will conduct to the execution of the second test.

Considering that RAIM requires a minimum of five satellites in order to perform fault detection and a minimum of six for fault isolation/exclusion[2], and that the RAIM availability test depends on the geometric matrix $\mathbf{H}$ necessary to compute the PL, the RAIM availability test will give precious informations about the state/quality of the constellation. Furthermore, if not enough satellites are visible or in presence of poor measurements, RAIM will be turned off, giving an information on the code quality and an insufficient number of visible satellites. These important informations can be used in the quality check stage in order to get informations on the constellation and receiver solution quality. It will be demonstrated that system integrity information provided by RAIM, i.e detection of satellite failure or measurement error, can

---

[2] In the case where only one satellite is affected by a failure at a time.

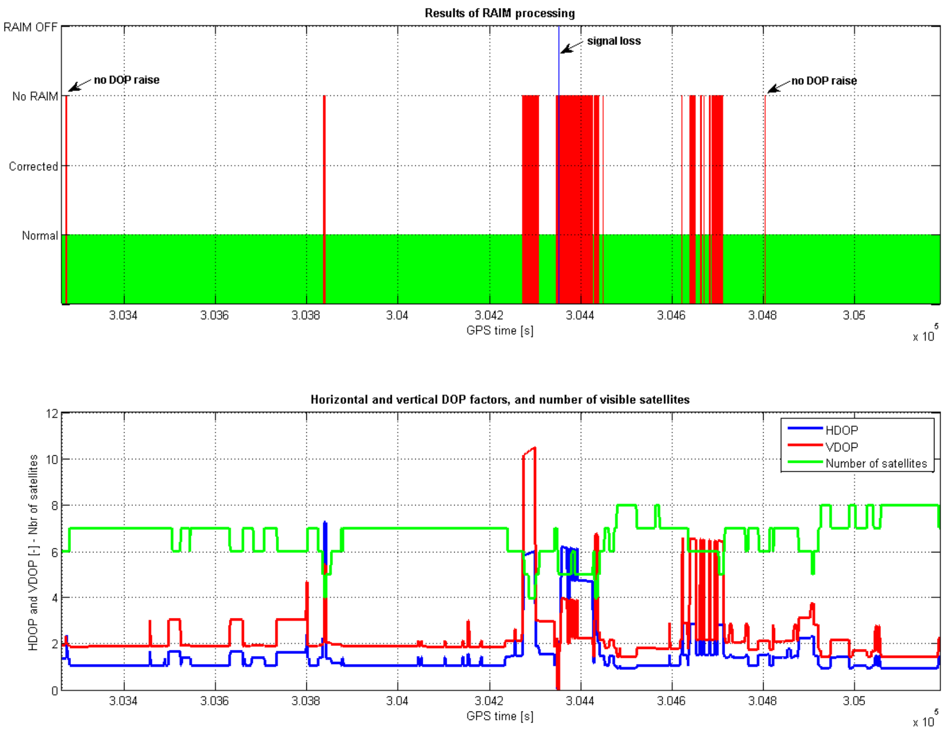

Figure 3.14: Results of RAIM processing (above) and comparison with horizontal (blue) and vertical (red) DOP factors and number of visible satellites (green).

be used in order to give an information on the quality of the signal and so indirectly on the chances to resolve the ambiguities in carrier-phase PP. The informations brought by the RAIM algorithm cover a large number of factors including quality of the constellation geometry, measurement quality and signal losses. Figure 3.14 shows RAIM processing results obtained for kinematic ground observations and their relationship with DOP factors and number of visible satellites. The red periods in the first graphic indicate availability test failures while the blue ones represent periods where RAIM was turned off. Availability test failures are mainly related to bad constellation geometry conditions since the DOP factors are often high during these periods. But poor measurements are also translated as a RAIM unavailability since two periods are critical despite good constellation conditions. The period where RAIM is turned off is due to signal loss. Furthermore, the alarm limit (AL) is the only parameter of the algorithm and could influence the sensitivity of the availability test and the FDI procedure. For the performed tests, the AL parameter was set to 556.6 [m] used for non-precision purposes[3].

---

[3] Informations on the role of the AL parameter in the algorithm can be found in [11].

3.4.2 Combining RAIM and L2 phase lock time analysis

Considering these results obtained for ground acquired data, it will now be investigated if RAIM processing results can be associated with informations on phase quality for detecting periods where the ambiguities are difficult to resolve in PP.

Ambiguity resolution is largely dependent on signal quality and particularly on satellite number and phase quality. In order to develop an efficient Signal Quality Monitoring (SQM) algorithm able to detect periods where ambiguities will be difficult to resolve, a kinematic GPS ground observation data sample is analyzed. The final solution was computed by mean of phase PP. Periods affected by bad measurement quality involve difficulties to resolve correctly the ambiguities. The figure 3.15 shows the ambiguity resolution status for the considered data sample. The red periods are those where the ambiguities could not be resolved and should be detected by the SQM algorithm. The first graphic in figure 3.16 shows the results of RAIM processing for the acquired observations. The second graphic presents the number of satellites that are not affected by cycle slips on L1 and L2 phase and the true horizontal and vertical errors obtained by computing the unsigned difference between the code solution and the PP solution. It is visible that periods where RAIM was turned off or not available correspond all to zones where the ambiguities could not be resolved. Furthermore, if the number of satellites that have not tracked L2 phase is variable after a RAIM alarm status, the ambiguities are difficult to resolve, too. So, large variability of non-affected satellite number as well as periods where RAIM availability test has failed can both form an indicator for conditions where the ambiguities could be difficult or even impossible to resolve. An SQM algorithm using these informations was developed and the results are shown in figure 3.17. The red periods indicate alarm states given by the SQM algorithm. They correspond to the times where RAIM indicates an anomaly and to periods where the available constellation was not stable during enough time to resolve correctly the ambiguities. The time interval during which the constellation should be stable in order to disengage alarm state after RAIM alarm is the unique parameter of the algorithm. This parameter has been set by default to 30 observations. By relating this result with the information given in figure 3.15, it can be seen that the alarm

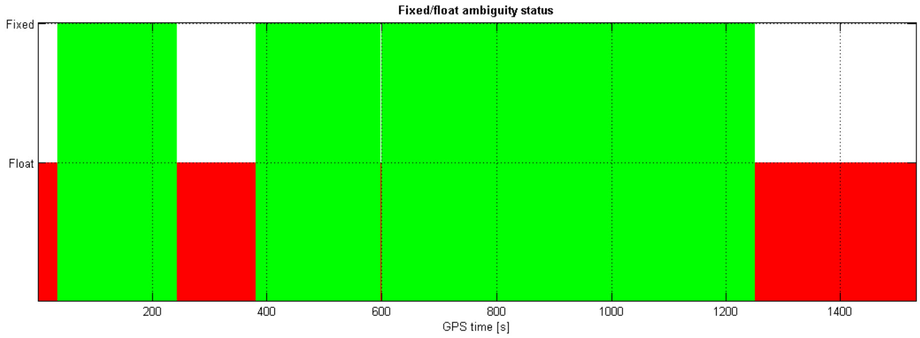

Figure 3.15: Ambiguity resolution status obtained after PP carrier-phase observations for the analyzed data sample. The red zones indicate periods where the ambiguities could not be resolved and form therefore problematic periods which should be detected by the RT application.

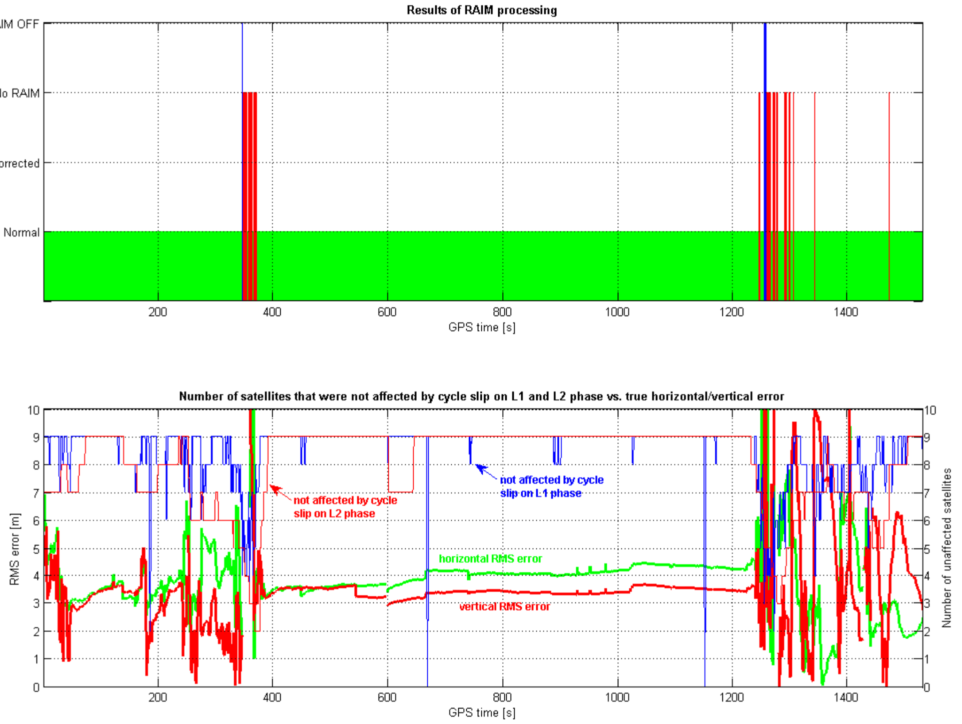

Figure 3.16: Results of RAIM processing (above) and comparison with true horizontal/vertical error and number of satellites that are not affected by cycle slips on either L1 or L2 carrier-phase. The high variability of the errors at the first and last parts are due to the fact that the ambiguities could not be resolved by PP carrier-phase for the reference trajectory.

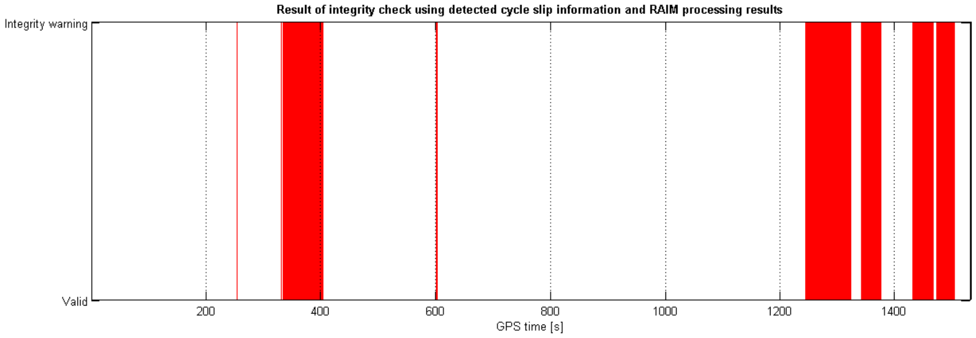

Figure 3.17: Results given by the developed SQM algorithm using RAIM and L2 phase track analysis for ground acquired kinematic data. The red periods correspond to alarm states.

periods correspond to problematic observations in the PP solution. It is now of interest to

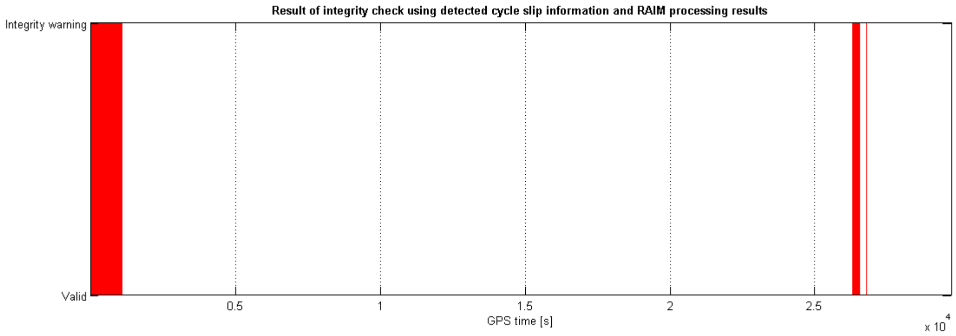

Figure 3.18: Results given by the developed SQM algorithm using RAIM and L2 phase track analysis for a survey flight. The red periods correspond to alarm states.

Figure 3.19: Results of RAIM processing (above) and comparison with horizontal (blue) and vertical (red) DOP factors and number of visible satellites for the analyzed flight data (green).

test the behavior of the SQM algorithm on real flight data where RAIM was enabled. One example of result is shown in figures F.3 where a flight data sample was submitted to the test. Figure F.4 indicates that the first epochs are characterized by low satellite number optimally detected by using RAIM. Furthermore, a period of noisy satellite constellation is characterized by a RAIM unavailability and a L2 phase track loss by the tracking loop. These periods are typical for causing problems during the PP. Nevertheless, the global quality of the data is good and the ambiguities could therefore be resolved for the whole period during PP. Other GPS data have been submitted to the SQM algorithm and the obtained results were found relevant for RT implementation. The value of the SQM algorithm parameter will be determinant for the resulting output after RAIM alarm was set. Knowing that RAIM alarm condition corresponds with high probability to problematic epochs during PP, the ambiguity resolution will still be difficult if cycle slips are further present during these periods. In order to rise the chances of resolving them correctly, no cycle slip should occur during a given time interval. If this interval is too large, the output will be less reliable. On the other hand, if the interval is too small, it is the phase quality component of the algorithm that will be reduced. The SQM algorithm parameter used in the presented examples has been set to 30 epochs according to the result obtained by PP with respect to ambiguity resolution.

3.5 Real-time implementation perspectives

Cycle slip detection results are the key indicators for evaluating the quality of the phase measurements. Several algorithms have been implemented in *Matlab* in order to evaluate their performances. According to the quality of the given results, the algorithm detecting cycle slips on L1 carrier-phase by means of time derivative of the ionospheric delay has been implemented in the PM quality check tool. Reliable cycle slip detection on L2 phase can be performed by making the assumption of cycle slip presence in case of L2 phase track loss. The analyzed data sample has shown that periods where numerous satellite signals have no L2 phase tracked are problematic for PP. It will therefore be appropriate to use this method for detecting the number of PRNs that have no L2 phase tracked. By this way, the phase quality can be evaluated with a very high reliability, making it the ideal algorithm for the RT application. The presented interference detection algorithm results are highly dependent on the value of the algorithm parameter. The sensitivity of the results issued from the first test to the value of the parameter for noisy airborne data affects the reliability of the given information. For this reason, the complete algorithm has been implemented in the PM tool while only the single threshold test will be integrated in the RT quality check process.

This chapter has demonstrated the advantages of using RAIM processing results since they provide a QI including several factors. Furthermore, the brought information can be completed by using phase QI in order to give a global indication on the chances of resolving more or less easily the ambiguities during the PP step. The algorithm has been tested on all the airborne-mapping GPS data samples where RAIM was enabled and the obtained results are relevant. This algorithm is particularly useful for RT quality check since a long period of alarm state gives immediately an indications on the bad quality of the current observations. So, if a flight line is largely affected by such an alarm, it will be useful to repeat the survey along the considered flight line.

The RT quality check application architecture will be designed by considering these conclusions. The priority is given on the algorithms providing reliable informations since reliability of the analyzed quality will largely affect decisions during the flight.

Chapter 4

Real-time position and velocity accuracy estimation

Modeling position and velocity errors as well as possible is of great importance for RT Kalman filtering in the GPS/INS integration step. This chapter analyzes the relevance of the receiver's accuracy measures and searches their potential improvements. The GPS position quality improvement by using EGNOS corrections and ionospheric and tropospheric corrections capabilities of the receiver are also evaluated in this chapter.

4.1 GPS accuracy

Accuracy can be measured by a statistical quantity called the standard-deviation assuming that the GPS measurements contain no systematic errors or blunders. The lower the standard-deviation the higher the accuracy. The currently used GPS stochastic model in the RT Kalman filter is directly derived from receiver estimations. In order to evaluate the receiver provided accuracy estimations, it seems relevant to first analyze receiver error behavior by mean of statistical modeling, considering the fact that a 3-σ tolerance is introduced in the GPS stochastic model. Some backgrounds related to GPS error is given in the following sections.

4.2 GPS error sources and estimates of user position

GPS accuracy depends in general on a lot of factors like the quality of the pseudorange observations or satellite ephemeris data for example. In order to analyse the effect of errors coming from different sources, the assumption is usually made that all these sources can be allocated to individual satellite pseudoranges [11]. This induces that these different errors are summarized in an equivalent error in the pseudorange observations, called *user-equivalent range error* (UERE). The composite UERE is modeled like a zero mean Gaussian random variable where its variance, σ_{UERE}, is computed by the sum of all the error's variance. Moreover, one assumes that UERE is independent and identically distributed from satellite to satellite [11].

The position accuracy is expressed as a function of a geometry factor and a pseudorange error factor. In general, the latter is approximated by satellite UERE while the first is expressed by a quantity, called the Dilution of Precision (DOP), taking in account the relative user/satellite geometry.

4.2.1 Pseudorange errors

Typical errors comprised in the satellite UERE come from

- satellite clock stability,
- predictability of satellite perturbations,
- thermal radiation,
- ephemeris prediction error,
- thruster performance,
- ionospheric delay,
- tropospheric delay,
- receiver noise and resolution,
- multipath.

Equation 3.1.1 represents the pseudorange model and the error components affecting the signal. All these error components are root-sum-squared to form the total system UERE expressed by his standard-deviation σ_{UERE}. This value has changed over time and the space, control and user segments improved. Considering the value given in *Javad*-receiver manual, the σ_{UERE} term is set to 2 [m] in this analysis. It will be shown later that DOP and UERE parameters can be combined to estimate horizontal and vertical position accuracy.

4.2.2 User to satellites geometry

As mentioned, user/satellite geometry influences position error. To illustrate the main idea of the DOP factors, one can take a 2D example. The figure 4.1 shows that in the presence of identical measurement errors, the shape of the error domain (shaded area) depends on the user/satellite geometry. On the left, the geometry is optimal since the two satellites form approximately a right angle while on the right, this angle is much smaller. In the first case, the error domain will be smaller than in the second case, even if the measurement errors are the same. This concept is comprised within the DOP factors which are derived from the trace of the parameter cofactor matrix given by

$$\mathbf{Q_{xx}} = (\mathbf{H}^T\mathbf{H})^{-1} = \begin{bmatrix} q_{EE} & q_{Ey} & q_{EU} & q_{E\delta t} \\ q_{NE} & q_{NN} & q_{NU} & q_{N\delta t} \\ q_{UE} & q_{UN} & q_{UU} & q_{U\delta t} \\ q_{\delta tE} & q_{\delta tN} & q_{\delta tU} & q_{\delta t\delta t} \end{bmatrix} \tag{4.2.1}$$

Horizontal and vertical DOP factors can both be deduced respectively by

$$HDOP = \sqrt{q_{EE} + q_{NN}} \tag{4.2.2}$$
$$VDOP = \sqrt{q_{UU}} \tag{4.2.3}$$

where

$\mathbf{H}$ = design matrix
$\mathbf{Q_{xx}}$ = parameter cofactor matrix
$HDOP$ = horizontal dilution of precision
$VDOP$ = vertical dilution of precision

Since the DOP factors only depend on the design matrix which expresses the relation between the user position and the satellites, they can be exploited for position accuracy estimation like it will be shown in the next section.

4.3 Relevance of receiver accuracy estimations

A GPS observation data sample provided by six airborne-mapping missions is used for evaluating the indicated accuracy. The receiver computed horizontal and vertical position accuracy is expressed by the distance Root Mean Square (RMS), noted $drms$, and by $du_{68\%}$ value expressing the 1-σ interval of vertical error, respectively. These two accuracy measures are developped and analyzed in this section to check their relevance.

4.3.1 Position accuracy estimation

Horizontal and vertical accuracy estimation are treated separately. First the vertical accuracy is considered since it represents a 1D case. Some concepts will be extended for the 2D case of horizontal accuracy.

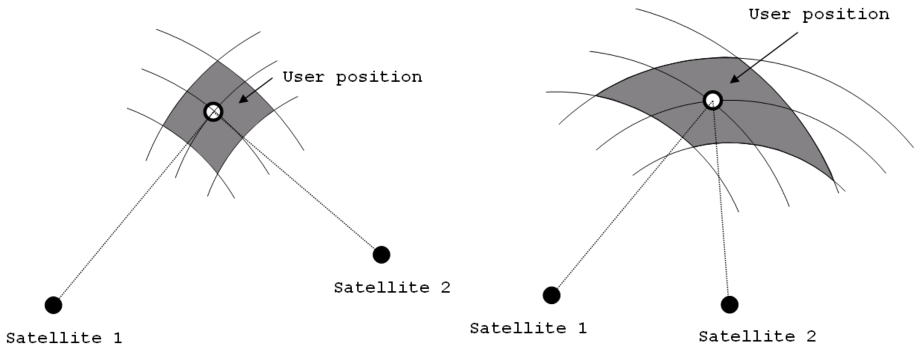

Figure 4.1: Dilution of precision and influence of relative user/satellite geometry on user error. Despite the fact that UERE is the same for both cases, the error domain size changes. (inspired from [11]).

Vertical error modeling

The differential carrier-phase post-processed solution is used as the true trajectory against which the RT computed code position is compared. The true unsigned (absolute) vertical error, noted $d\tilde{u}$, is obtained by the difference

$$d\tilde{u} = |u_{pp} - u_{code}| \tag{4.3.1}$$

where

u_{pp} = true considered vertical coordinate in ENU frame
u_{code} = receiver computed vertical coordinate in ENU frame

The u_{pp} component comes from the post-processed solution obtained by using *GrafNav* software. The empirical probability density function of the computed $d\tilde{u}$ values is shown in figure 4.2. According to [11] and [24], the signed vertical error distribution is assumed as zero mean and jointly Gaussian. The Gaussian behavior of the vertical error of airborne GPS data is verified by the figure 4.3 showing the correspondence between the measured vertical error distribution and the Gaussian distribution. It is generally assumed that each observation is independent and identically distributed [11], i.e. an observation is uncorrelated with the observations at previous epochs. So, knowing that the error behavior is nearly Gaussian, one can now express the accuracy estimation by means of Gaussian error statistics. The figure E.2 in appendix E shows a Gaussian cumulative distribution with mean zero of absolute (unsigned) error. This model is useful to set up the relationship between RMS, 95% and 99% probability, noted respectively $du_{68\%}$, $du_{95\%}$ and $du_{99\%}$, which are all commonly used 1D accuracy measures. It is important to understand that each vertical observation error can be seen as a realization of a Gaussian process. Therefore, it can be estimated by applying one of the mentioned statistic analysis. According to [14], one assumes that

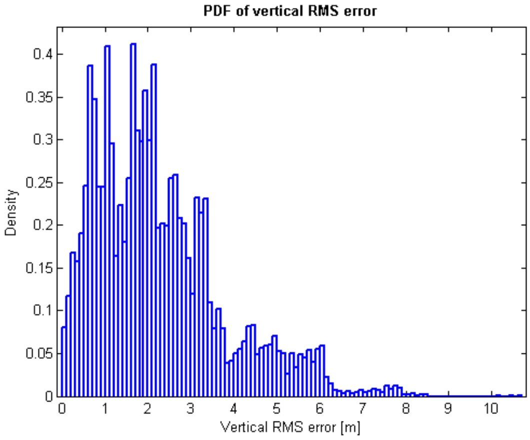

Figure 4.2: Empirical PDF of true RMS vertical error.

$$d\tilde{u} \sim N(0, VDOP \cdot \sigma_{UERE}) \tag{4.3.2}$$

since the VDOP component is derived from the trace of $\mathbf{Q_{xx}}$. The vertical error can be seen as the product of $VDOP$ and a random variable $UERE$ whose distribution is given by

$$UERE \sim N(0, \sigma_{UERE}) \tag{4.3.3}$$

By this mean, the standard-deviation of equation 4.3.2 can be expressed as

$$du_{x\%} = K \cdot VDOP \cdot \sigma_{UERE} \tag{4.3.4}$$

where

K = coefficient depending on the wanted confidence interval
$du_{x\%}$ = accuracy measure with probability $x\%$

The work in [14] shows that this relation is statistically correct even when position and time are variables. The value of K depends on the size of the wanted confidence interval associated to a probability that the true error lies within. A value of $K = 1$ means that 68% of the measurements fall within ± one standard-deviation of the mean. A value of $K = 2$ and $K = 3$ mean that respectively 95% and 99% of the values fall within ± two and ± three standard-deviations of the mean. So, the different error statistics can be approximated by

$$du_{68\%} \approx 1.0 \cdot VDOP \cdot \sigma_{UERE} \tag{4.3.5}$$

$$du_{95\%} \approx 2.0 \cdot VDOP \cdot \sigma_{UERE} \tag{4.3.6}$$

$$du_{99\%} \approx 3.0 \cdot VDOP \cdot \sigma_{UERE} \tag{4.3.7}$$

at each observation epoch. The result of the comparison between the estimation given in equation 4.3.5 and the true vertical error given by the *GrafNav* post-processed solution for the analyzed data sample is shown in figure 4.4. The green lines represent the unsigned true vertical error and the blue lines the obtained $du_{68\%}$ accuracy estimation (which is provided

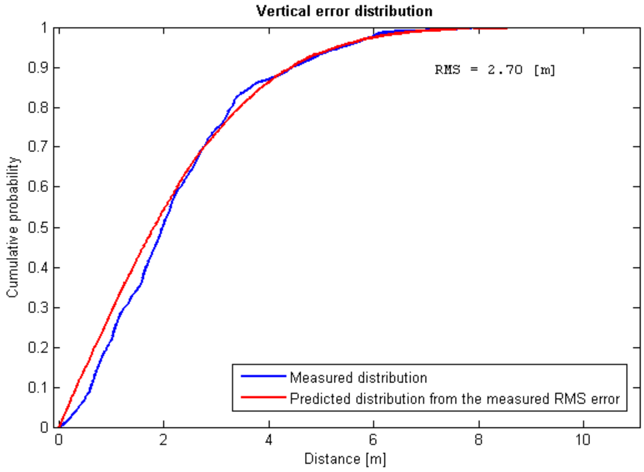

Figure 4.3: Vertical RMS error distribution modeled by a Gaussian distribution (the values are unsigned errors).

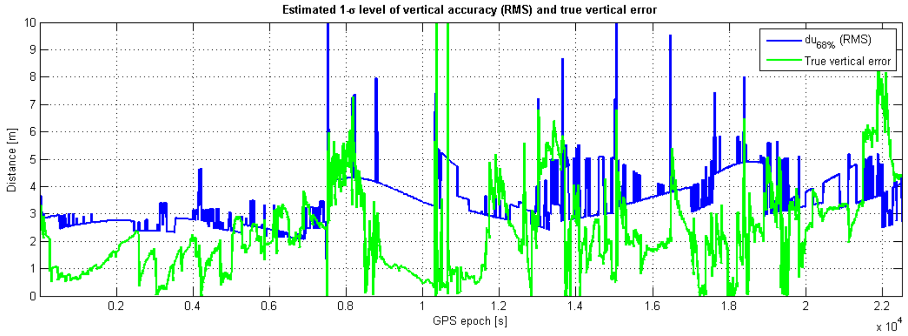

Figure 4.4: Evaluation of $du_{68\%}$ vertical accuracy measure provided by the receiver and comparison with true vertical error.

directly by the receiver). The next step is to check if this estimation is relevant according to the true error. Since each epoch is considered as independent and identically distributed and since only one realization is given for each epoch, no classical statistical test can be applied. For these reasons, the difference between the error and the estimated median, noted $du_{50\%}$, will be considered. The estimation of the median can be derived from $du_{68\%}$ considering the Gaussian nature of vertical error distribution and will therefore be given by

$$du_{50\%} = 0.67 \cdot du_{68\%} \tag{4.3.8}$$

It is assumed that this new serie is normally distributed with zero mean[1]. The bias of the obtained distribution will be the indicator of the relevance of the estimation. Figure 4.5 shows the normalized distribution of the series and compares it with the zero mean and 1-σ normal distribution. The major part of the estimation differences is comprised between ± 2.00 [m]. It is also visible that the distribution is reasonably well centered, indicating that about 50% of the true error lies below the $du_{50\%}$ accuracy measure. Since the 3-σ interval is considered for Kalman filtering, it is also relevant to check the $du_{99\%}$ estimation given by the red curve in figure 4.6. All the vertical errors are comprised in the 99% interval. So, one can conclude that the estimation provided by the receiver is statistically relevant and could be used as a realistic stochastic model for Kalman filtering.

Horizontal error modeling

The vertical error analysis has shown that uncertainty in position can be defined as the probability that the actual error will not exceed a certain amount. It has been demonstrated that vertical error, which is one-dimensional, can be modeled like a Gaussian distribution. In the case of horizontal error modeling, this assumption has other consequences. According to [11] and [24], it is assumed that the distribution of GPS fixes can be approximated by a bivariate normal distribution without correlation between the two variables. Thus, this

---

[1] Since a lot of factors are comprised in the vertical error, the central limit theorem enables to make this assumption.

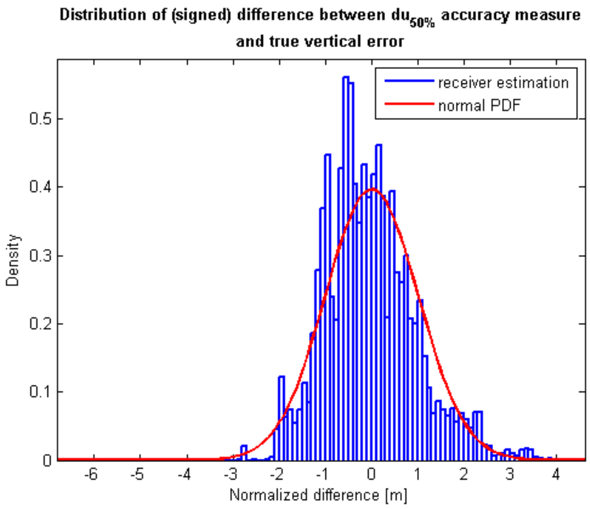

Figure 4.5: Normalized distribution of estimation difference time serie.

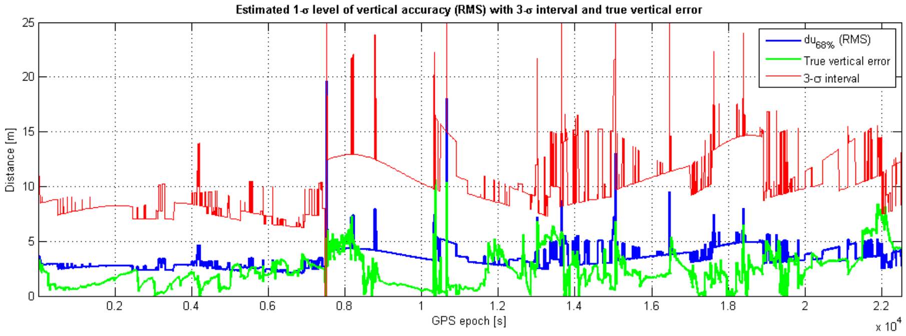

Figure 4.6: Evaluation of $du_{99\%}$ vertical accuracy measure provided by the receiver for representing the 99% confidence interval.

probability can be related to the magnitude of the standard-deviation. In the case of a 1D accuracy measure and a Gaussian distribution, the standard-deviation corresponds to a 68.27% confidence interval, while a 95% confidence level will be obtained by multiplying the standard-deviation by 1.96. By extending this concept to two dimensions, one obtains an elliptical area whose size corresponds to a certain error probability. In the practice, this area, called error ellipse[2], is approximated by a circle whose radius is a function of the wanted error statistics. That means that the probability that the true error lies within the circle will vary with the value of the radius and that one might assume the same variance in each direction [24]. Since

---

[2] Details on the concept of error ellipse can be found in [1].

the distribution of the error along the east and north axes are Gaussian, the distribution of the horizontal error $\tilde{dh}$ obtained by

$$\tilde{dh} = \sqrt{d\tilde{e}^2 + d\tilde{n}^2} \tag{4.3.9}$$

where

$d\tilde{e}$ = true error along east axis
$d\tilde{n}$ = true error along north axis

will be modeled by a χ^2 distribution with 2 degrees of freedom[3].

The true errors $d\tilde{e}$ and $d\tilde{n}$ are obtained by the unsigned difference between the post-processed trajectory and the receiver provided position. Figure 4.7 shows the horizontal error distribution. In a similar manner as presented in the previous section, we can check if these errors behave like a Rayleigh distribution, which is a particular case of the χ^2 distributions. If this is the case, we can use this distribution to compute adequate confidence intervals, to check if the estimation provided by the receiver is relevant and to switch from one confidence level to another. Figure 4.8 shows empirical cumulative distribution function (CDF) and Rayleigh CDF. It seems apart for the errors near 5 [m] that the Rayleigh distribution can adequately model horizontal error behavior. This high frequency of errors near 5 [m] come from the same flight and thus, the Rayleigh model stays adequate for the rest of the data. The figure E.3 in appendix E represents a Rayleigh CDF with the traditional accuracy measures.

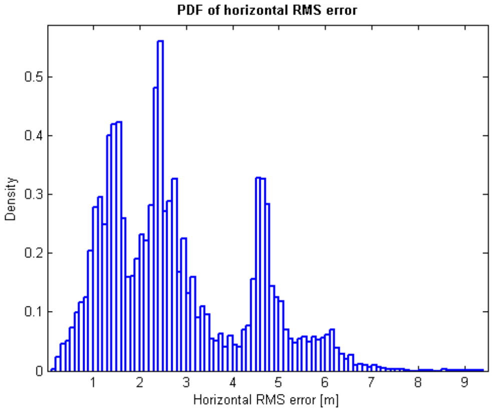

Figure 4.7: Empirical PDF of true horizontal RMS error.

There exist several 2D accuracy measures that are commonly used in the practice. The most used are the distance root-mean-squared error, noted *drms*, the circular error probable, noted *CEP*, the 2*drms* accuracy measure, and sometimes the 99% error probability noted *R*99.

---

[3] The demonstration is given in appendix E.

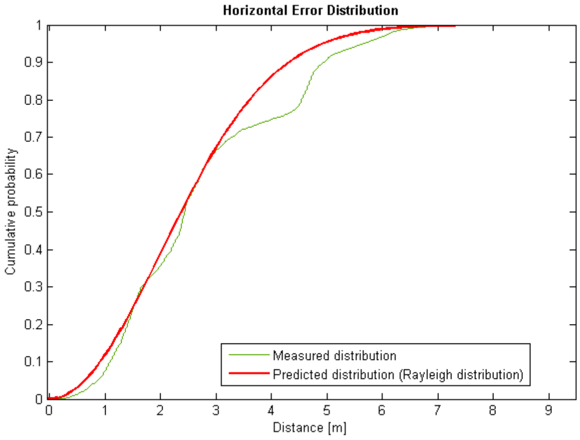

Figure 4.8: Adequation between Rayleigh CDF and empirical CDF.

Distance Root-Mean-Squared error The *drms*, is a single quantity expressing 2D accuracy. This quantity corresponds to the equivalent expressed in 2D of the value of one standard deviation of the error in the 1D case. It is given by

$$drms = \sqrt{\sigma_{EE}^2 + \sigma_{NN}^2} \tag{4.3.10}$$

where

σ_{EE} = standard-deviation of estimated Easting coordinate
σ_{NN} = standard-deviation of estimated Northing coordinate

The *drms* can be related to DOP factors by the covariance matrix of the parameters given by

$$\mathbf{C} = \begin{bmatrix} \sigma_{EE}^2 & \sigma_{Ey}^2 & \sigma_{EU}^2 & \sigma_{E\delta t}^2 \\ \sigma_{NE}^2 & \sigma_{NN}^2 & \sigma_{NU}^2 & \sigma_{N\delta t}^2 \\ \sigma_{UE}^2 & \sigma_{UN}^2 & \sigma_{UU}^2 & \sigma_{U\delta t}^2 \\ \sigma_{\delta tE}^2 & \sigma_{\delta tN}^2 & \sigma_{\delta tU}^2 & \sigma_{\delta t\delta t}^2 \end{bmatrix} \tag{4.3.11}$$

This covariance matrix can be related to the cofactor matrix by

$$\mathbf{C} = \mathbf{Q_{xx}}\sigma_{UERE}^2 \tag{4.3.12}$$

By considering equations 4.2.2 and 4.3.12, it appears that

$$\sqrt{\sigma_{EE}^2 + \sigma_{NN}^2} = HDOP \cdot \sigma_{UERE} \tag{4.3.13}$$

The left term quantifies the *drms* accuracy measure. The probability that the computed position falls within a circle of radius *drms* from the true location depends on the geometry of the position solution, i.e. the shape of the error ellipse. The probability can vary from 0.63 to 0.69. Figure 4.9 shows the *drms* accuracy measure provided by the receiver and the correspondence with the true horizontal error. The relevance of this estimation will be checked using the same methodology as in the previous section.

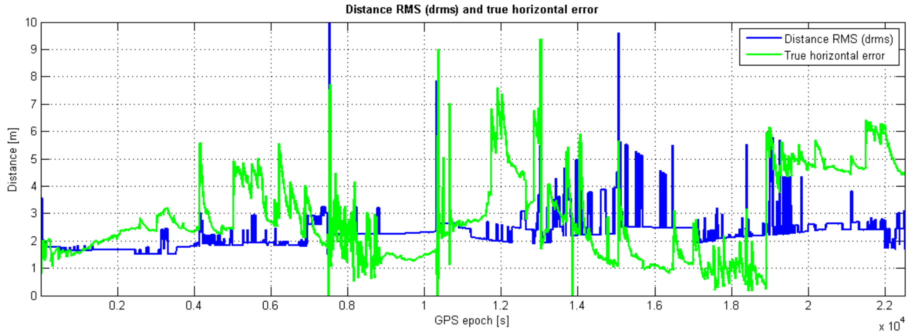

Figure 4.9: True horizontal error and *drms* estimation provided by the receiver.

Circular Error Probable (CEP) Strictly speaking, the CEP defines a circle whose radius catches 50% of the error distribution when centered at the true position [11]. The CEP can be estimated by multiplying the horizontal DOP factor and pseudorange error component by a constant defining the probability. The relation is given by

$$CEP \approx 0.75 \cdot HDOP \cdot \sigma_{UERE} \tag{4.3.14}$$

Twice the distance Root-Mean-Squared error $2drms$ defines a probability range between 0.95 and 0.98 that the horizontal error is within a circle of radius $2 \cdot drms$. In the practice, it is assumed that this value defines the 95% limit for the magnitude of the horizontal error [11]. The performance of the estimated $2drms$ values is shown in figure 4.10. About 14% of the values are above the true horizontal error, indicating a possible underestimation of the receiver derived *drms* value.

R99 accuracy measures The $R99$ accuracy measure defines the area around the true position where there is a probability above 99% that the true error lies within. It can be approximated by

$$R99 \approx 3 \cdot HDOP \cdot \sigma_{UERE} \tag{4.3.15}$$

The Stanford plot[4] in figure 4.10 indicates that about 1.4% of the true horizontal errors are outside of the probability circle. The choice of this coefficient is motivated by the fact that the 3-σ interval is considered in the Kalman filter. Thus, $R99$ defines a probability that is higher than 99%.

4.3.2 Analysis of possible position accuracy estimation assessment

A lot of factors influence the position error. As seen previously, the contribution of all these errors are summarized in the *UERE* term. Nevertheless, the main idea of this section is to check if there could be an assessment of the code solution accuracy estimation by correcting

---

[4] See appendix E for details on the Stanford plots.

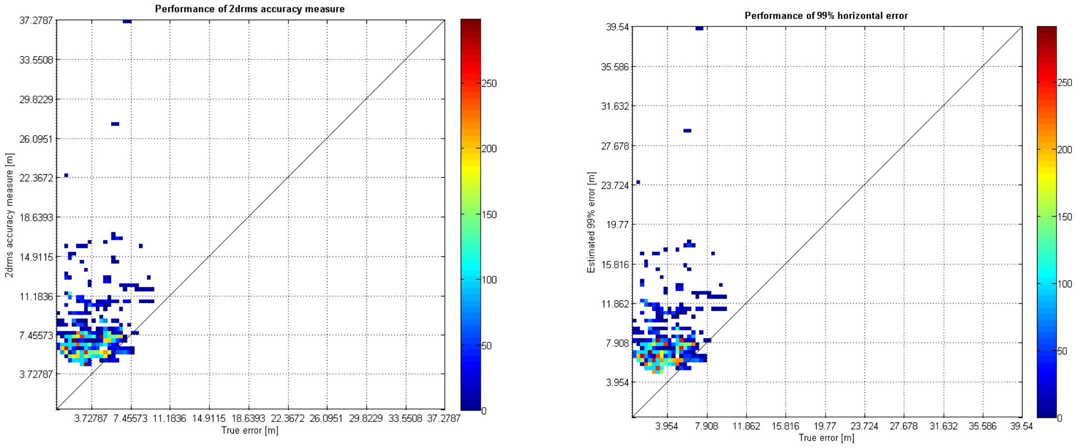

Figure 4.10: Stanford plot of estimated $2drms$ (left) and $du_{99\%}$ (right) accuracy measure against true horizontal and vertical error, respectively.

the receiver estimation and by using receiver estimated Spherical Error Probable (SEP). One should bear in mind that cycle slips only affect the phase and thus have only limited influence on the code solution.

Application of a correction factor on accuracy estimation

Previously, it as been checked that horizontal error can be modeled like a Rayleigh distribution. The estimated $drms$ value should reflect the radius of the circle where there is a probability of about 63% that the true error lies within. Multiplying the $drms$ value by two changes this probability to near 98%, and so on. It will now be checked if a correction factor could improve the estimation of different distribution points. To do that, it is important to understand that each error at each epoch is considered as independant and identically distributed. So, the true horizontal error at each epoch is a single realisation of a Rayleigh random process and it is its standard-deviation (and not the error) that is estimated. This implies that no classical statistical test can give informations on the relevance of the parameter estimation. Therefore, an empirical approach was chosen in order to improve the parameter estimation at each epoch. The difference between the true error and the median estimation is formed. According to the central limit theorem, it will be assumed that this new series follows a near Gaussian process since a lot of factors are implied in the phenomenon. In the best case, the normalized[5] sample should have a centered distribution with a small variance. By plotting the empirical distribution of the samples, it is visible that the distribution is not centered and that the median estimation underestimates the truth. So, the estimation, i.e. the sample, is multiplied by a coefficient until the distribution is centered. The result is shown in figure 4.11 where the blue distribution represents the non-corrected estimation while the green one is issued from the corrected median estimation by using a coefficient of 1.80. This means that

---

[5] Division by the standard deviation.

about 50% of the true errors lies below the corrected median. From that, the 99% can be recomputed and it appears that all the true errors (against 98% for the non-corrected sample) lie in the estimated confidence interval.

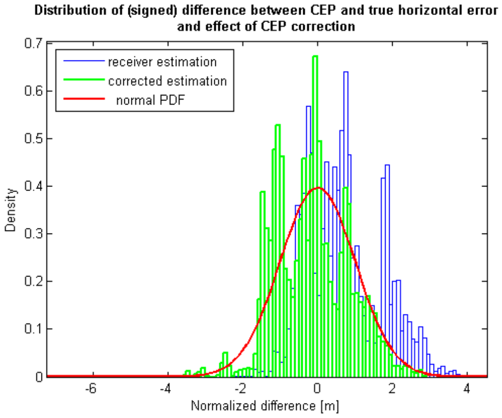

Figure 4.11: Effect of the correction coefficient on the CEP accuracy measure.

Use of Spherical Error Probable accuracy measure

Another possibility is to use the SEP estimation provided by the receiver to compute 2D and vertical accuracy measures. The SEP is strictly speaking the 3D equivalent of the CEP accuracy measure. It represents a 3D accuracy with various probability and can be defined like the radius of a sphere centered at the true position, containing the position estimate in 3D with a probability of 50%. CEP, $drms$ and $du_{68\%}$ values can be derived from SEP by doing some assumptions. [23] states that the relation between CEP, $drms$ and SEP is given by

$$CEP \approx \frac{SEP}{2.0} \tag{4.3.16}$$

$$drms \approx \frac{SEP}{1.7} \tag{4.3.17}$$

$$du_{68\%} \approx \frac{SEP}{0.88} \tag{4.3.18}$$

These relations have been applied to the analyzed GPS data samples in order to derive accuracy measures from the SEP computed by the receiver. The results are shown and compared with the direct computation of $drms$ and CEP in figure 4.12. It appears clearly that these indirect computations of CEP and $drms$ don't improve significantly the error estimation. This can be confirmed by analyzing the distribution of the difference between the true error and the SEP derived horizontal and vertical 50% accuracy measures (figure 4.13). Direct vertical accuracy measure is very relevant and no changes should be made. Nevertheless, computing 99% confidence interval from SEP derived accuracy measure gives little better results than by using directly the $drms$ measure. But one should bear in mind that these results depend strongly on the size of the sample and relevant conclusions can only be made for a very large sample.

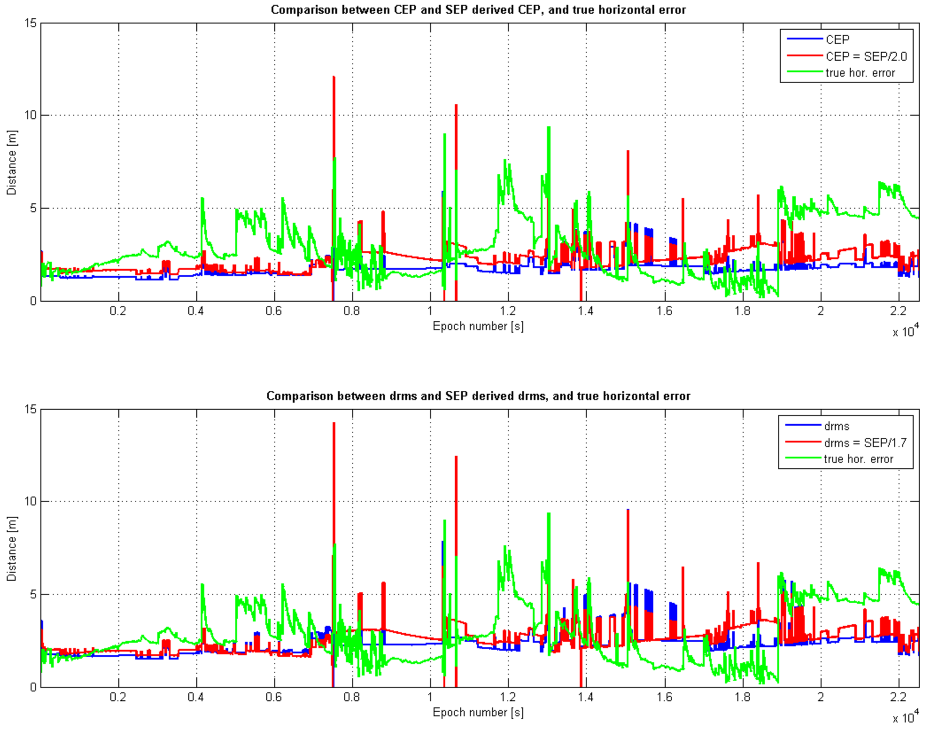

Figure 4.12: Comparison of CEP and *drms* values obtained by direct computation and by using SEP values.

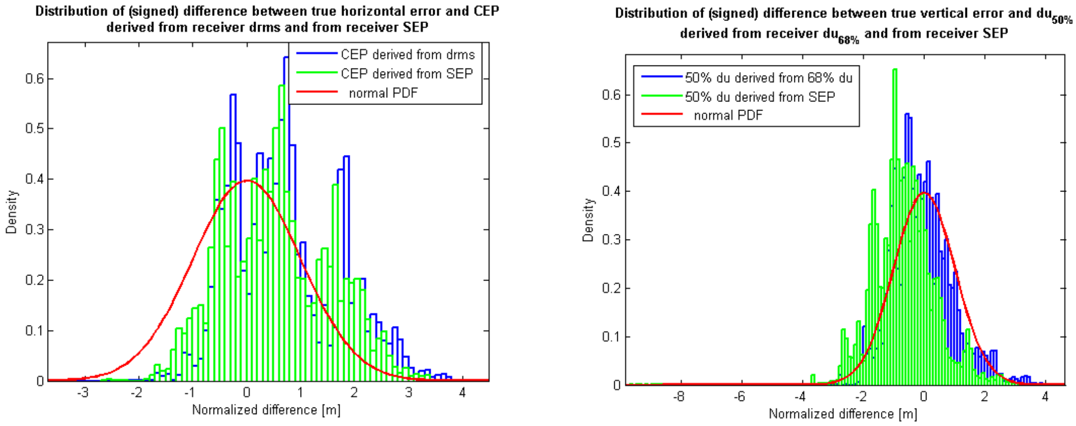

Figure 4.13: Comparison of CEP and *drms* values obtained by direct computation and by using SEP values.

Note One should bear in mind that the assumption that an error is independent from what happens previously has been made. But this is in fact a quite strong assumption and the autocorrelation functions of true horizontal and vertical errors show that the reality is not as simple (figure 4.14). Indeed, errors are very strongly correlated for a very long period.

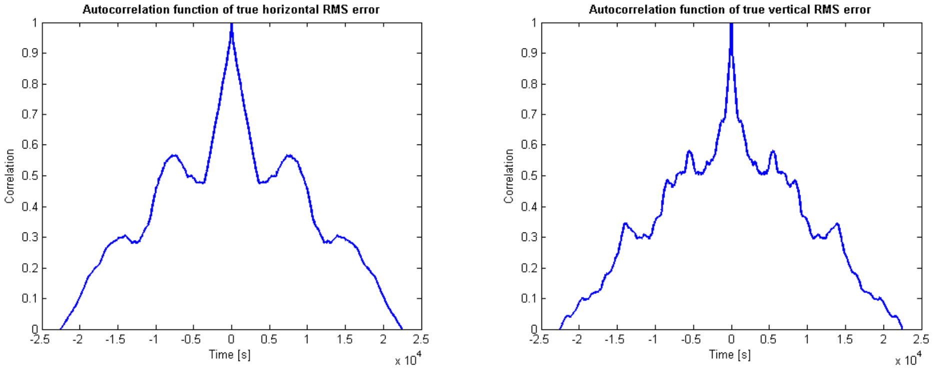

Figure 4.14: Autocorrelation functions of true horizontal error (on the left) and true vertical error (on the right).

4.4 GPS data quality assessment using receiver ionospheric and tropospheric corrections

The ionosphere is a dispersive medium where UV rays from the sun ionize a portion of gas molecules and release sol free electrons. This electrons perturb GPS wave propagation. The dual frequency receivers are able to correct group delay due to ionospheric effects by applying the relationship (following ICD-GPS-200 revision C)

$$R_{corr} = \frac{R_2 - \alpha R_1}{1 - \alpha} \tag{4.4.1}$$

where

R_{corr}	=	pseudorange corrected for ionospheric effects
R_i	=	pseudorange measured on the L-band channel indicated by the subscripts

The α constant is given by equation 3.2.8. The troposphere is a non-dispersive environment for frequencies up to 15 [GHz]. The phase and group velocities on both L1 and L2 are equally delayed with respect to free-space propagation [11]. This delay depends on the tropospheric refractive index which depends on the local temperature, pressure and relative humidity. There exist numerous tropospheric delay compensation models that can be found in the literature. The example found in [11] is outlined in order to understand the basic principles behind the receiver processing. The model is given by

$$\delta_{tro,k} = \frac{10^{-6} N_{k,0}}{(r_k - r_0)^4} \int_{r_0}^{r_k} \frac{r(r_k - r_0)^4}{\sqrt{r^2 - r_0^2 sin(E)^2}} dr \tag{4.4.2}$$

with

$$r_k = \sqrt{(R_E + h_k)^2 - r_0^2 cos(E)^2} - r_0 sin(E) \tag{4.4.3}$$

where

$\delta_{tro,k}$ = path length difference
$N_{k,0}$ = wet and dry component refractivity at standard sea level
r_0 = $R_E + h$
R_E = Earth radius
h = user's height
E = satellite elevation angle
k = subscript denoting either wet or dry component

One often models the refractivity by using both a dry and wet component. The first gives rise to about 90% of the tropospheric delay and can be predicted very accurately [11] while the latter, arising from the water vapor, is more difficult to predict because of uncertainties in the atmospheric distributions. More informations can be found in [11].

In order to test the relevance of these corrections, a static test using two receivers at the same time and place was performed[6]. One receiver was configured in such a way that corrections were applied before computing position while the corrections were disactivated in the second receiver. The true position were calculated by differential PP. The differences between the true position and the observed positions are shown in the figure 4.15. One can see that the corrections are particularly important for the vertical component. This can be confirmed by transforming the coordinates in an ENU local frame centered on the true positions. Corrected and non-corrected horizontal and vertical error distributions are shown in figure 4.16. The vertical component error is more than two times lower when the corrections are applied. By considering these results, it appears that it is of importance to apply ionospheric and tropospheric corrections since the ameliorations are relevant. Detailed error statistics are presented in table 4.1 where the vertical error is largely improved by such corrections. Considering these results, the tropospheric and ionospheric corrections should be activated on a dual frequency receiver.

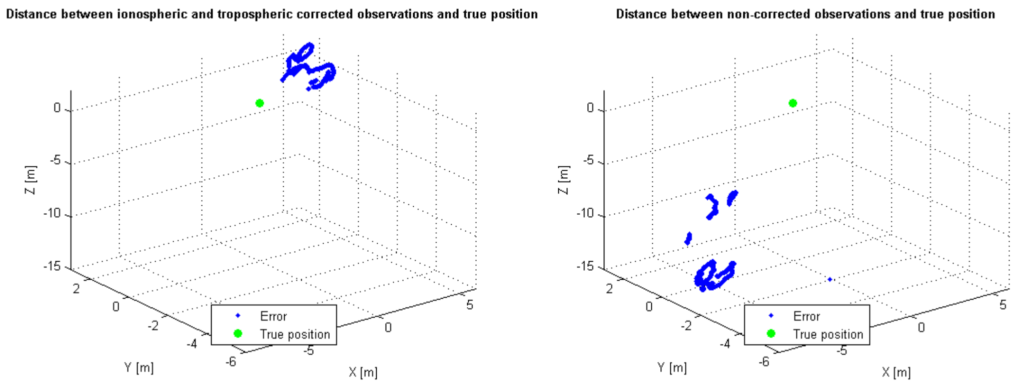

Figure 4.15: Difference between the true position (green) and the observations for the two receivers. On the left, corrections were activated.

---

[6] The assumption of identical conditions can be made knowing that the same type of antennas were used.

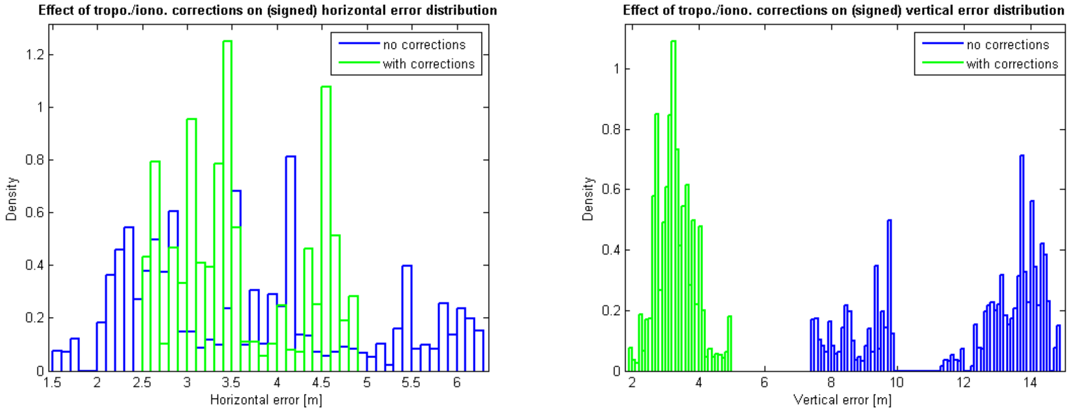

Figure 4.16: Error distribution of non-corrected observations (blue) and tropospheric and ionospheric corrected observation (green) for horizontal error (left) and vertical error (right).

Error type	With corrections	No corrections
95% horizontal error	4.69	6.03
95% vertical error	4.31	14.47
Mean horizontal error	3.58	3.67
Mean vertical error	3.31	11.99
CEP	3.45	3.50
Median vertical error	3.24	13.09

Table 4.1: Obtained error decreasing in meters using ionospheric and tropospheric corrections.

4.5 Real-time GPS data quality assessment using EGNOS equipped GPS receiver

One of the main objectives of the thesis is to evaluate the possible benefits of using WAAS/EGNOS equipped receiver in the context of airborne mapping. EGNOS will provide additional ranging capabilities, integrity information, and differential corrections on the L1 frequency which is broadcasted from geostationary satellites. The latter will correct the σ_{UERE} error component of equations 4.3.4 and 4.9 and by this mean, the *drms* and $du_{68\%}$ values computed by the receiver should be more relevant. Furthermore, the accuracy and the precision of the observations should be improved since only errors affecting the receiver will remain. In order to apply correctly the differential corrections in the receiver computed solution, the receiver must be configured in such a way that all corrections can be applied. Furthemore, the differential mode must be activated.

EGNOS sends different Message Types (MT) each second that define the nature of the signals and indicate the nature of the use enabled by the Signal In Space (SIS). To do that, it is important to note that there are two possible modes: the MT0 and MT0/2. The MT0 is used to indicate that the system is on test. Since April 2003, there is an additional signal, described as MT0/2 that consists of a new MT providing fast corrections, ionosphere corrections and ranging data. For practical distribution, the MT0/2 is overlapping the frame of MT0. The MT0/2 mode means that the MT0 bit stream includes MT2 data. The MT0/2 will allow all receiver units to process and use the corrections broadcast by EGNOS for multi-modal non-safety of life applications. Therefore, the receiver must be configured in such a way that the MT0 is interpreted like the MT2 in order to apply the corrections for all the satellites.

A static test using two receivers with the same type of antenna was performed in order to compare the performances. The two antennas were placed at a distance of about two meters in order to have the same conditions. One receiver was configured in standalone mode while the second receiver was in differential mode (EGNOS). The obtained observation cloud of the two receivers are shown in figure 4.17. It can be seen that the precision and accuracy are much higher in the case of applied EGNOS corrections. Figure 4.18 shows the distributions of the error components. The effect of the corrections are particularly high on the vertical component, since the bias of near 3 [m] has completely been removed in the EGNOS corrected solution. It is now of interest to check if the accuracy measure provided by the receiver in differential mode is relevant. To do that, the same empirical methodology as in the previous section was applied. It has been observed that the RMS provided by the receiver is much too optimistic and should therefore be corrected by applying a correction factor. The effects of the corrections are shown in figure 4.19 where the distributions have been centered. The applied correction coefficients are 3.0 and 2.0 for respectively the horizontal and the vertical accuracy measures. The result of the corrected accuracy measures provided by the receiver as well as the 3-σ interval are shown in figure 4.20. The behavior of the true error is better modeled than by using a constant σ_{UERE}, which is visible by observing the adequation between the blue and the green curves. The performance of the 3-σ accuracy measures, which is of importance for the Kalman filtering, is shown in the two Stanford plots of figure E.1 in appendix E. Only 0.45 % and 0.44 % of the true horizontal and vertical errors respectively lie outside of the 99% interval (against respectively 39.3% and 14.1% without correction coefficient), by considering 11'000 observations.

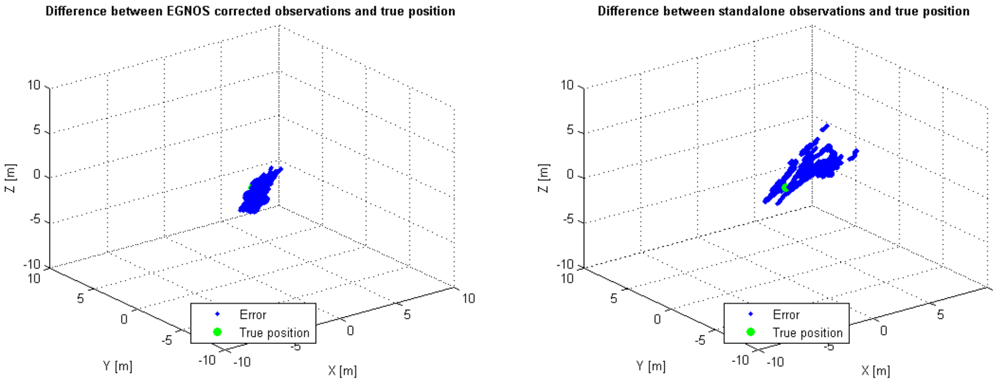

Figure 4.17: Point clouds of EGNOS corrected data (left) and standalone GPS data (right).

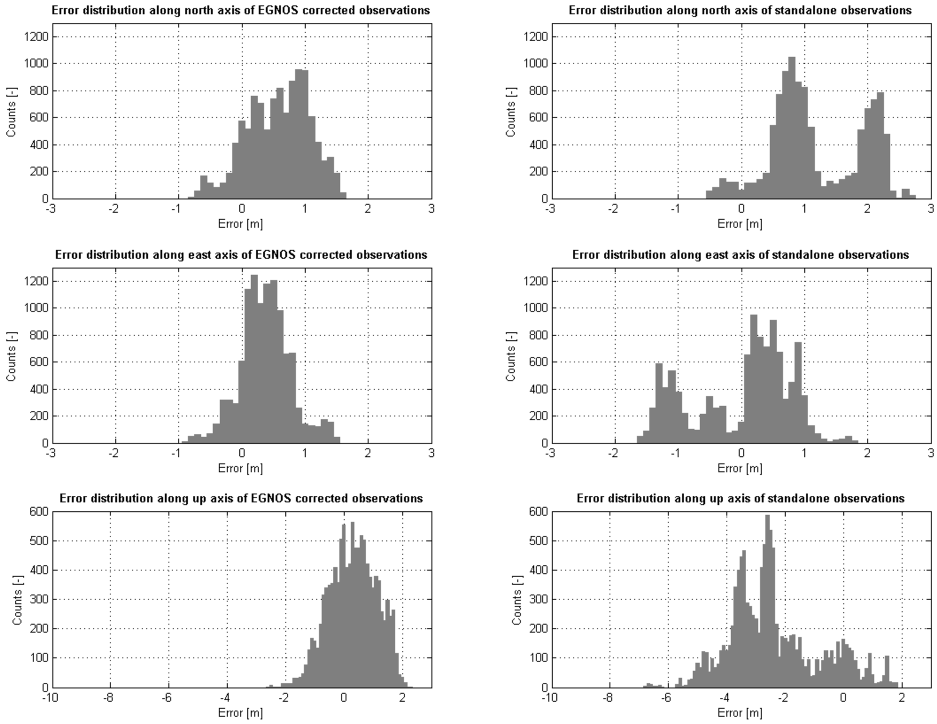

Figure 4.18: Error distribution of standalone observations (right) and EGNOS differential observations (left) for the three ENU components.

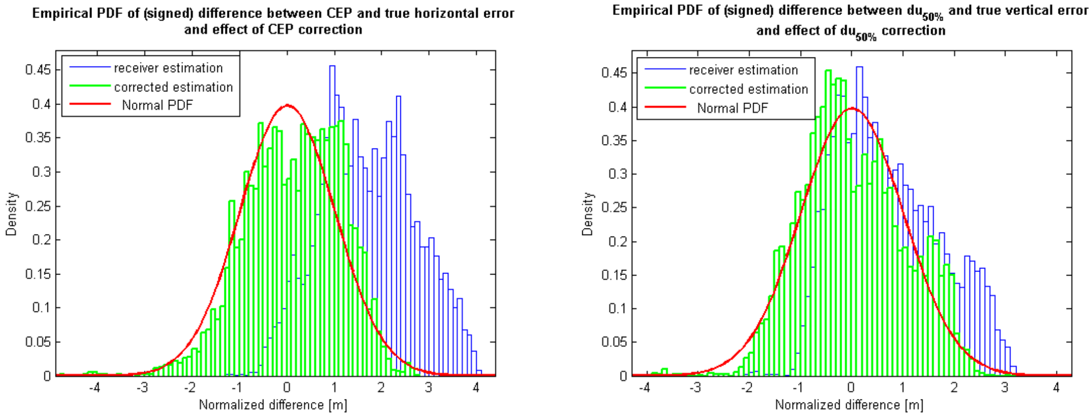

Figure 4.19: Effect of the application of a correction factor on the provided accuracy measures in EGNOS differential mode.

4.6 Discussion

The results presented in this chapter show that the statistical approach for RT accuracy measure processing adopted by the receiver for the code solution stays the relevant method

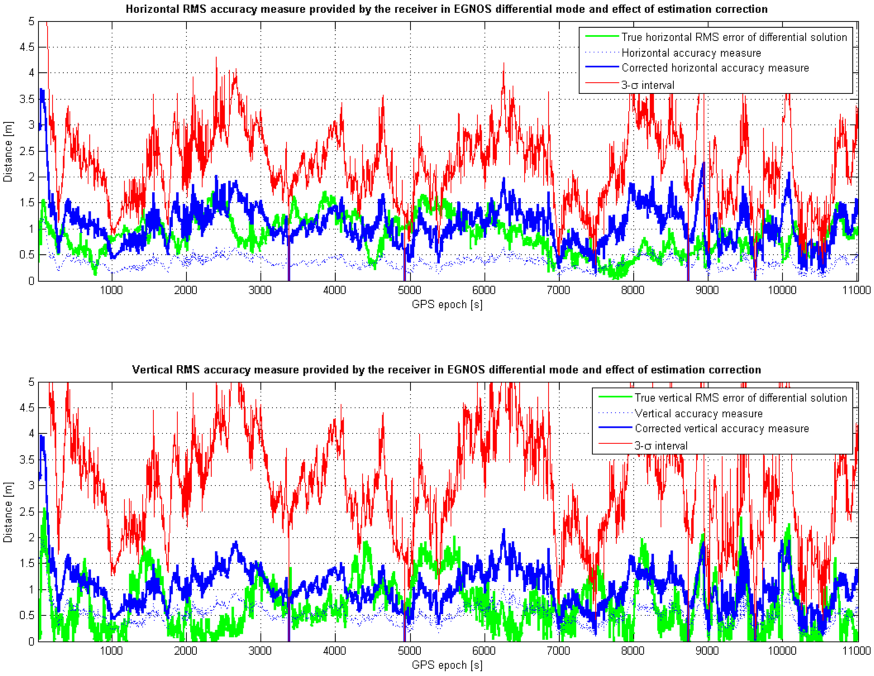

Figure 4.20: Corrected and non-corrected $drms$ (above) and $du_{68\%}$ (below) accuracy measures with 3-σ interval (in red).

to use for RT applications. It should be remembered that this approach takes into account the geometry factor (DOP factors) and the pseudorange errors (UERE) and is statistically valable even if the geometry is variable. It has been demonstrated that the direct vertical accuracy estimation given by $du_{68\%}$ is relevant from a statistical point of view. The horizontal accuracy measure, however, is too optimistic and should therefore be corrected by multiplying the estimations by a constant coefficient. The results of velocity accuracy estimation are not shown because of the strong link with the position accuracy. The conclusion that can be drawn however are the same.

The use of WAAS/EGNOS corrections have been tested in a static experiment. The advantageous in terms of accuracy and precisions are irrefutable in such a configuration since the horizontal and vertical accuracy measures have been improved approximately by a factor 1.5 and 2, respectively. Nevertheless, kinematic tests need to be performed in order to obtain relevant results within the airborne mapping context. The main weakness of using EGNOS corrections lies in the fact that the receiver doesn't store some parameters (like the ionospheric delay for example) in the internal memory, so that the time to first fix may be longer than that of GPS SVs. The classical EGNOS integrity information used in the aviation domain is derived by the processing of a PL as explained in [3]. This processing capabilities are most of the time specific to avionic receivers. The use of the EGNOS differential mode is also of interest for providing realistic accuracy measures. Nevertheless, the provided accuracy indicators must therefore be corrected since they are too optimistic again.

Chapter 5

Benefits of using on-board RTK-GPS

The benefits of using RTK-GPS on-board solution for direct georeferencing and integrity purposes are discussed in this chapter. Communication link design and required setup will be described and tested in a real survey flight. The obtained results are analyzed and some recommendations proposed.

5.1 Potential of on-board RTK-GPS

The laser-scanning system developed at EPFL has the ability of integrating GPS/INS data and generating a laser-point cloud in RT. The accuracy of this point cloud depends directly on the accuracy of the trajectory. The use of RTK-GPS positioning could significantly improve the accuracy and therefore avoid PP. Furthermore, effects of isolated float or standalone solutions could be decreased through the RT Kalman filtering by using a realistic stochastic model. RTK-GPS has a great potential in terms of quality checks since a fixed RTK solution indicates good phase quality. In order to evaluate the usability of such architecture in the airborne-mapping context, a test flight was performed by using RTK-GPS direct georeferencing. Before presenting the obtained results, some RTK principles are presented in the next section.

5.2 RTK-GPS principle

RTK-GPS surveying is a carrier-phase-based relative positioning technique that requires two receivers simultaneously tracking the same satellites. The base receiver remains stationary over a point whose coordinates are known and is connected to a radio transmitter while the rover is a moving receiver whose coordinates are unknown. Since RTK-GPS is based on carrier-phase measurements of both receivers, the integer ambiguities must be resolved in order to estimate the baseline properly. The base receiver measurements and coordinates are formated and transmitted via the communication link to the rover receiver which is also attached to a radio receiver. Often used communication link options are radio/modem, cellular phone, FM-subcarrier or satellite link. The communication link range dictates the potential distance that the rover can operate from the base station. Another important feature is that the position calculation performed by the rover usually requires synchronized packets from the base to be paired with time-matched measurements from the rover receiver. Any delay in the base receiver data will translate directly into the age or latency of the computed position. The transmission bandwidth of the communication link directly affects the latency of the rover position. A datalink that has a 9600 baud transmission bandwidth will acquire data from the base station to rover four times faster than a datalink with a 2400 baud bandwidth. The built-in software in the rover receiver combines and processes the measurements acquired at both, the base and the rover receivers to obtain rover coordinates. The ambiguity parameters are determined using on-the-fly (OTF) ambiguity resolution where the initialization is performed during very short observational time spans. There exist several OTF techniques but all are based on the same concepts that are described in this section.

Through the communication link between the two receivers, the base and rover observables can be combined to form double differenced observations. An initial adjustment using least-squares or Kalman filtering technique is then performed to obtain the initial rover position with the covariance matrix. The use of the covariance matrix enables to form a confidence region around the estimated real-value ambiguity parameters. The size of this ambiguity search space is mainly dependent on the geometry and code accuracy. The shape of the region is an hyperellipsoid around the estimated ambiguity parameters in the case where the number of satellites is more than four. This hyperellipsoid will contain the likely integer ambiguity parameters at a certain probability level. This means that for a given probability level p, there is a p [%] chance that the true integer ambiguity parameters are located inside that hyper-ellipsoid. Since the true ambiguity parameters must be integer values, gridlines intersecting at integer values inside the hyperellipsoid can be modeled. Figure 5.1 shows a simplified 2D example of the confidence region and the potential ambiguity parameter values. A statistical test is then applied on all potential solutions applying rejection/acceptance criteria. The most probable solution among all possible solutions is selected according to a criterion of minimum variance. The chosen solution is validated statistically and a final adjustment is performed to obtain the rover coordinates at centimeter-level accuracy. The general strategy for OTF ambiguity resolution is summarized in figure 5.2.

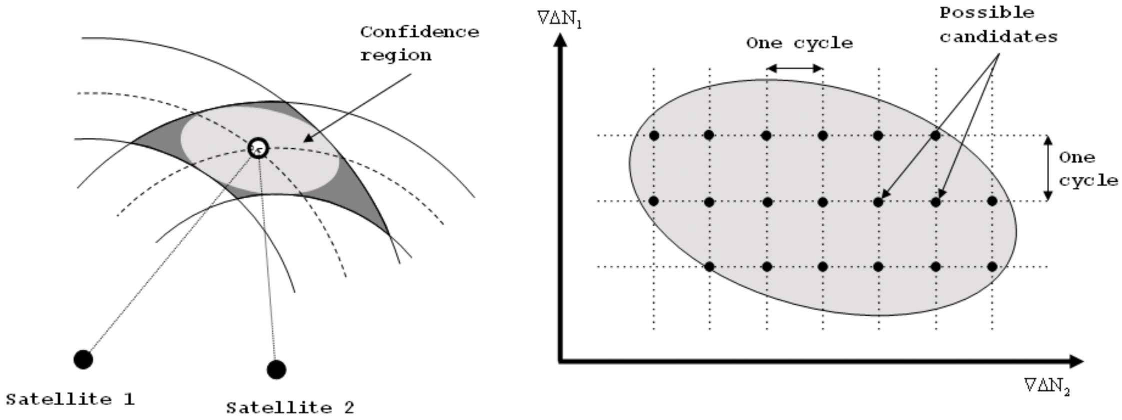

Figure 5.1: Principle of OTF ambiguity resolution (inspired from [2]).

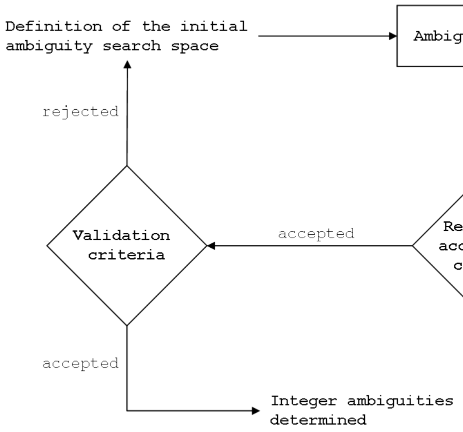

Figure 5.2: Strategy for OTF ambiguity resolution (from [2]).

5.3 Correction data transmission via radio channel

Different RTK corrections message formats exist. The Radio Technical Commission of Maritime Services (RTCM) has proposed a standard on the content of correction messages, called RTCM SC-104. Each RTCM data record contains several MT for various contents. Each message comprises header and body. Table D.2 in appendix D shows the different RTCM message types and their content. For carrier-phase positioning systems, two pairs of RTK messages are defined in the RTCM standard. The MT 18 and 19 contain raw carrier phase and pseudorange measurement information while MT 20 and 21 contain corrections for the carrier-phase and pseudorange measurements respectively. The corrections are defined as

$$\delta\phi = \frac{1}{\lambda_i}(\rho_{exp} - b_{sv}c + b_{base}c) - \phi_j - A \tag{5.3.1}$$

$$\delta R = \rho_{exp} - b_{sv}c + b_{base}c - R_j \tag{5.3.2}$$

where

ρ_{exp} = computed range from the base to the satellite
b_{sv} = satellite clock offset computed from the downlink satellite clock model
b_{base} = estimated clock offset of the base receiver
A = arbitrary constant integer number of cycles chosen at the start of tracking to keep the size of the correction small

These corrections can be applied directly to the rover measurements rather than doing a difference between the base and the rover measurements. However, there are some significant limitations to the RTCM standard which should be considered for RT applications. The RTCM SC-104 MT 18 to 21 provide most of the information required for a successful RTK system, however the size of the messages and their framing overhead make them inefficient for high frequency observations [21].

Another commonly used message format is the CMR (Compact Measurement Record[1]) developed by *Trimble* which encompasses both a message protocol and a compression/decompression algorithm for measurement data. Three MT are defined for RTK positioning: measurements, reference station location and reference station description. Measurement compression technique enables a data transmission at a 2400 baud bandwidth. Details on the used techniques are described in [21]. So, while RTCM SC-104 requires at least a 4800 baud communication link between the base and the rover units, the CMR format provides a compressed transmission standard which requires less than half the bandwidth of the equivalent RTCM message.

5.4 Test flight using GPS-RTK on board solution for direct georeferencing

A survey flight above the calibration field near Sion was organized in order to test a GPS-RTK architecture. The goals of the test are (1) to define an optimal setup (receiver configuration and hardware design), (2) to check the communication link quality between the base and the rover receivers, (3) to provide a first evaluation of the quality RTK-GPS observation and (4) to present the first results on the RT-point-cloud generated by using RTK trajectory.

5.4.1 Architecture

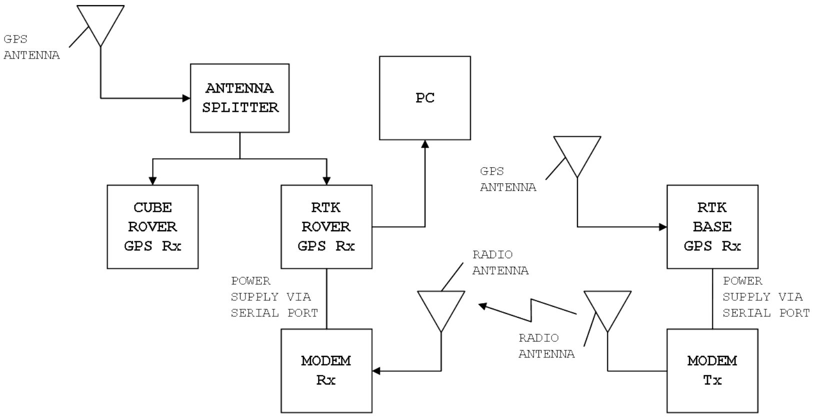

Figure 5.3: GPS-RTK solution architecture used during test flight.

The weak point of the GPS-RTK solution lies in the communication link between the base and the rover receiver. The long base lines as well as the mountainous topography of most of the flights involve the need of sufficient signal strength for receiving RTK corrections. The selected radio transmitter power is therefore as such to enable a range of about 6 to 8 [km] in situations where no major obstacles hinder wave propagation. The radio receiver antenna was mounted directly on the mapping sensor head, pointing down. The CMR+ correction message format was chosen because of the advantages mentioned in section 5.3. The hardware design is

---

[1] The new version of CMR format is called CMR+.

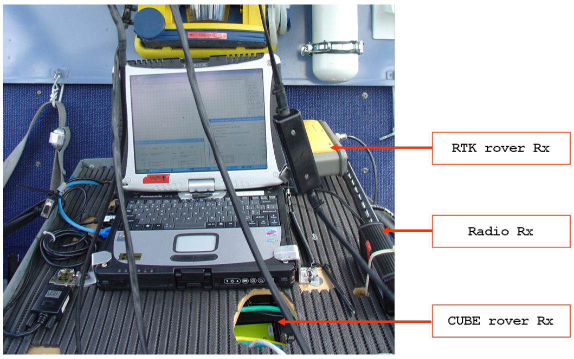

Figure 5.4: Architecture realization on the rover used during the test flight.

shown in figure 5.3. Two GPS receivers (rovers) are connected through a splitter to the same antenna. One receiver (CUBE) is configured in standalone mode enabling the classical carrier-phase PP for comparison, while the other runs in RTK mode. The modem is connected to the GPS receiver via serial port providing 12 [Volts] output for powering the radio receiver. Due to the distance between the CUBE and the sensors, it was necessary to use a cable between the radio antenna and the radio box, despite the fact that some losses could occur.

5.4.2 Results

In order to evaluate the quality of the RTK observations, a reference trajectory obtained by PP carrier-phase using *GrafNav* software is considered. The ambiguities could be resolved for the entire treated trajectory in the reference solution. Figure 5.5 shows the reference trajectory (black line with squares) as well as the RTK provided points. The green points are fixed solutions while the red ones are standalone code solutions. The rover receiver was configured in such a way that if no correction message is received at a given epoch, the receiver will either provide the current standalone solution or compute the position later when the message arrives. This delay is problematic in kinematic mode because the provided delayed position will be given at the current GPS time, involving two solutions for one position (one standalone and one corrected) but with two different GPS times! A *Matlab* routine was implemented to correct this and to remove the standalone solution for the epochs where a delayed fixed solution is present. The zoom in figure 5.5 shows two fixed solutions and two standalone points. At the epoch preceding the lack of two observations (second point from the left), no correction message was received. So, a standalone solution was provided by the receiver for this epoch and later removed. The correction message was received at the epoch corresponding to the third point. At this time, the receiver processes the RTK solution for the previous point and doesn't enable a solution for the current time. That is the reason why no solution is provided at the third epoch. This add-hoc correction was necessary in order to use the data file for integrating the GPS positions with those provided by the IMU and the laser unit, and to compare the solutions with the reference trajectory. If we consider the post-processed positions as errorless reference, the obtained accuracy of fixed RTK positions expressed in a local frame (shown by the green dots in figure 5.6) is mainly below 10 [cm]. The existing bias on the vertical could be related to the station height at the reference point. The performance of

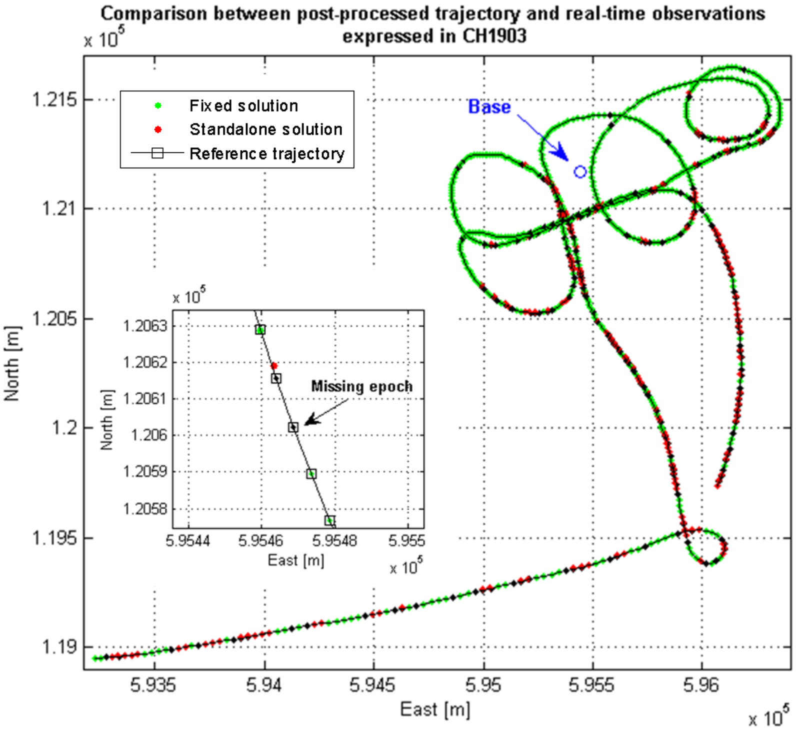

Figure 5.5: Comparison between post-processed trajectory and RTK observations.

the provided RTK accuracy measure is shown in figure 5.7 presenting the Stanford plots of the horizontal and vertical error 3-σ intervals. It can be seen that the receiver estimated accuracy is too optimistic according to the real error computed by using the reference trajectory, and could therefore be corrected by applying a correction factor in a similar manner as presented in section 4.5.

The radio link signal quality is analyzed for the entire flight in order to evaluate the operational range. The quality is mainly above 80 [%], and this even for base lines which have a length of 7 [km]. This suggests that the practical communication link range could be above 10 [km] for the given radio output power. The base line length is only one factor determining signal degradation. The flight dynamic, and particularly the speed have strong influences on the radio link quality because of the type of used radio receiver antenna. The figure 5.8 confirms this by showing that bad radio signal quality occurs mainly during the transfers and the turns where the receiver antenna is not vertical.

Considering these results, several changes should be made to optimize the results provided by RTK-GPS. First of all, the processing of correction messages should be configured to extrapolation mode. In this mode, the rover will extrapolate the missed base station's carrier-phase measurements when computing its RTK solution. This should improve the stability and fixed solution availability. Furthermore, in such a setup, further correction are needed to match the GPS times. Secondly, the radio receiver antenna structure should be rigid in order to remove the dependence on the flight speed, i.e. antenna instability, of the radio link quality.

The next section presents the first results of the laser point cloud generation by using directly the time corrected RTK-GPS trajectory. The architecture of the RT data processing system developed at EPFL that enables the production of a georeferenced laser point cloud is briefly described in chapter 6.

5.5 Direct laser point cloud georeferencing using RTK-GPS/INS integration

The RTK provided observations are integrated with the IMU observations in the RT Kalman filter in order to obtain position and attitude data at a sufficient rate for the laser point georeferencing. Theoretically, if some isolated standalone positions affect the trajectory, the Kalman filter should reduce their influence through adequate stochastic modeling. The accuracy estimation provided by the receiver is adapted according to the solution type. Nevertheless, a long period of adjacent standalone points could seriously affect the quality of the filtered trajectory, and thus the quality of the generated laser-point cloud.

A reference laser-point cloud was computed by using post-processed observations and served estimating the accuracy of the RT-generated-laser point cloud. The accuracy of the point

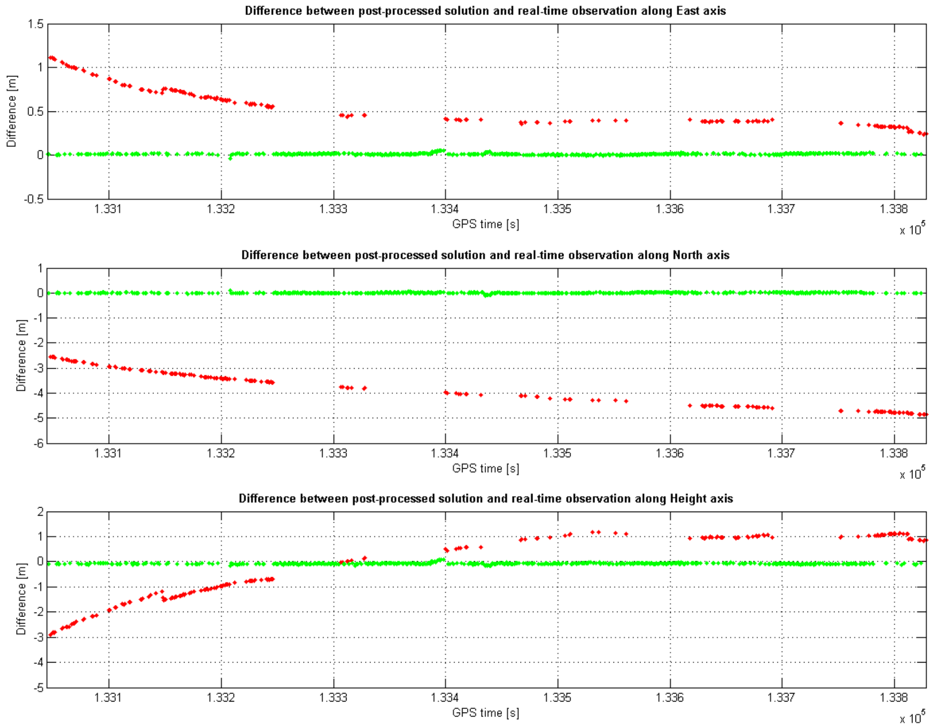
Difference between post-processed solution and real-time observation along East axis

Difference between post-processed solution and real-time observation along North axis

Difference between post-processed solution and real-time observation along Height axis

Figure 5.6: Accuracy of the RTK (green) and standalone (red) solutions along the three axis obtained by computing the unsigned difference between the reference points and the real-time acquired positions.

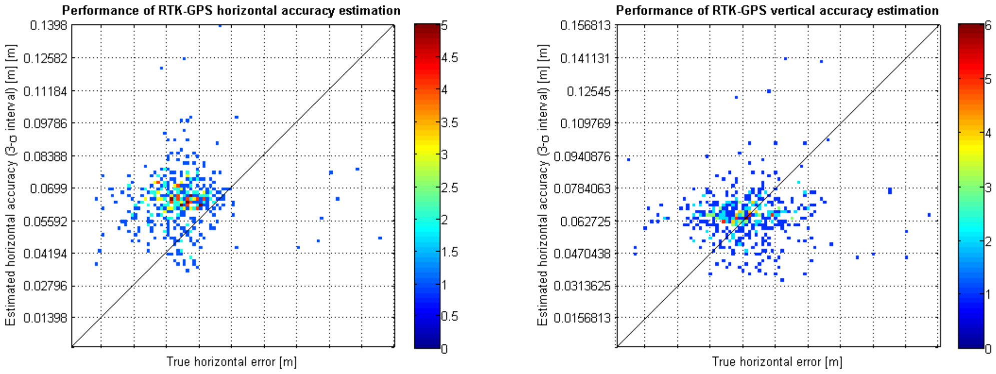

Figure 5.7: Performance of RTK-GPS 3-σ horizontal (left) and vertical (right) accuracy estimation by comparing with the true error.

coordinates are shown in figure 5.9. The planimetric accuracy lies in range of 1 to 4 [cm]. The altimetric accuracy is affected by a bias of 10 [cm] which could be a consequence of some imprecisions in the reference antenna height measurement, which was also observed in the GPS-RTK solution. It should be noted that only the flight lines with high frequency of fixed positions are treated in order to evaluate the potential of this approach. Effects of standalone solutions in the Kalman filter solution as well as the influence of the Kalman filter in-flight initialization are not investigated in this work. A stabilization of the ambiguity fixing through optimal receiver configuration and hardware design as well as optimal Kalman filter tunning should largely improve the results. Nevertheless, further tests need to be performed to evaluate the behavior of the RTK architecture, i.e. the radio link and solution type behavior, in less favorable conditions than those of this test flight.

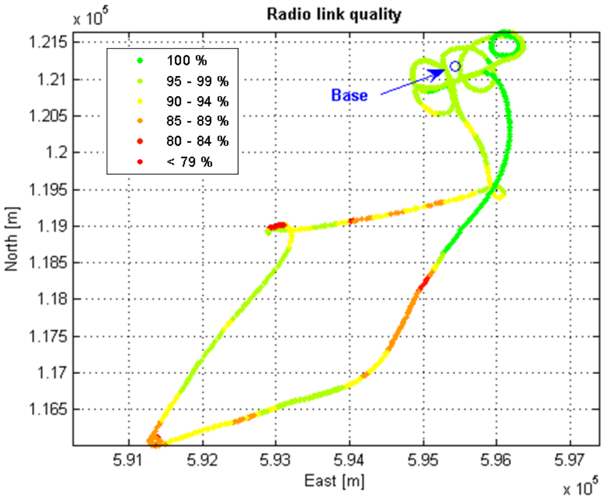

Figure 5.8: Radio link quality obtained during the flight.

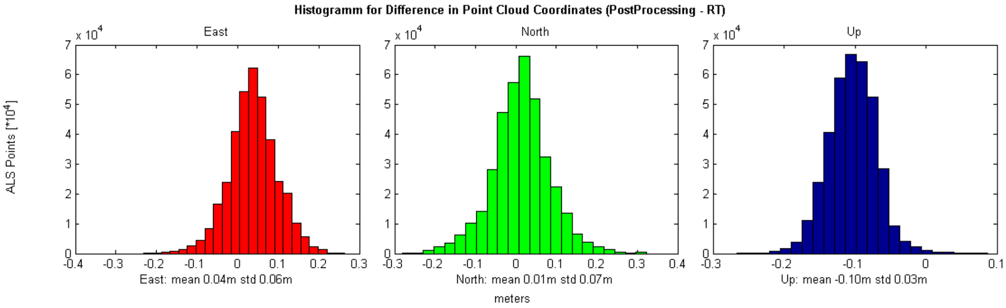

Figure 5.9: Histogram for difference in point cloud coordinates (PP - RT).

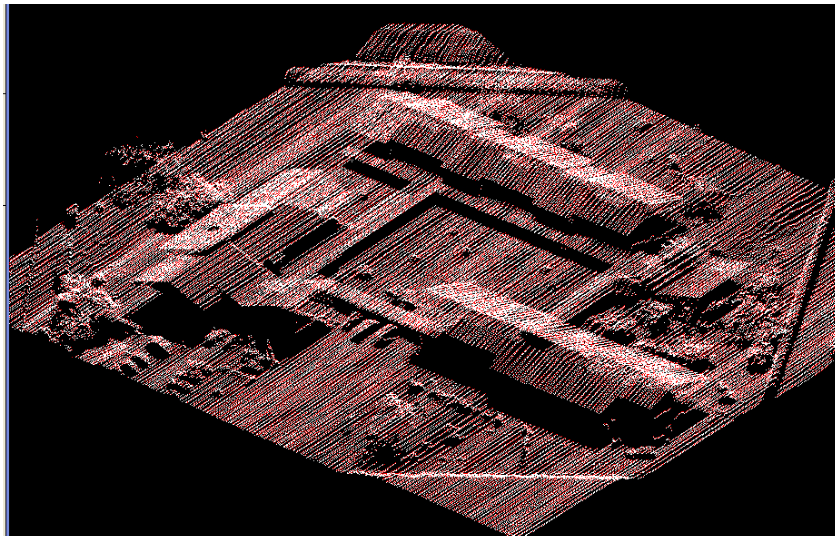

Figure 5.10: RT point cloud (red points) and reference point cloud (white points) issued from PP observations.

5.6 Conclusion

The potential of using and RTK-GPS in-flight solution with radio communication channel has been demonstrated. The optimal receiver configuration as well as the main hardware design have been highlighted in order to obtain a fully operational system. The first test shows that in good conditions (high fixed position rate), a RT-generated-laser point cloud can be obtained with an accuracy below 10 [cm]. This is an attractive alternative in cases where results must be obtained shortly after the flight as well as an ultimate control for positioning integrity (e.g. by means of laser scanning overlap between times).

Chapter 6

Real-time integrity monitoring system architecture

This chapter deals with the developed integrity check tools as well as their integration in the RT GPS/INS/Laser monitoring system available at TOPO lab. The final approach adopted for representing the GPS quality information is also described and represented by mean of illustrations.

6.1 System architecture

The quality check approaches presented in chapter 3 need to be integrated in a single environment following a "best from available" strategy. According to the adopted development strategy, all the selected algorithms evaluated in chapter 3 have been combined in a C++ tool called *Visint*. Nevertheless, it has been shown in chapter 3 that cycle slip detection on L1 carrier-phase as well as interference detection are subject to the sensitivity of the chosen parameters. This will seriously affect the reliability of the given results and requires therefore further tunning of the algorithm. According to these considerations, it has been chosen to use only algorithms that provide reliable information for the RT quality check. This choice is motivated by the fact that false alarms provided by the quality check procedure during flights could have strong economical consequences. Figure 6.1 presents the global architecture of the quality monitoring tool. Details of the used algorithms for PM and RT integrity checks are described in the following sections.

6.2 Integrity check tool VISINT

According to the defined strategy (see chapter 2), the tested QI and algorithms in chapter 3 have been implemented into a quality control tool called *Visint*. It follows the architecture presented in figure 6.1. This application enables fast decoding and processing of the raw GPS log files and generates an ASCII quality check report file shortly after the flight. Furthermore, the development of such a tool enables the validation of the translation of the algorithms from

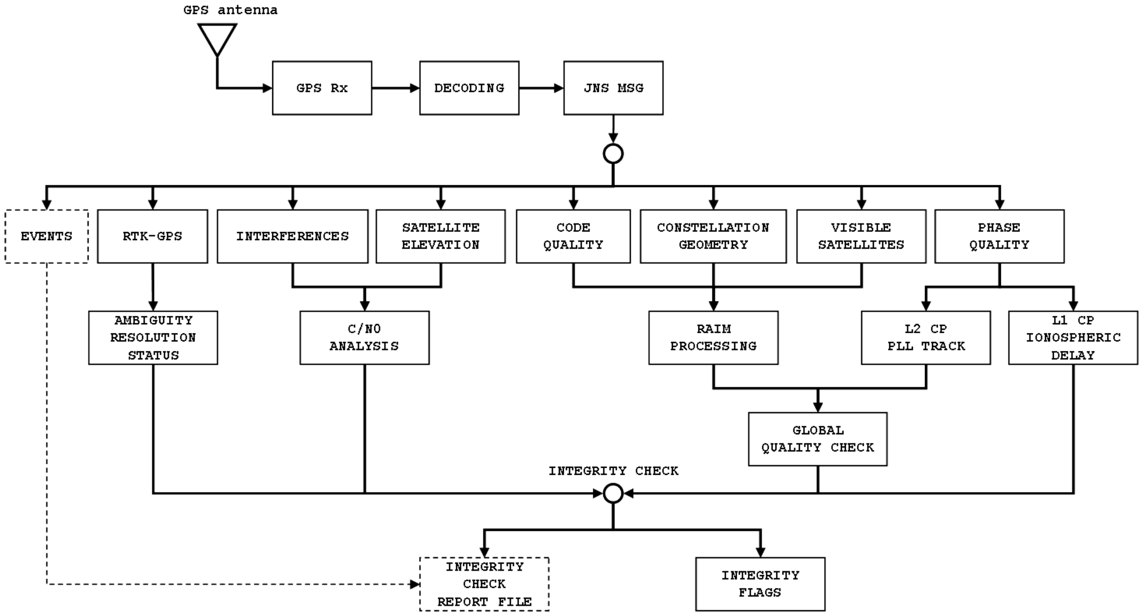

Figure 6.1: Global integrity check architecture. The spotted boxes are specific to the post-mission integrity check tool.

the *Matlab* to the C++ language with a perspective of RT implementation. The figure 6.2 shows an example of report file provided by *Visint*. A satellite specific report enables a quick view on the detected cycle slips and interferences for each epoch. Furthermore, the number of visible satellites provides a direct view on possible signal losses. The RAIM processing results as well as the solution type are also indicated. The tool enables several options like the choice of the cycle slip detection algorithm for example. L2 cycle slips are assumed in epochs where the phase tracking loop hasn't locked any signal while L1 cycle slips are detected by using ionospheric features (see section 3.2). RAIM processing results as well as the complete proposed interference detection algorithm described in 3.3 are also used and presented in the report file. Despite the fact that the given result is very similar to the one obtained by the *TEQC* tool [4], the main interests of *Visint* lie in the detection and representation of the camera events and in faster processing[1]. Through this approach, the relation between the GPS quality and the importance of the epochs can be associated with flight lines, which improves the decision in the airborne-mapping context. For example, bad GPS observation quality during transfer flights will have less importance than problems occurring within flight lines.

6.3 HELIPOS environment for in-flight data quality monitoring

Helipos is an in-flight data quality monitoring and flight management tool currently under development at EPFL. The RT sensor integrations as well as the RT point cloud georeferencing

---

[1] This is due to the fact that the TEQC tool requires a RINEX file. Thus, the receiver log file needs first to be converted. Furthermore, the RINEX file doesn't contain all needed QI messages.

```
GPS INTEGRITY CHECK REPORT (VISINT)
***********************************

   IC file date:                   Wed May 07 13:35:52 2008
   Readed JNS file:                travers.gps
   IC file:                        OUT.txt
   Observation interval:           32 [obs]  (32 [sec])
   Number of observations:         4499
   GPS observation frequency:      1 [Hz]
   Satellite elevation mask:       15.00 [deg]
   GPS time of start of window:    10:31:25 2007
   GPS time of end of window:      11:46:23 2007
   Cycle slip detection mode:      L1 phase lock time analysis

Satellite specific IC and interference detection

   Events                       *                                 ***** ****  ****** ***** ******   ****** ****** ****** ****** *****         ********
   SV 11          ----x-------------------------------------------------------II----------------------------------------------------------------------I-------------
   SV 20          ----x-------------------------------------------------------II------------------------------------------------------------------------------------
   SV  1          ----x-------------------------------------------------------II------------------------------------------------------------------------------------
   SV 14          ----x-----------------    I  III--IIII------IIII II^^^^^^^      II^^^^^^^^     II^^^^^^^^I   III^^^^^^
   SV 23          ----x--------------II----------------IIIIIII--------IIIIII--II------------------------------------------------------------------------------------
   SV 19          ---^^^^^^^^^^^^^^^^III^^^^^^^^       II
   SV 31          ^^^^^^^^^^^^^^^^^^^-----------------------------------------II------------------------------------------------II--II---IIIII------------------II--
   SV 28          IIIIIIIIIIIII      IIIIIIIIIIII III^I
   SV 32          ----x-------------------  II--------------------------------II--   II------------II------------III--I   II-I-IIIIIII- I-        IIIIIIIIIII
   SV 17              I-IIIIII--------------IIIIIIII--------------------------II-----------------------------------------------------------------------------II-----
   SV 13          -                                                           I^^^^    I III^^^^^^      III^^^^^^      I^^^----III I----II---IIIII----       I-----
   SV  4          -                                                                                           III^^^^^^II^^^^^^^^^^^^ III^^^^I^ I^^^^^^^^^^^II^^
   SV 25                                                                                                      I^            II^II^  IIIIIII    I^I^^^
   Interf.            X
   Time           |+++++++++|+++++++++|+++++++++|+++++++++|+++++++++|+++++++++|+++++++++|+++++++++|+++++++++|+++++++++|+++++++++|+++++++++|+++++++++|+++++++++|++++++++|
                  10:31:25                                                                                                                                  11:46:23

   Legend:        ' ' = sat. not observed    '-' = sat. observed    'x' = interference    'I' = cycle slip    '^' = sat. below elevation mask

Solution types

   Status:        ~~~~~~~~~~~~~~~~~~~~~~~~~~~~~~~~~~~~~~~~~~~~~~~~~~~~~~~~~~~~~~~~~~~~~~~~~~~~~~~~~~~~~~~~~~~~~~~~~~~~~~~~~~~~~~~~~~~~~~~~~~~~~~~~~~~~~~~~~~~~~~~~~~~~~~

   Legend:        '~' = standalone    '-' = DGPS    '/' = RTK float    '|' = RTK fixed

Results of RAIM processing

   Status:        -x-------------------------------------------xx---------------------------------xxxx--0xxxxxxx--------------xxxxxxx------x-----x------------------

   Legend:        '-' = normal    'x' = no RAIM    'I' = Fault detected and excluded    '0' = RAIM off
```

Figure 6.2: VISINT integrity check report file.

and analysis is performed in this environment. The figure 6.3 shows the global architecture of the *Helipos* environment. The data provided by the GPS and the IMU sensors are integrated through RT Kalman filtering. His output enables the generation of precise position and attitude observations at high frequency (400 Hz) for the RT laser point cloud georeferencing. The position and attitude given by the Kalman filter are also sent to the *Helipos* interface enabling the data viewing and especially the current tracked position representation. The RT

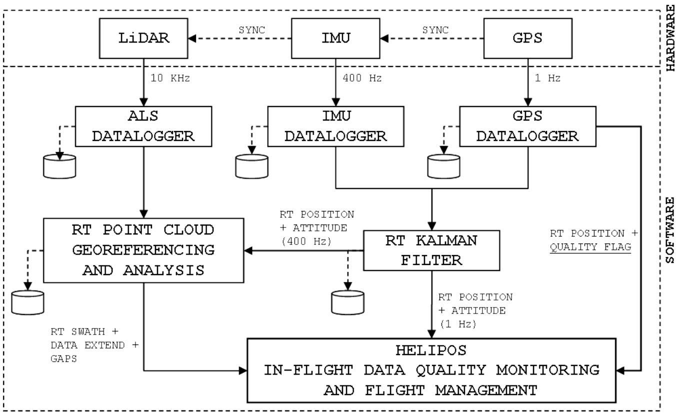

Figure 6.3: Architecture of the *Helipos* environment under development at EPFL. The quality check class is implemented at the GPS datalogger output and the flag is sent via binary message directly to *Helipos* interface.

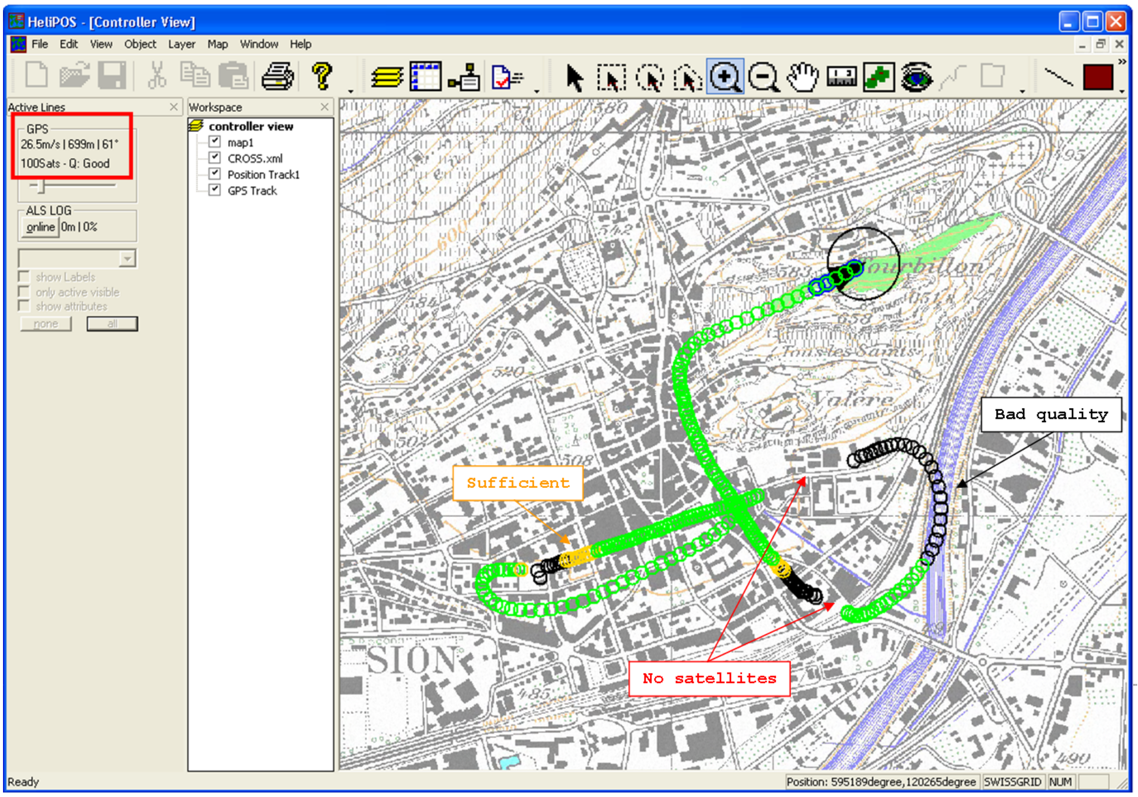

GPS
26.5m/s | 699m | 61°
100Sats - Q: Good

ALS LOG
online 0m | 0%

Position: 595189degree,120265degree

Figure 6.4: Representation of the GPS quality in the *Helipos* environment.

GPS quality check tool has been coded and implemented as an independent C++ class called at the output of the GPS datalogger. After GPS message decoding step, the raw messages are given as input in the class and a resulting quality flag is sent after processing through predefined binary message to the *Helipos* for representation (see figure 6.3). The adopted representation of the GPS observation quality is shown in figure 6.4 as a snapshot view of the interface during the flight. The GPS quality is shown through two indicators. The first is the actual GPS quality field (red frame on the top left in figure 6.4) while the second is represented as a history of color-coded circles on the map. Four colors have been defined for each possible flag: `good` (green), `sufficient` (red), `critical` (yellow) and `bad` (black). This approach provides a simple and clear view of the quality information during the flight and improves decision making for the flight-operator.

6.4 Performance of the system

The results obtained by the *Visint* tool have been tested on all the available log files and then compared with results obtained by the *GrafNav* and *TEQC* tools. Furthermore, the application has been successfully engaged during the last surveying flights. The RT GPS quality monitoring tool has been implemented in a flight simulator whose GPS module is called *RFlows*. It enables the time serving of datas read from raw GPS data files as well as

IMU and laser scanner observation files. This enables the replaying of past flights as well as the visualisation and management simulation through the *Helipos* interface. The developed GPS quality check class has been debugged and tested in this simulator with a perspective for its future implementation in the real environment. The problematic time intervals previously identified in the PP solutions have been compared with the QI provided in *Helipos* during the flight replaying. The example in figure 6.4 shows a problematic part of the flight in terms of satellite signal tracking. The results correspond to the conclusions made in chapter 3 with respect to algorithms and indicators.

Note As the simulation is based on raw GPS data, epochs containing not enough observations for obtaining a position fix are not present in the logfile. This is the reason why no QI are given during these periods.

Chapter 7

Conclusion

This chapter provides the synthesis of the main results obtained in this thesis and identifies interesting possibilities for further development.

7.1 Synthesis

This work aimed to improve the GPS data quality control in the context of airborne-mapping missions that requires differential carrier-phase processing. In cases where data from the reference receiver are not available in RT, we focused on identifying the relevant QI for signals tracked by the rover. From that following conclusions can be drawn

1. The detection of cycle slips on the carrier-phases is of great importance and should therefore be performed in RT to provide indications on the phase quality.
2. The use of RAIM provides a synthetic and complete information on the signal quality since it covers a large number of factors like the constellation geometry, the number of satellites or the code quality. Furthermore, the combination of RAIM processing with phase quality monitoring by mean of cycle slip detection forms a relevant signal quality indicator with respect to PP.
3. WAAS/EGNOS differential corrections improve significantly the positioning quality and provides relevant accuracy measures after the application of a correction factor on the receiver estimations. Further kinematic tests need to be carried out to confirm these advantages.
4. RT quality monitoring for airborne-mapping missions enhance GPS integrity by providing informations that warn immediately the mission-operator about problematic flight-lines. For achieving this goal, QI like C/N0, cycle slip presence and RAIM are combined to provide a quality information for each epoch.

Later, we focused on testing RTK in a flight, as an ultimate integrity check for the differential phase data. Based on this experience the following conclusion can be made.

1. The obtained GPS positioning accuracy is below 10 [cm] in the case of optimal communication link quality between the base station and the moving rover. Nevertheless, further tests need to be carried out in less favorable conditions that those of the experimental flight.

2. The potential of using RTK solution is high since a RT laser-point cloud could be calculated with an accuracy comprised between ± 10 [cm]. Effects of RT Kalman filtering as well as the use of the provided accuracy for integrity purposes must be developed.

7.2 Outlook

The outcome of the thesis resulted in a GPS quality monitoring tool working in RT. It is now possible to detect problematic periods in terms of bad code and phase quality as well as in terms of insufficient number of satellites. Further work could be made to impre the GPS solution by using WAAS/EGNOS differential corrections. If the static experiment presented in this thesis has the first conclusions, a kinematic test needs to be carried out in order to provide relevant conclusions within the airborne-mapping context. But the main potential for direct georeferencing lies in the use of the RTK-GPS. By performing further tests with the configuration proposed in chapter 6, the encountered problems should be resolved and the laser-point cloud could be acquired with the accuracy fulfilling the requirements directly in RT. To achieve this, the effect related to the Kalman filter initialization and the reliability of the RTK accuracy measures need to be further investigated.

Bibliography

[1] Carosio, A. (1994): *Fehlertheorie und Ausgleichungsrechnung*, Band 1, Eidgenoessische Technische Hochschule Zuerich.

[2] El-Rabbany, A. (2002): *Introduction to GPS, the Global Positioning System*, Artech House, Boston, London.

[3] ESA (2005): *EGNOS factsheet 3: Integrity Explained.* http://www.egnos-pro.esa.int/Publications/fact.html

[4] Estey, L.H. and Meertens, C.M. (1999): *TEQC: The Multi-Purpose Toolkit for GPS/-GLONASS Data*, GPS Solution, Vol. 3, No. 1, pp. 42-49.

[5] Gao,S. and al. (2004): *Analysis of Regional Ionospheric Disturbance with HK GPS Network*, 2004 Int. Symposium on GNSS/GPS, Sydney, Australia.

[6] Gerdan, G.P. (1995): *A Comparison of Four Methods of Weighting Double-Difference Pseudorange Measurements*, Trans Tasman Surveyor, Vol. 1, No. 1, Canberra, Australia.

[7] Hartinger, H. and Brunner, F.K. (1998): *Attainable Accuracy of GPS Measurements in Engineering Surveying*, Proceedings of FIG XXI International Conference, 21-25 July, Brighton, U.K., Commission 6, pp. 18-31.

[8] Hoffman-Wellenhof B., Legart K. and Wieser M. (2003): *Navigation - Principles of Positioning and Guidance*, Springer Verlag, Wien, New York.

[9] Hugentobler, U., Schaer S, Fridez P. (2001): *Bernese Manual Reference 4.2*, University of Berne, Switzerland.

[10] Jin, X. (1996): *Theory of Carrier Adjusted DGPS Positioning Approach and Some Experimental Results*, Ph.D. thesis, Delft University Press, The Netherlands.

[11] Kaplan, E.D (1996): *Understanding GPS: Principles and Applications*, Artech House Publishers.

[12] Kim, D. and Langley, R.B. (2001): *Instantaneous Real-time Cycle-slip Correction of Dual-frequency GPS data*, in Proc. KIS 2001, pp. 255-264, Banff Alberta, Canada.

[13] Langley, R.B. (1997): *GPS Receiver System Noise*, GPS World, Vol. 8, No. 6, pp. 40-45.

[14] Leva, J.L. (1994): *Relationship between Navigation Vertical Error, VDOP, and Pseudorange Error in GPS*, IEEE Transactions On Aerospace And Electronic Systems, Vol. 30, No. 4, pp. 1138-1142.

[15] Lipp, A. and Gu, X. (1994): *Cycle-slip Detection and Repair in Integrated Navigation Systems*, PLANS, pp. 681-688.

[16] Ndili, A. and Enge, P. (1998): *GPS Receiver Autonomous Interference Detection*, Presented at the 1998 IEEE Position, Location and Navigation Symposium - PLANS 1998.

[17] Neumann, J.B., Van Dierendonck, K.J., Manz, A., Ford, T.J. (2000): *Real-time carrier phase positioning using rtcm standard message types 20/21 and 18/19*, GPS-ION 2000.

[18] Satirapod, C. and Wang, J. (2000): *Comparing the Quality Indicators of GPS Carrier Phase*, Geomatics Research Australasia, No. 73, pp. 75-92.

[19] Sleewaegen, J.M. (1997): *Multipath Mitigation, Benefits from Using the Signal-to-Noise Ratio*, 10th Int. Tech. Meeting of the Satellite Division of the U.S., Inst. of Navigation GPS ION'97, Kansas City, Missouri, pp. 531-540.

[20] Talaya, J. (2003): *Algorithms and methods for robust geodetic kinematic positioning*, Ph.D. thesis, Universitat Politécnica de Catalunya.

[21] Talbot, N.C. (1996): *Compact data transmission standard for high-precision gps*, GPS-ION 1996.

[22] Tiemeyer, B. (2002): *Performance Evaluation of Satellite Navigation and Safety Case Development*, Eurocontrol Experimental Centre, Report no. 370.

[23] Van Diggelen, F. (1998): *GNSS Accuracy: Lies, Damn Lies, and Statistics*, GPS World, Vol. 9, No. 1, pp. 41-45.

[24] Wilson, D.L. (2008): *David L. Wilson's GPS Accuracy Web Page*, http://users.erols.com/dlwilson/gps.htm.

[25] Xu, G. (2007): *GPS: Theory, Algorithms and Applications*, Berlin: Springer,2nd ed. edition.

Appendix A

VISINT post-mission quality check tool

A.1 Use of VISINT

The *Visint* PM quality check tool decodes *Javad/Topcon* binary files based on the JNS messages that can be found in the GPS Receiver Interface Language (GRIL) manual[1]. The minimum program arguments must be specified by

```
>visint infile outfile
```

The `infile` argument represents the receiver logfile that must be entered by his full name (with the file extension) while `outfile` is the chosen output filename in which the quality report is written. Several options are available for the generation of the report file. These options must be specified as additional arguments

```
>visint infile outfile [-f ****] [-i ****] [-cs ****] [-mask ****]
```

The `****` fields must be replaced by the desired value. The `-f` option can be used to change the GPS observation frequency. By default, this value is set to 1 [Hz]. The `-i` option represents the desired time span used for summarizing the quality information. By default, the interval is computed in such a manner that the report file can be printed in A4 format. The `-cs` option enables to choose the used cycle slip algorithm that will be applied on L1 carrier-phase. The different possible values are

- `L1ionodelay`: use of time derivative of ionospheric delay,
- `L1locktime`: use of phase tracking loop output,
- `L1doppler`: use of Doppler integration,
- `nocycleslip`: no cycle slip detection wanted.

---

[1] This manual can be found on `www.javad.com`

By default, only the cycle slips on L2 are detected by using the phase tracking loop output for the L2 carrier-phase. The `-mask` option enables to specify the elevation mask in degrees. By default, this value is set to 15 [deg].

A.2 Structure

The global structure of the `VISINT` application is shown in figure A.1.

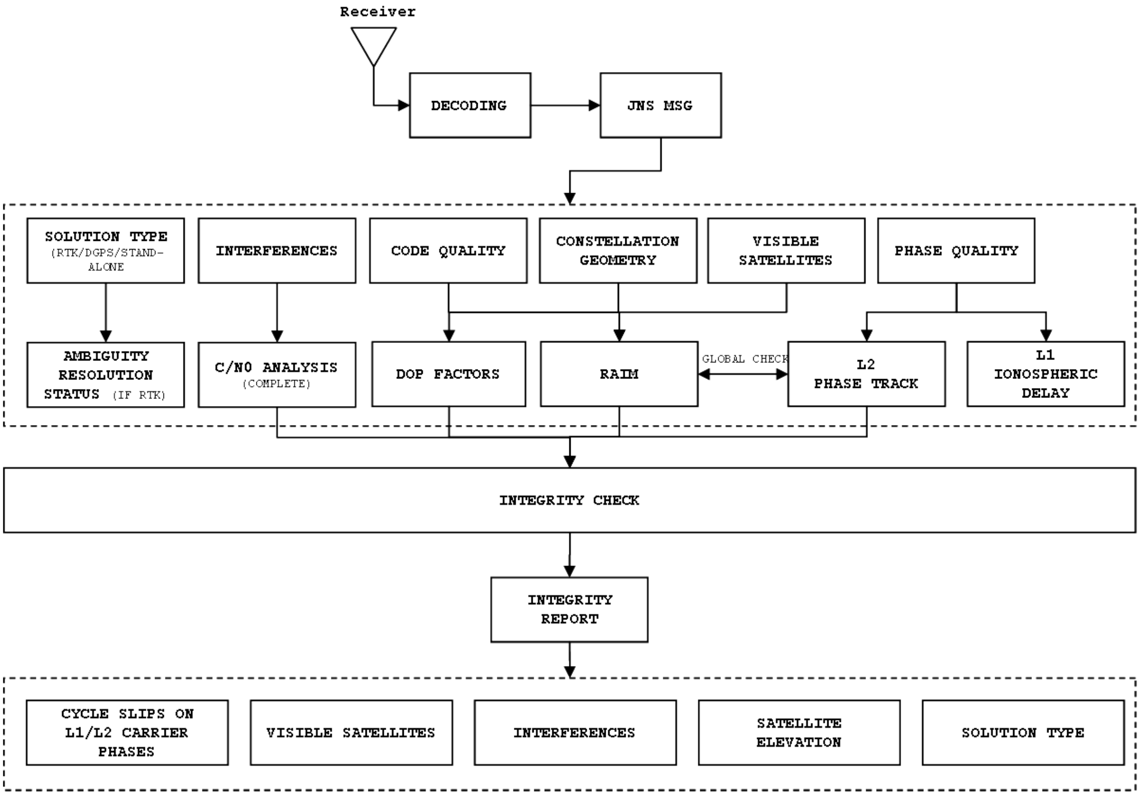

Figure A.1: Global structure of the `VISINT` application.

A.3 C++ code

The complete C++ code for the *Visint* application is provided in the additional CD.

Appendix B

C++ real-time quality check class

B.1 Structure

The global structure of the `integrity` class implemented in *Helipos* is shown in figure B.1.

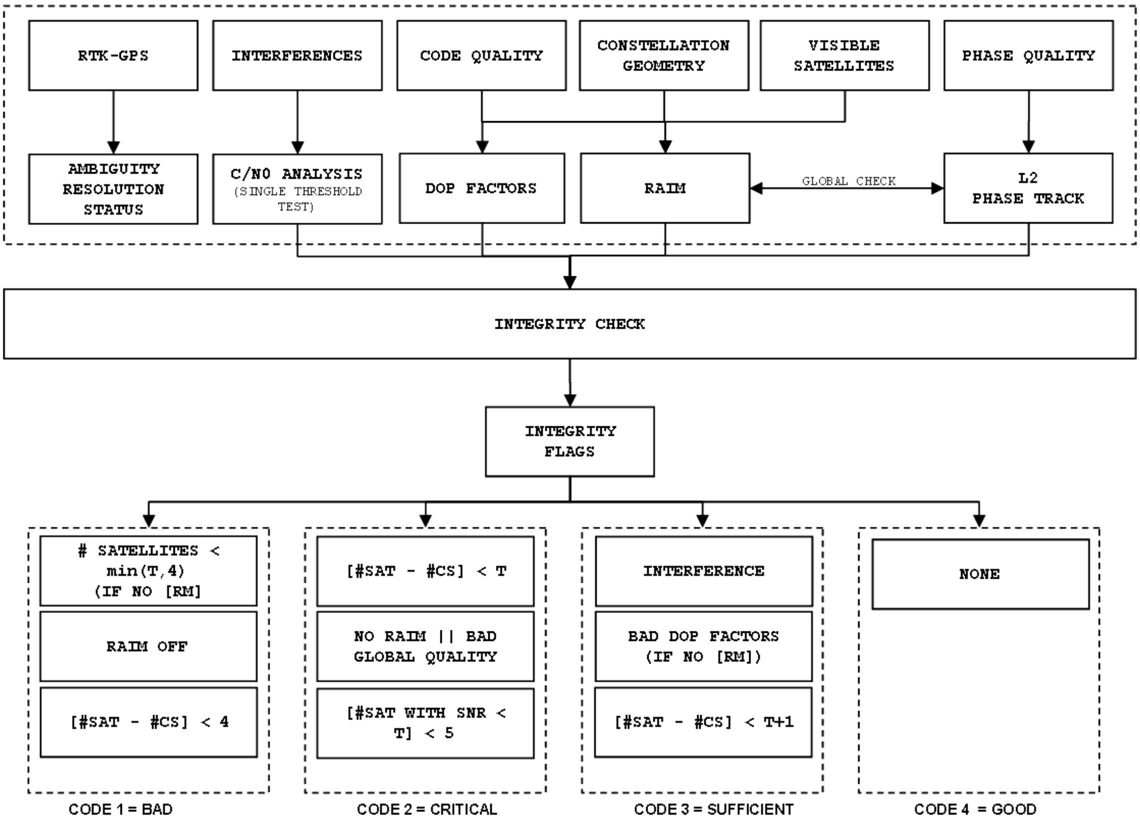

Figure B.1: Global structure of the `integrity` class.

B.2 C++ code

The C++ source file of the `integrity` class is given below. The output of the different algorithms shown in figure B.1 are classified according to their degree of importance. So if two algorithms give a warning, the worst case will be given as output and therefore as quality flag.

```

#include "stdafx.h"
#include "integrity.h"

//
//  FUNCTION: CGPSQual()
//
//  PURPOSE: CGPSQual class default constructor.
//
//  PARAMETERS:
//    None.
//
//  RETURN VALUE:
//    None.
//
//  COMMENTS:
//
//    This is the default constructor of the CGPSQual class.
//    Initializes the classe's attributes.
//
CGPSQual::CGPSQual()
{
    Tsat            = 5;
    Tdop            = 10;
    Tsnr            = 20;
    elevMask    = 10;
    raimAl      = false;
    alarm       = false;
    prev            = 0;
    counter     = 0;
    GloCheck    = false;
}

//
//  FUNCTION: ~CGPSQual()
//
//  PURPOSE: CGPSQual class destructor.
//
//  PARAMETERS:
//    None.
//
//  RETURN VALUE:
//    None.
//
//  COMMENTS:
//
//    This is the destructor of the CGPSQual classe.
//
//
CGPSQual::~CGPSQual()
```

```
{
}

//  FUNCTION: check( SMsgDP &dp , SMsg2P &twop , SMsgEL &el, SMsgEC &ec, ...
//            SMsgRM &rm, int &nrSat, QCFLAG &Prev ,  bool &Alarm, ...
//            bool RaimAl, QCFLAG Counter, bool RAIM )
//
//  PURPOSE: GPS quality check
//
//  PARAMETERS:
//    - SMsgDP &dp: [DP] JNS message
//    - SMsg2P &twop: [2P] JNS message
//    - SMsgEL &el: [EL] JNS message
//    - SMsgEC &ec: [EC] JNS message
//    - SMsgRM &rm: [RM] JNS message
//    - nrSat: number of satellites
//    - Prev: number of remaining unaffected satellites of
//      previous epoch
//    - Alarm: status of global check algorithm
//    - RaimAl: status of RAIM in global check algorithm
//    - Counter: number of stable epochs in global raim
//      algorithm
//    - RAIM: true if RAIM wanted
//
//  RETURN VALUE:
//    Quality flag
//
//  COMMENTS:
//
//    This is the main method to call for quality check.
//
QCFLAG CGPSQual::check( SMsgDP &dp , SMsg2P &twop , SMsgEL &el, SMsgEC &ec,
    SMsgRM &rm,...
        int &nrSat, QCFLAG &Prev ,  bool &Alarm, bool RaimAl, QCFLAG Counter,
            bool RAIM )
{
    QCFLAG flag(11);

    if ( nrSat < Min(Tsat,4) )
        flag = 1;                                           //1

    if ( nrSat < Tsat )
        flag = 1;                                           //1

    if ( L2TrackCheck( twop, nrSat ) < Min(Tsat,4) )
        flag = 2;                                           //1

    if ( L2TrackCheck( twop, nrSat ) < Tsat )
        flag = Min(flag,3);                          //2

    if ( L2TrackCheck( twop, nrSat ) < Tsat + 1 )
        flag = Min(flag,4);                          //3

    if ( DOPCheck( dp ) )
        flag = Min(flag,5);                          //3

    if ( InterfCheck( ec, el, nrSat ) < Tsat )
```

```
        flag = Min(flag,6);                         //3

    if (RAIM)
    {
        switch ( RaimRes(rm) )
        {
        case 1:
            // no RAIM
            flag = Min(flag,7);                     //2
            break;

        case 3:
            // RAIM turned off
            flag = 10;                                      //1
            break;
        }

        if ( ( RaimRes(rm) == 1 ) && ( L2TrackCheck( twop, nrSat ) < Tsat ) )
            flag = 8;                                           //2

        // Global check using RAIM and CS wanted
        if (GloCheck)
        {
            if ( L2RaimCheck( rm, twop, nrSat, Prev, Alarm, RaimAl, Counter ) )
                flag = Min(flag,9);                 //2
        }
    }

    // Return integrity flag
    return flag;
}

//
//  FUNCTION: L2TrackCheck( SMsg2P &twop, int &nrSat )
//
//  PURPOSE: Return number of unaffected satellites
//
//  PARAMETERS:
//    - twop: [2P] JNS message
//    - nrSat: number of satellites
//
//  RETURN VALUE:
//    Number of unaffected satellites
//
//  COMMENTS:
//
//    This method returns the number of satellites that
//    are not affected by L2 phase track loss.
//
QCFLAG CGPSQual::L2TrackCheck( SMsg2P &twop, int &nrSat )
{
    // Counter initialization
    QCFLAG c(0);

    // Test if variable is numerical or not
    for ( int i = 0 ; i < nrSat ; i++ )
```

```
    {
        if ( &twop.rcpP2[i] != 0 )
        {
            if ( isNan( twop.rcpP2[i]) )
                c++;
        }
        else
        {
            break;
        }
    }

    // Return number of unaffected satellites
    return (nrSat-c);
}

//
//  FUNCTION: InterfCheck( SMsgEC &ec, SMsgEL &el, int &nrSat )
//
//  PURPOSE: Detect low C/N0 values
//
//  PARAMETERS:
//    - ec: [EC] JNS message
//    - el: [EL] JNS message
//    - nrSat: number of satellites
//
//  RETURN VALUE:
//    Number of unaffected satellites
//
//  COMMENTS:
//
//    This method returns the number of satellites that
//    are not affected by low C/N0 value.
//
QCFLAG CGPSQual::InterfCheck( SMsgEC &ec, SMsgEL &el, int &nrSat )
{
    // Initialize counter
    QCFLAG c(0);

    for ( int i = 0 ; i < nrSat ; i++ )
    {
        if ( (&ec.cnrCAT[i] != 0) && (&el.elev[i] != 0) )
        {
            if ( ( (el.elev[i] > elevMask) && (ec.cnrCAT[i] < Tsnr) ) || (el.
               elev[i] < elevMask) )
                c++;
        }
        else
        {
            return nrSat;
        }
    }

    // Returns number of affected satellites
    return (nrSat-c);
}

```

```
//
//  FUNCTION: isNan( double input )
//
//  PURPOSE: Check if input is numeric or not
//
//  PARAMETERS:
//    - input: variable to check
//
//  RETURN VALUE:
//    Success if variable is not numeric
//
//  COMMENTS:
//
//    This method checks if the input variable
//    is numeric or not. This is usefull for
//    checking if L2 phase was tracked or not.
//
//
bool CGPSQual::isNan( double input )
{
    if ( !(input/input) )
        return true;

    return false;
}

//
//  FUNCTION: DOPCheck( SMsgDP &dp )
//
//  PURPOSE: Check if DOP factors are high
//
//  PARAMETERS:
//    - dp: [DP] JNS message
//
//  RETURN VALUE:
//    Success if HDOP or VDOP is above threshold
//
//  COMMENTS:
//
//    This method checks for DOP factors
//
//
bool CGPSQual::DOPCheck( SMsgDP &dp )
{
    // NOT WORKING PROPERLY
    /*
    if ( ( dp.hdop > Tdop ) || ( dp.vdop > Tdop ) )
        return true;
    */
    return false;
}

//
//  FUNCTION: RaimRes( SMsgRM &rm )
//
//  PURPOSE: RAIM processing result check
//
```

```
//   PARAMETERS:
//     - rm: [RM] JNS message
//
//   RETURN VALUE:
//     RAIM status
//
//   COMMENTS:
//
//     This method returns the RAIM status that can
//     take the following values:
//             - 0 : normal
//             - 1 : no RAIM
//             - 2 : FDI
//             - 3 : RAIM off
//
QCFLAG CGPSQual::RaimRes( SMsgRM &rm )
{
    char *pch = &rm.RMtext[18];

    // Return RAIM processing result
    return ( (QCFLAG) ( atoi( pch ) ) );
}

//   FUNCTION: L2RaimCheck( SMsgRM &rm, SMsg2P &twop, int &nrSat, ...
//             QCFLAG &Prev, bool &Alarm, bool RaimAl, short unsigned int Counter
    )
//
//   PURPOSE: Global check of code and phase signals, and constellation quality
//
//   PARAMETERS:
//     - rm: [RM] JNS message
//     - twop: [2P] JNS message
//     - nrSat: number of satellites
//     - Prev: number of remaining unaffected satellites of
//       previous epoch
//     - Alarm: status of global check algorithm
//     - RaimAl: status of RAIM in global check algorithm
//     - Counter: number of stable epochs in global raim
//       algorithm
//
//   RETURN VALUE:
//     Success if the algorithm is in alarm state
//
//   COMMENTS:
//
//     This method make a global check by using RAIM processing results
//     and L2 phase track analysis. The alarm state is disengaged if
//     the following observations are stable.
//
bool CGPSQual::L2RaimCheck( SMsgRM &rm, SMsg2P &twop, int &nrSat, QCFLAG &Prev
    , bool &Alarm, bool RaimAl, short unsigned int Counter )
{

    // If RAIM detects anomaly, set alarm state
    if ( (RaimRes(rm) == 1) || (RaimRes(rm) == 3) )
    {
        alarm = true;
```

```
        raimAl = true;
        counter = 0;
    }
    // If quality is not stable, maintain alarm state
    else if ( ( (Prev - L2TrackCheck( twop, nrSat)) != 0 ) && (RaimAl) )
    {
        alarm = true;
        raimAl = true;
    }
    // If quality is stable, engage epoch counter and maintain alarm state
    else if (  ( Prev - L2TrackCheck( twop, nrSat) == 0 )  && (RaimAl) )
    {
        counter = Counter + 1;
        alarm = true;
        raimAl = true;
    }
    // If large number of epoch were stable...
    if ( counter > Interval )
    {
        alarm = false;
        raimAl = false;
    }

    // store last number of remaining satellite
    prev = L2TrackCheck( twop , nrSat );

    // return status
    return alarm;
}

//
//  FUNCTION: SetGPSQual(int tsat, int tsnr, int tdop, bool raim, int elev, ...
//          bool glocheck, int interval)
//
//  PURPOSE: Set the GPS quality parameters
//
//  PARAMETERS:
//    - tsat: satellite threshold
//    - tsnr: C/NO threshold
//    - tdop: DOP threshold
//    - raim: RAIM wanted or not
//    - elev: elevation mask
//    - glocheck: global check wanted or not
//    - interval: parameter for global check
//
//  RETURN VALUE:
//    Success if all the parameters are correct.
//
//  COMMENTS:
//
//    This method sets the GPS quality parameters
//
bool CGPSQual::SetGPSQual(int tsat, int tsnr, int tdop, bool raim, int elev, bool glocheck, int interval)
{
    Raim     = raim;
```

```
    Tsat     = tsat;
    Tdop     = tdop;
    Tsnr     = tsnr;
    elevMask = elev;
    GloCheck = glocheck;
    Interval = interval;

    // Return sucess
    return true;
}

//
//  FUNCTION: Min(int x , int y )
//
//  PURPOSE: Return the minimum of two integers
//
//  PARAMETERS:
//    - x,y: integers
//
//  RETURN VALUE:
//    Minimum between x and y.
//
//  COMMENTS:
//
//    This method returns the minimum of two integers
//
int CGPSQual::Min(int x , int y )
{
    return (x<y)?x:y;
}
```

The header file of the `integrity` class is given below.

```

// Header files
#include "jnsMsg.h"         // Javad GPS receiver messages

// Structure
typedef short unsigned int QCFLAG;

// CGPSQual class
class CGPSQual
{
    public:

        // Constructor/Destructor
        CGPSQual();
        ~CGPSQual();

        // Methods
        QCFLAG  check(  SMsgDP &dp, SMsg2P &twop, SMsgEL &el, SMsgEC &ec,
            SMsgRM &rm, int &nrSat, QCFLAG &Prev, bool &alarm, bool raimAl,
            QCFLAG counter, bool RAIMon );
        bool    SetGPSQual(int tsat, int tsnr, int tdop, bool raim, int elev,
            bool glocheck,int interval);

        // Attributs
        QCFLAG   prev;
```

```
        bool     raimAl, alarm;
        short unsigned int  counter;

    private:

        // Methods
        QCFLAG   L2TrackCheck( SMsg2P &twop, int &nrSat );  // L2 phase track
            analysis
        QCFLAG   InterfCheck( SMsgEC &ec, SMsgEL &el, int &nrSat );
        QCFLAG   RaimRes( SMsgRM &rm );
        bool     DOPCheck( SMsgDP &dp );                           // Check
            DOP factors
        bool     isNan( double input );                     // Check if input
            is numeric or not
        bool     L2RaimCheck( SMsgRM &rm, SMsg2P &twop, int &nrSat, QCFLAG &
            Prev, bool &Alarm, bool RaimAl, short unsigned int Counter );
        int      Min (int x, int y);

        // Attributs
        QCFLAG   Tsat, Tdop, Tsnr;
        bool     Raim, GloCheck;
        int      elevMask, Interval;

};
```

B.3 Use of the class

This section presents the code extract that calls the integrity class after the JNS message decoding step. The main method is called `check` and requires the decoded JNS messages as input arguments. The method returns a quality flag for each epoch.

```
// GPS quality settings
pCommController->m_pGPSQual->SetGPSQual(CTsat, CTsnr, CTdop, CRaim, CElev,
    CGloCheck, CInterval);
                }

// Check GPS quality
pCommController->qflag = pCommController->m_pGPSQual->check( dpMsg, twopMsg,
    elMsg,ecMsg, rmMsg, nrSats, pCommController->Prev , pCommController->Alarm
    , pCommController->RaimAl, pCommController->Counter, true);
```

Appendix C

Structure of the developed algorithms

C.1 Interference detection algorithm

C.1.1 Structure

The global structure of the proposed interference algorithm based on the C/N0 is presented in figure C.1. First, the JNS messages relative to the C/N0 and the satellite elevation angle are decoded. Only the satellites which have their elevation angle above the defined elevation mask are considered. The number of satellites is corrected by removing the satellite below the mask from the total observed satellites. After that, the minimum and the mean C/N0 value are computed in the buffer whose size is previously defined, and then combined and compared to the current standard deviation. The latter is adapted at each epoch[1]. If the comparison test is successful, an interference can be presumed. This test checks also if the minimum value of the buffer is below a defined threshold in order to take in account satellites with low C/N0. A second parallel test is performed by comparing each C/N0 (from each satellite) to a single threshold. In the case of a positive outcome, an interference is detected.

C.1.2 Matlab code

The *Matlab* algorithm is shown below. The single threshold test is not included in this extract.

```
% Read courant epoch
for time = 1:length(TIMEVEC);

    % Initialization of number of visible satellites
    Avsats = 0;

    % Analyse of each visible satellite at readed epoch
    for sat = 1:length(PRN)

        % Insertion of C/N0 value in the corresponding buffer line
        buffer(sat,k) = SNR(time,sat);

```

---

[1] Another possibility is to use the standard deviation of the buffer, but the results are not as good.

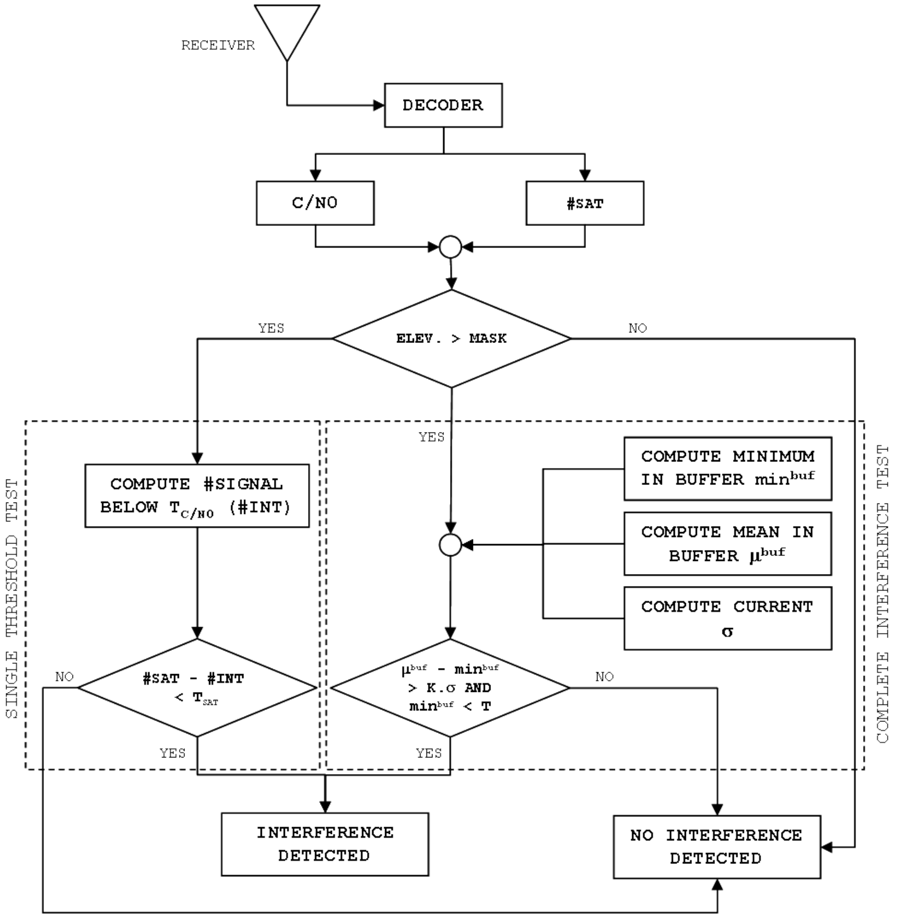

Figure C.1: Interference detection algorithm based on $C/N0$ ratio.

```
        % Check if C/N0 value is available and above the elevation mask
        if (~isnan(SNR(time,sat))) && (ELEVATION(time,sat) > elevationMask)

            % Computation of the courant global C/N0 mean
            itSum(sat)  = itSum(sat) + SNR(time,sat);
            meanGlobal(sat)     = itSum(sat)/time;

            % Computation of the courant global C/N0 standard deviation
            itSigma(sat)   = itSigma(sat) + ...
                (SNR(time,sat) - meanGlobal(sat))^2;
            sigma(sat)  = sqrt(itSigma(sat)/(time-1));

            % Determination of courant available satellite number
            Avsats      = Avsats + 1;

            % Check if the buffer is full
            if mod(k,bufferLength) == 0

                % Computation of the buffer mean for the readed satellite
                prevMeanBuffer(sat) = meanBuffer(sat);
                meanBuffer(sat)        = mean(buffer(sat,:));
```

```

                % Computation of the buffer standard deviation for the
                % readed satellite
                stdBuffer(sat)       = std(buffer(sat,:));

                % Computation of the buffer minimum value for the readed
                % satellite
                minBuffer(sat)        = min(buffer(sat,:));

                % *** Interference presence test ***
                if (prevMeanBuffer(sat)-minBuffer(sat)) > K*sigma(sat)

                    % Count how many satellites are affected by a soudain
                    % decrease of C/N0 value
                    count    = count + 1;

                end

            end

        end

    end

    % If the buffer is full, initialization of the buffer iterator
    if mod(k,bufferLength) == 0, k = 0; end;

    % *** Case where a large number of satellite is affected at the courant
    % epoch. If the remaining unaffected satellite number is less than 5,
    % set an interference alarm. The total available satellite number
    % should be more than 4.
    if (Avsats - count)  <= 5 && (Avsats > 4)

        detInterference(time) = true;

    else

        detInterference(time) = false;

    end

    % Initialization and incrementation of iterators and counters
    count = 0;
    k      = k+1;
end
```

C.2 Signal quality monitoring algorithm

C.2.1 Structure

The structure of the proposed SQM algorithm using RAIM and L2 phase lock time is shown in figure C.2. RAIM alarm is engaged if the RAIM function detects an anomaly. At each following epoch, the number of satellites that have their L2 phase tracked is compared to

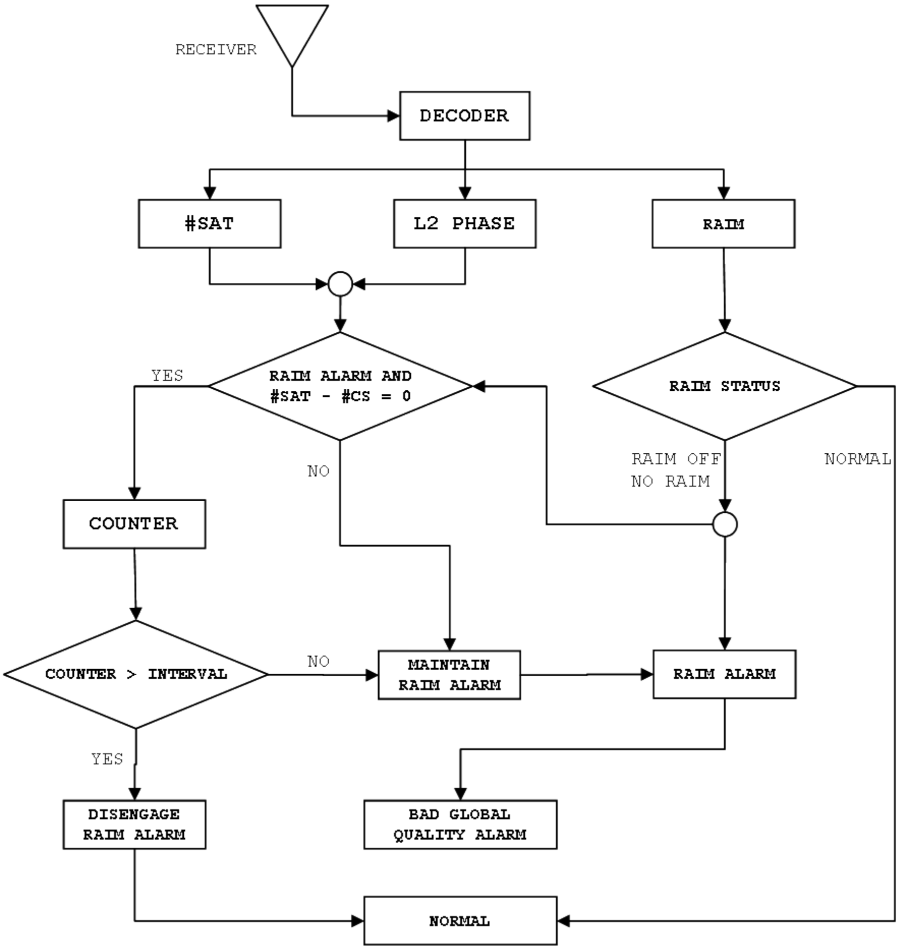

Figure C.2: SQM algorithm based on RAIM processing results and L2 phase tracking loop output.

the number of satellites to form the unaffected satellite number. If this number is not null, the RAIM alarm state is maintained. On the other hand, if a defined number of consecutive epochs have no affected satellites, the RAIM alarm state is disengaged.

C.2.2 Matlab code

The *Matlab* algorithm is shown below.

```

% Variable initialization
raimflag     = false;
intflag      = zeros(length(raim),1);
c            = 0;

% **** Parameter ****
% Time interval during which no constellation variation should occur in
% order to disengage alarm state
interval     = 30;
```

```

for i = 1 : length(t)

    % Case where RAIM detects anomaly
    % No RAIM: bad geometry or limited number of satellites
    % RAIM turned off: not enough satellites (<5)
    if ((raim_noraim(i) > 0) || (raim_turnedoff(i) > 0))

        % Set alarm mode
        intflag(i)  = true;
        raimflag    = true;

    end

    % The variable "remsat2" contains the number of remaining satellites
    % that are not affected by a cycle slip on L2 (phase lock loss) at
    % current epoch
    if (remsat2(i) < 5)

        intflag(i)  = true;

    end

    if i > 1

        % If unaffected constellation is not stable after RAIM has detected
        % anomaly, alarm state is maintained
        if (remsat2(i-1) - remsat2(i) ~= 0) && (raimflag == true)

            % maintain integrity alarm
            intflag(i)  = true;

        end

        % If unaffected constellation is stable under alarm mode, increment
        % time counter
        if (remsat2(i-1) - remsat2(i) == 0) && (raimflag == true)

            c           = c + 1;
            intflag(i)  = true;

        end

    end

    % If unaffected constellation was stable during enough time (given by
    % variable "c"), disengage alarm state and initialize time counter
    if c > interval

        c           = 0;
        intflag(i)  = false;
        raimflag    = false;

    end

end
```

Appendix D

Content of the RTCM message types

D.1 RTCM message types

The table D.2 shows the content of the different RTCM message types. MT 18 to 21 are of particular interest for RTK-GPS positioning.

MT	Description	Remark
1	Differential GPS corrections	
2	Delta differential GPS corrections	
3	GPS reference station parameters	
4	Reference station datum	
5	GPS constellation health	
6	GPS null name	
7	DGPS beacon almanac	
8	Pseudolite almanac	
9	GPS partial correction set	
10	P-code differential correction	
11	C/A code, L1, L2 delta corrections	
12	Pseudolite station parameter	
13	Ground transmitter parameter	
14	GPS time of week	
15	Ionospheric delay message	
16	GPS special message	
17	GPS ephemerids	
18	RTK uncorrected carrier phases	added in RTCM2.1
19	RTK uncorrected pseudorange	added in RTCM2.1
20	RTK carrier phase corrections	added in RTCM2.1
21	RTK pseudorange corrections	added in RTCM2.1
22	Extended reference station parameters	

Table D.1: Content of the RTCM message types.

23	Antenna type definition	added in RTCM2.3
24	Reference station: ARP parameter	added in RTCM2.3
25,26	Undefined	
27	Extended DGPS radio beacon almanac	
28..30	Undefined	
31	Differential GLONASS corrections	added in RTCM2.2
32	Differential GLONASS reference station	added in RTCM2.2
33	GLONASS constellation health	added in RTCM2.2
34	GLONASS partial differential correction set and GLONASS null name	added in RTCM2.2
35	GLONASS radio beacon almanac	added in RTCM2.2
36	GLONASS special message	added in RTCM2.2
37	GNSS system time offset	
38..58	Undefined	
59	Proprietary message	
60..63	Multipurpose usage	

Table D.2: Content of the RTCM message types.

Further informations can be found on the RTCM Official Website.

Appendix E

Complements on the accuracy measures

E.1 How to read a Stanford plot

The stanford plot enables to check the relevance of an accuracy estimation by providing a simple and clear graphical view. The horizontal axis represents the true errors that are derived from the PP solution in this thesis. The vertical axis represents the accuracy measure provided by the receiver. So, to each provided accuracy corresponds his true error, which is represented by a point in the graphic. The color represents the point density. Thus, if the color tends to be red, the point density is high. The Stanford plots are initially used to represent the integrity performance. They are used in this thesis for checking the relevance of accuracy measures like the 3-σ interval. The points that are located below the diagonal mean that the true error is higher than the estimated interval limit, i.e. the true error lies outside of the interval.

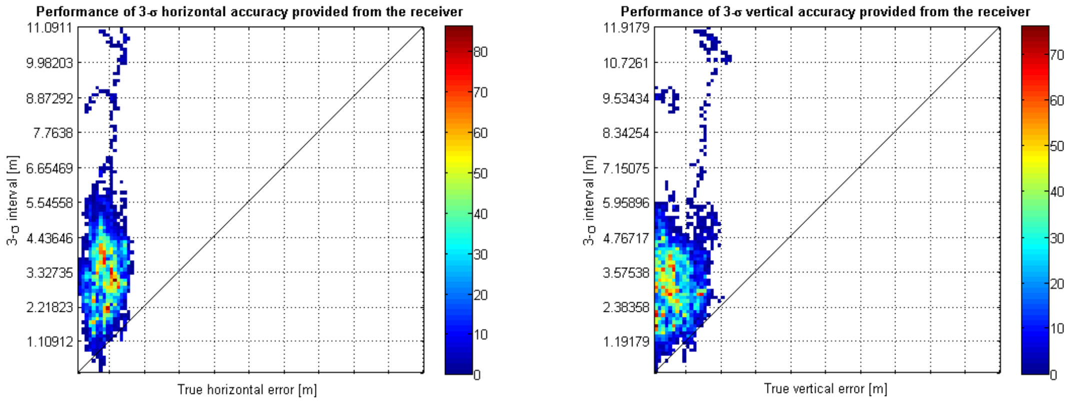

Figure E.1: Stanford plots showing the performance of the 3-σ horizontal (left) and vertical (right) accuracy measure after applying a correction coefficient.

The stanford plots presented in figure E.1 give as example the performance of the EGNOS differential mode accuracy estimation that have been corrected by applying a correction coefficient (see chapter 4). The 3-σ interval is considered and it is visible that very few observations are outside of the interval (near 0.4% for both cases). This indicate that the analyzed accuracy measure is relevant.

E.2 Gaussian distribution features

The statistics of the Gaussian distribution are showed in figure E.2.

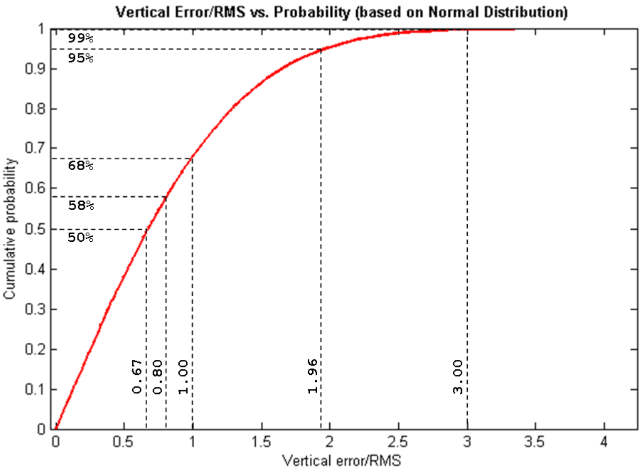

Figure E.2: Gaussian CDF used for modeling the vertical error behavior and deriving classical one-dimensional accuracy measures.

The table E.1 can be used to estimate different error statistics by multiplying the error statistic on the rows for obtaining the corresponding error statistic in the wanted column.

	Median (50%)	Mean (58%)	RMS (68%)	95% error	99% error
Median (50%)	1.00	1.20	1.50	2.95	3.84
Mean (58%)	0.83	1.00	1.25	2.46	3.21
RMS (68%)	0.67	0.80	1.00	1.96	2.57
95% error	0.34	0.41	0.64	1.00	1.31
99% error	0.26	0.31	0.39	0.76	1.00

Table E.1: Relationship between different error statistics for vertical error by assuming a Gaussian distribution.

E.3 Rayleigh distribution

E.3.1 Features

The statistics of the Rayleigh distribution are shown in figure E.3.

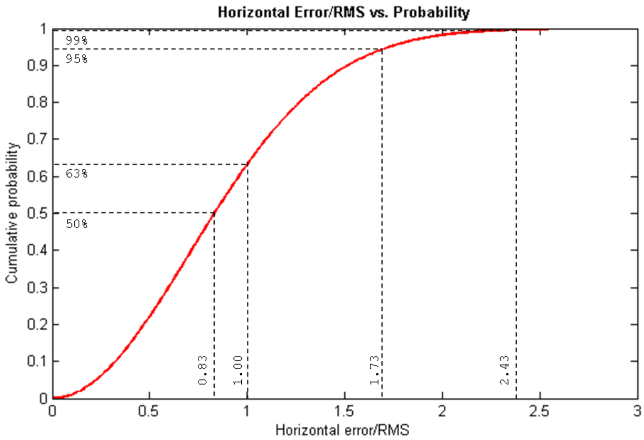

Figure E.3: Rayleigh CDF need for modeling horizontal error behavior.

The table E.2 can be used to estimate different error statistics by multiplying the error statistic on the rows for obtaining the corresponding error statistic in the wanted column.

	CEP (50%)	Mean (54%)	RMS (63%)	95% error	99% error
CEP (50%)	1.00	1.06	1.20	2.08	2.62
Mean (54%)	0.94	1.00	1.13	2.01	2.45
RMS (63%)	0.83	0.89	1.00	1.73	2.18
95% error	0.48	0.50	0.58	1.00	1.26
99% error	0.38	0.41	0.46	0.79	1.00

Table E.2: Relationship between different error statistics for horizontal error by assuming a Rayleigh distribution.

E.3.2 Deriving the Rayleigh distribution from Gaussian distributions

This section deals with the derivation of a Rayleigh distribution from normal distributions. This is essential for understanding position error behavior.

If X is a random variable whose density is f_X, the cumulative distribution function of $Y = X^2$ is given by

$$\begin{aligned} F_Y(y) &= P(Y \leq y) \\ &= P(X^2 \leq y) \\ &= P(-\sqrt{y} \leq x \leq \sqrt{y}) \\ &= F_X(\sqrt{y}) - F_X(-\sqrt{y}) \end{aligned} \tag{E.3.1}$$

The density function of Y can be obtained by

$$\begin{aligned} f_Y(y) &= \frac{d}{dy} F_Y(y) \\ &= \frac{d}{dy}\left[F_X(\sqrt{y}) - F_X(-\sqrt{y})\right] \\ &= \frac{1}{2\sqrt{y}}\left[f_X(\sqrt{y}) + f_X(-\sqrt{y})\right] \end{aligned} \tag{E.3.2}$$

We assume that Y follows a standard normal distribution whose density can be written as

$$f(x) = \frac{1}{\sqrt{2\pi}\sigma} e^{-(x-\mu)^2/2\sigma^2} \tag{E.3.3}$$

By inserting this relation in equation E.3.2, we get

$$\begin{aligned} f_{X^2}(y) &= \frac{1}{2\sqrt{y}}\left[\frac{1}{\sqrt{2\pi}} e^{-\sqrt{y}^2/2} + \frac{1}{\sqrt{2\pi}}\; e^{-\sqrt{y}^2/2}\right] \\ &= \frac{1}{\sqrt{y}} \frac{1}{\sqrt{2\pi}} e^{-y/2} \\ &= \frac{\frac{1}{2} e^{-1/2y} \left(\frac{1}{2} y\right)^{\frac{1}{2}-1}}{\sqrt{\pi}} \end{aligned} \tag{E.3.4}$$

which is the Gamma density function with parameters $\left(\frac{1}{2}, \frac{1}{2}\right)$

Now that we have demonstrated that

$$X^2 \sim Gamma\left(\frac{1}{2}, \frac{1}{2}\right) \tag{E.3.5}$$

and if we consider theorem E.3.1, we have

$$Z = X^2 + Y^2 \sim Gamma\left(1, \frac{1}{2}\right) \tag{E.3.6}$$

Theorem E.3.1 *If X and Y are two independent random variables following a Gamma distribution of parameter (s, λ) and (t, λ) respectively, then the sum $X + Y$ will also be distributed following a Gamma distribution of parameter $(s + t, \lambda)$.*

This relation states that

$$Z \sim \chi^2 \tag{E.3.7}$$

with two degrees of freedom since the chi-square distribution is nothing else than a Gamma distribution of parameter $\left(\frac{n}{2}, \frac{1}{2}\right)$ whose density is given by

$$\begin{aligned} f_{\chi_n^2}(y) &= \frac{\frac{1}{2} e^{-y/2} \left(\frac{y}{2}\right)^{n/2-1}}{\Gamma\left(\frac{n}{2}\right)} \\ &= \frac{e^{-y/2} y^{n/2-1}}{2^{n/2}\Gamma\left(\frac{n}{2}\right)} \end{aligned} \tag{E.3.8}$$

If we consider two degrees of freedom, we can obtain

$$f_{\chi_2^2} = \frac{e^{-y/2} y}{2y} = \frac{1}{2y} e^{y/2} \tag{E.3.9}$$

which is the density function of a Rayleigh distribution.

This demonstration is important for the error analysis since we can demonstrate that the RMS error expressed as

$$dR = \sqrt{dx^2 + dy^2} \tag{E.3.10}$$

where

$$\begin{aligned} dx &\sim N(\mu_{dx}, \sigma_{dx}) \\ dy &\sim N(\mu_{dy}, \sigma_{dy}) \end{aligned}$$

follows a Rayleigh distribution. For doing that, we can express the following problem. If we write $r = g_1(x, y) = \sqrt{x^2 + y^2}$ and $\theta = g_2(x, y) = \arctan(y/x)$ where r and θ are polar coordinates parameters, we can calculate the partial derivatives

$$\begin{aligned} \frac{\partial g_1}{\partial x} &= \frac{x}{\sqrt{x^2 + y^2}} \\ \frac{\partial g_1}{\partial y} &= \frac{y}{\sqrt{x^2 + y^2}} \\ \frac{\partial g_2}{\partial x} &= \frac{-y}{x^2 + y^2} \\ \frac{\partial g_2}{\partial y} &= \frac{x}{x^2 + y^2} \end{aligned} \tag{E.3.11}$$

The Jacobian can be derived as

$$J(x, y) = \frac{x^2}{(x^2 + y^2)^{3/2}} + \frac{y^2}{(x^2 + y^2)^{3/2}} = \frac{1}{\sqrt{x^2 + y^2}} = \frac{1}{r} \tag{E.3.12}$$

The joint probability density function of X and Y is given by

$$f(x, y) = \frac{1}{2\pi} e^{-(x^2+y^2)/2} \tag{E.3.13}$$

Thus, the joint probability function of R and θ will be

$$f(r, \theta) = \frac{1}{2\pi} r e^{-r^2/2} \tag{E.3.14}$$

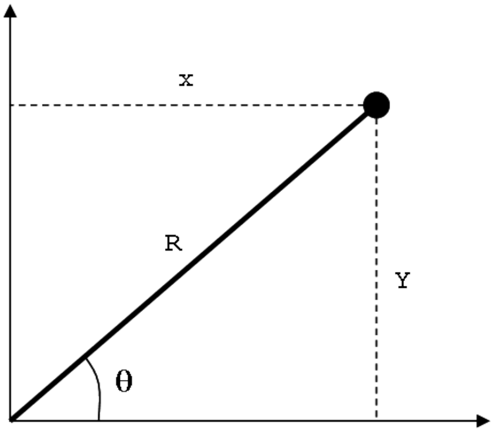

where $0 < \theta < 2\pi$ and $0 < r < \infty$. This density is decomposable in marginal density functions, these two variables will therefore be independent. θ is uniformly distributed on $(0, 2\pi)$, while R follows a Rayleigh distribution whose density is given by

$$f(r) = re^{-r^2/2} \tag{E.3.15}$$

So if we consider that the horizontal and vertical errors follow a standard normal distribution, the distance between the true position and the observed position follows a Rayleigh distribution.

E.4 Velocity accuracy estimation

Since the receiver velocity accuracy measure is related to the position accuracy measure, the same conclusion as for the position can be made. This section presents the main conclusions.

Appendix F

Reference solution of cycle slip detection for a given GPS data sample

This chapter provides the result of the cycle slips detection by using *GrafNav* post-processing software for a chosen data sample. These results have been considered as the reference to which the tested algorithms from chapter 3 should tend.

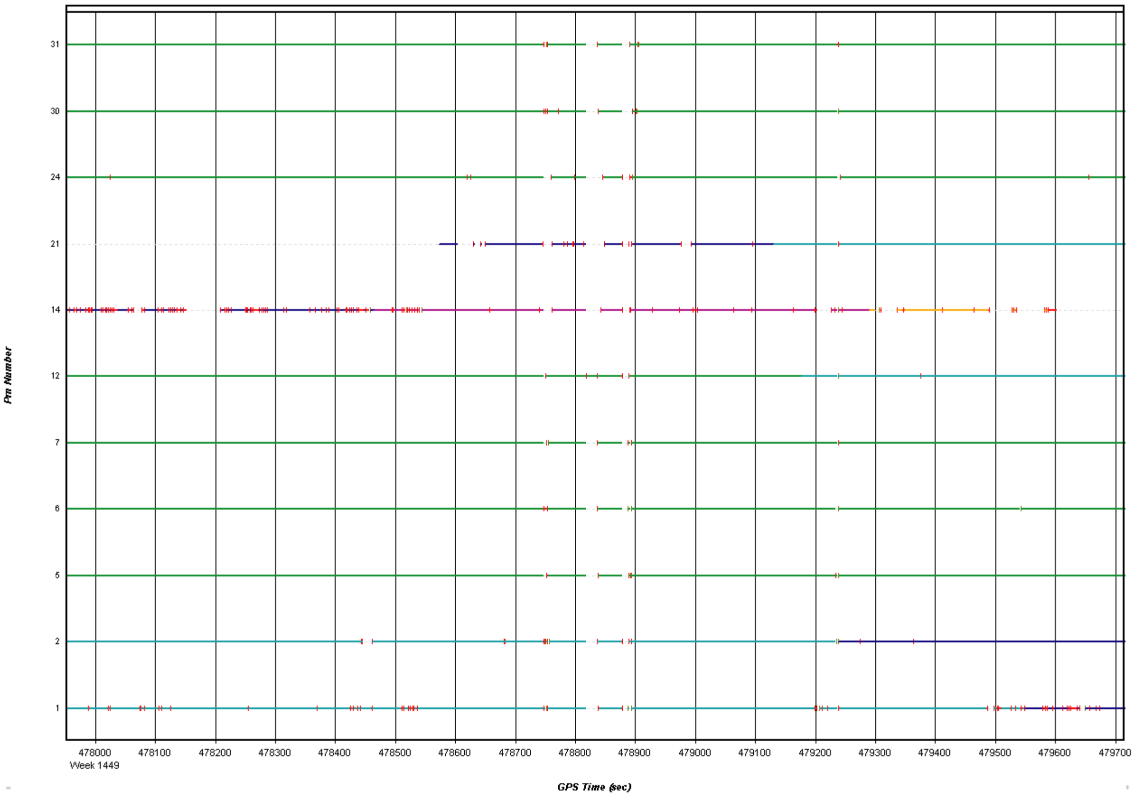

Figure F.1: Result of cycle slip detection on L1 carrier phase.

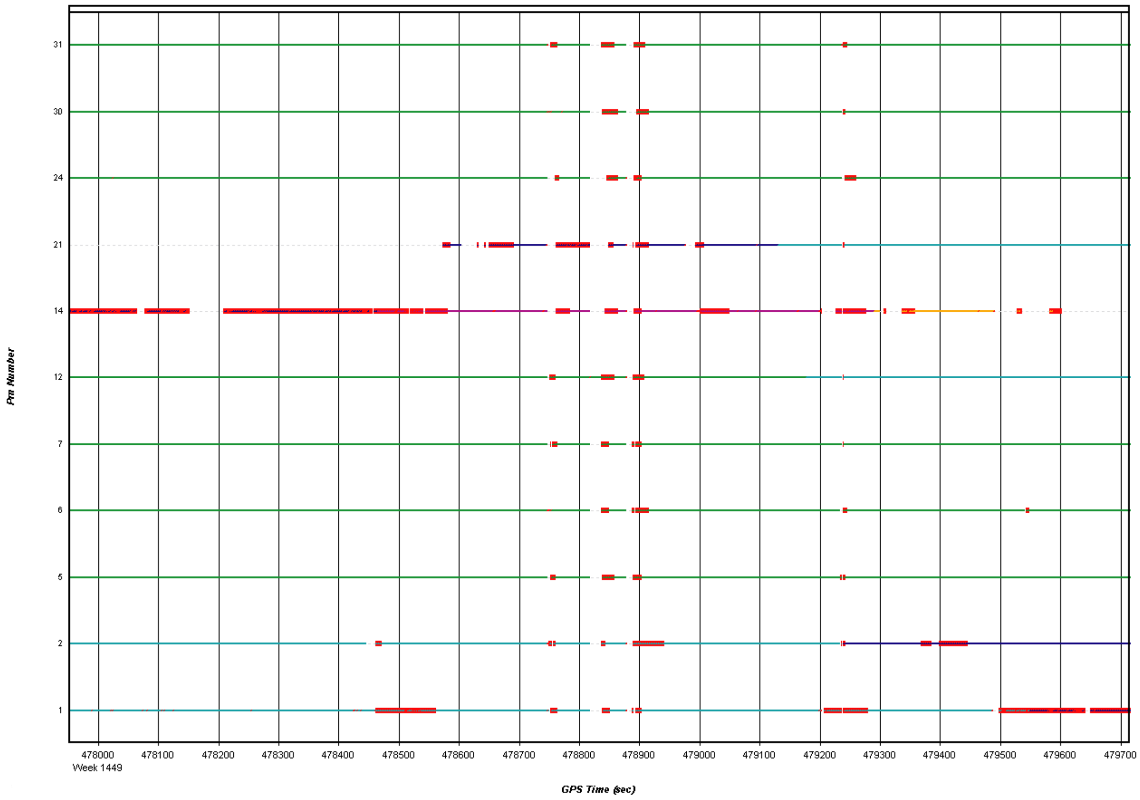

Figure F.2: Result of cycle slip detection on L1 carrier phase.

The cycle slips are indicated by the red marks on the lines. *GrafNav* uses the locktime read or the computed locktime in the decoder combined with a Doppler check to detect L1 phase cycle slips. The default L2 cycle slips detection method utilizes L2 locktime datas. Furthermore, Kinematic Ambiguity Resolution (KAR) and relative ionospheric processing can be used for detecting small cycle slips on L2 by comparing it against the L1 phase. More informations about the *GrafNav* processing methods can be found in the software manual[1].

---

[1] www.novatel.com